# PH.D. THESIS

Joint Detection and Decoding of High-Order Modulation Schemes

for CDMA and OFDM Wireless Communications

*by Yingjiu Xu*
*Advisor: Prof. John S. Baras*

**CSHCN PhD 2003-1**
**(ISR PhD 2003-2)**

ABSTRACT


Title of Dissertation:   JOINT DETECTION AND DECODING OF

HIGH-ORDER MODULATION SCHEMES FOR

CDMA AND OFDM WIRELESS COMMUNICATIONS

Yingjiu Xu, Doctor of Philosophy, 2003


Dissertation directed by:   Professor John S. Baras
                            Department of Electrical and Computer Engineering



Wireless communications call for high data rate, power and bandwidth effi-
cient transmissions. High-order modulation schemes are suitable candidates for
this purpose as the potential to reduce the symbol period is often limited by
the multipath-induced intersymbol interference. In order to reduce the power
consumption, and at the same time, to estimate time-variant wireless channels,
we propose low-complexity, joint detection and decoding schemes for high-order
modulation signals in this dissertation.

We start with the iterative demodulation and decoding of high-order CPM
signals for mobile communications. A low complexity, pilot symbol-assisted co-
herent modulation scheme is proposed that can significantly improve the bit
error rate performance by efficiently exploiting the inherent memory structure

of the CPM modulation. A noncoherent scheme based on multiple symbol differential detection is also proposed and the performances of the two schemes are simulated and compared.

Second, two iterative demodulation and decoding schemes are proposed for quadrature amplitude modulated signals in flat fading channels. Both of them make use of the iterative channel estimation based on the data signal reconstructed from decoder output. The difference is that one of them has a threshold controller that only allows the data reconstructed with high reliability values to be used for iterative channel estimation, while the other one directly uses all reconstructed data. As the second scheme has much lower complexity with a performance similar to the best of the first one, we further apply it to the space-time coded CDMA Rake receiver in frequency-selective multipath channels. We will compare it to the pilot-aided demodulation scheme that uses a dedicated pilot signal for channel estimation.

In the third part of the dissertation, we design anti-jamming multicarrier communication systems. Two types of jamming signals are considered - the partial-band tone jamming and the partial-time pulse jamming. We propose various iterative schemes to detect, estimate, and cancel the jamming signal in both AWGN and fading channels. Simulation results demonstrate that the proposed systems can provide reliable communications over a wide range of jamming-to-signal power ratios.

Last, we study the problem of maximizing the throughput of a cellular multicarrier communication network with transmit or receive diversity. The total throughput of the network is maximized subject to power constraints on each mobile. We first extend the distributed water-pouring power control algorithm

from single transmit and receive antenna to multiple transmit and receive antennas. Both equal power diversity and selective diversity are considered. We also propose a centralized power control algorithm based on the active set strategy and the gradient projection method. The performances of the two algorithms are assessed with simulation and compared with the equal power allocation algorithm.

JOINT DETECTION AND DECODING OF

HIGH-ORDER MODULATION SCHEMES FOR

CDMA AND OFDM WIRELESS COMMUNICATIONS


by

Yingjiu Xu



Dissertation submitted to the Faculty of the Graduate School of the
University of Maryland, College Park in partial fulfillment
of the requirements for the degree of
Doctor of Philosophy
2003




Advisory Committee:

        Professor John S. Baras, Chairman/Advisor
        Professor John J. Benedetto
        Dr. Evaggelos Geraniotis
        Professor Steve Tretter
        Professor Sennur Ulukus

## DEDICATION


Dedicated to my parents and to my wife

## ACKNOWLEDGEMENTS

First, I would like to express my gratitude to my advisor, Professor John S. Baras, for his genuine and generous help. He came to help me when my former advisor left the school and has kindly shielded me from many difficulties in the last stage of my graduate study. His help is crucial to the completion of this work. I would also like to take this opportunity to thank my former advisor, Dr. Evaggelos Geraniotis, for his continuous guidance, encouragement and direction during the entire course of preparation for this dissertation.

I am indebted to Professor John J. Benedetto, Professor Steve Tretter, and Professor Sennur Ulukus for serving as committee members of my dissertation.

I am deeply thankful to the chairman of the Electrical and Computer Engineering Department, Professor Steven Marcus, and the director of the Institute for Systems Research, Professor Eyad Abed, for their help and caring for the benefits of students.

I would also like to thank my fellow graduate students for many helpful discussions and for their encouragement.

Finally, my deepest appreciation and gratitude goes to my parents and my wife for their constant love, understanding, and support.

TABLE OF CONTENTS

# LIST OF TABLES

LIST OF FIGURES

xiii

JOINT DETECTION AND DECODING OF
HIGH-ORDER MODULATION SCHEMES FOR
CDMA AND OFDM WIRELESS COMMUNICATIONS

Yingjiu Xu

July 31, 2003

This comment page is not part of the dissertation.

# Chapter 1

# Introduction

High-speed data transmission over wireless channels has been an area of intensive research in past years. One of the frequently occurring problems in wireless communications is signal multipath – the transmitted signal arrives at the receiver through multiple propagation paths with different delays. As a result, those signal components from different paths may add up destructively or constructively, causing signal fading – variation in the received signal strength. This situation is aggravated by the time-variant nature of wireless channels, where those multiple propagation paths vary with time. To demodulate the received signal coherently, this time-variant channel state information must be accurately estimated.

According to Proakis [1], the error rate in Rayleigh fading channels decreases only inversely with signal-to-noise ratio (SNR), while it decreases exponentially with SNR in nonfading channels. Therefore in multipath fading channels, a large amount of transmitting power is required to achieve a low probability of error. But to do this, one has to consider the high cost of high power amplifier on top of high power consumption. Otherwise, he has to push the limit of the low cost amplifier and face the amplitude nonlinearity problem. For this purpose,

1

continuous phase modulation (CPM), with its constant envelope, is well suited for wireless communications because of its compact power spectrum and its insensitivity to nonlinear distortions. But the BER performance of continuous phase modulation provided by current receivers is generally worse than that of the memoryless modulation like MPSK (minimal phase-shift keying). This is in part due to the correlation in signals introduced by the memory in continuous phase modulation, which is obvious in uncoded signals. In the case of coded CPM signals, however, the improper handling of the inherent memory in CPM signals by current CPM receivers is more to be blamed for the bad performance than the CPM memory itself. There is either no information or at most hard decisions vulnerable to error propagation exchanged between CPM demodulators and channel decoders.

There is also a limit on the maximum transmit power in the practical situation, not only for economical reasons but also because there are situations where high-powered signals would be interfering with each other. In the latter situation, the effective signal-to-interference-ratio (SINR) would saturate when the transmit power goes to infinity. Therefore, it is extremely important to develop power and bandwidth efficient communication systems for high data rate wireless communications.

Another difficulty posed by the multipath is intersymbol interference (ISI) – signals associated with different symbol periods arrive at the receiver at the same time and interfere with each other. In this case, because the coherent bandwidth of the channel is smaller than the signal bandwidth, different frequency components of the signal are subject to different gains and phase shifts across the band. This kind of fading channel is said to be frequency-selective.

There are mainly two kinds of solutions for static or very slowly fading channels. One solution to ISI is equalization, which is expensive in the amount of computation under severe frequency-selective fading. The other is multicarrier communications, which divide the transmitted data into a number of bit streams and transmitting them through different frequency subchannels, within each of which the fading is approximately flat. Recently, a special form of multicarrier communications, orthogonal frequency-division multiplexing (OFDM), has received much attentions due to its simplicity in implementation – it uses the IFFT at the transmitter and the FFT at the receiver.

For fast multipath fading channels, it remains a challenging task to estimate time-variant and frequency-selective channel state information efficiently. Since the fading on each individual path can be treated as flat, efforts have been made to resolve multiple paths and estimate the parameters of each path separately. One of them is the Rake receiver for DS-CDMA (Direct-Sequence Code Division Multiple Access), where each Rake finger handles one path with a certain delay. But the resolution of this method depends on the channel bandwidth, which limits it mostly to wide-band signals. For narrow-band signals, oversampling, either spatial or temporal, must be used to resolve multiple paths. With multiple antennas coming into use more and more frequently, the problem of channel estimation in fast multipath fading channels demands more and more attention.

Although the multipath problem is created by nature, not all problems in wireless communications are caused by nature. Some are due to human beings themselves, either deliberately or inadvertently, which could pose damages from severely degrading the performance of wireless communication systems to knocking them completely out of services. Hence these problems have to be addressed

for reliable communications over wireless channels.

Among inadvertently artificial problems, one of them is the cochannel interference due to frequency reuse in a cellular network. The presence of the cochannel interference greatly complicates the design of a high performance network. When there is only a single cell, the problem of maximizing the system throughput against the frequency-selective fading in a wireless channel can be achieved through water-pouring power allocation and adaptive modulation among OFDM subchannels. In a multi-cell mobile communication environment, one would tend to increase the frequency reuse in order to increase the spectral efficiency with given bandwidth, which, however, introduces severe cochannel interferences and complicates the problem of maximizing the system throughput.

Jamming belongs to problems deliberately caused by man in hostility. Anti-jamming design is especially important for military purposes. Many of the current anti-jamming systems make use of bandwidth redundancy by resorting to spread-spectrum techniques, either code-division multiple access or frequency-hopping. An interesting problem is how to achieve some kind of anti-jamming capability without bandwidth redundancy, by exploiting signal structure to estimate and cancel jamming signals and/or by reallocating resources such as power and bandwidth to avoid jamming signals.

In order to improve power and bandwidth efficiency, and to combat fading and artificial interferences, we propose approaches to system design based on the following ideas: joint detection and decoding, pilot symbol-assisted channel estimation (PSAM), jamming signal estimation and cancellation, transmit and receive diversity, power control and adaptive modulation. In particular, we pursue our research in the following aspects: iterative demodulation and de-

4

coding of high-order CPM signals in flat fading channels, pilot symbol-assisted demodulation of turbo-coded quadrature amplitude modulation in Doppler fading channels, anti-jamming multicarrier communication systems, power control and adaptive modulation for OFDM with transmit and receive diversity. A more detailed description of each part will be presented in the following sections.

## 1.1 Iterative Demodulation and Decoding of High-Order CPM Signals in Flat Fading Channels

Continuous phase modulation is a highly attractive modulation scheme for wireless communications because of its compact power spectra and its insensitivity to nonlinear distortion. However, the subject of coherent detection of CPM signals, especially high-order CPM signals in fading channels, has received less attention because of the common belief that it is difficult to accurately estimate the phase of the received signal in such an environment. Differential detection techniques have thus been widely used in the reverse link to combat phase uncertainties caused by fading. But the performance of differential detection is significantly inferior to that of coherent demodulation. Furthermore, differential detection has irreducible error floor in fast fading channels.

In [2], Gertsman and Lodge demonstrated that joint data detection and channel estimation can be done accurately by integrating linear prediction into the branch metric calculation for digital phase-modulated demodulation. Although it has obtained a BER performance never reached before, the receiver com-

plexity grows linearly with the constellation size to the power of the predictor length, limiting this technique to modulation schemes with small constellation size. To reduce the complexity, it is necessary to separate channel estimation from CPM demodulation. Pilot symbol-assisted modulation can be used for this purpose. However, in continuous phase modulation, pilot symbols cannot be inserted directly into the data stream as in linear modulation on account of the cross-symbol signal dependency. Ho and Kim [3] demonstrated that data dependent pilot symbols can be used in continuous phase modulation with rational modulation index.

Once the channel state information is estimated by using pilot symbols, iterative processing can be applied to coded CPM signals by using the "generalized turbo principle" proposed by Hagenauer [4]. According to Rimoldi [5], continuous phase modulation can be decomposed into a continuous phase encoder and a linear modulator. With the channel interleaver between the channel encoder and the CPM modulator, the entire coded CPM transmitter can be regarded as a serial concatenated turbo encoder. Therefore the demodulation can be greatly enhanced by passing the soft extrinsic information between the CPM demodulator and the channel decoder.

To further improve the performance, channel estimation error can be reduced by using the iterative filtering technique mentioned before. What makes channel estimation more complicated here is that the inherent memory of the CPM signal will introduce severe error propagation when the receiver reconstructs the transmitted signal for channel estimation. So far this problem has not been dealt with in literature.

We propose to use iterative demodulation and decoding schemes for high-

order continuous phase modulated signals in Doppler fading channels. We propose to treat the continuous phase encoder of CPM signals as the recursive inner decoder and the convolutional encoder as the outer decoder so that the entire CPM transmitter can be treated as a serial concatenated convolutional code. Thus the CPM receiver can achieve significant performance improvement by applying iterative demodulation and decoding.

To estimate the time-variant channel state information, we propose two approaches. One is demodulation based on the pilot symbol-assisted modulation with iterative channel estimation, which has low computational complexity but has a little power and bandwidth loss due to the introduction of pilot symbols. The other one is based on multiple-symbol differential detection, which combines channel estimation with CPM demodulation. Although it can achieve slightly better performance at medium signal-to-noise ratio and it does so without power and bandwidth loss due to pilot symbols, the computational complexity is much higher than the PSAM based approach. Please also note that instead of generating a common estimate of channel state information for each symbol period, the second method generates many estimates simultaneously depending on the state. So the demodulation based on this method actually belongs to noncoherent demodulation. We will evaluate those two approaches using numerical methods and compare their computational complexity as well as performance.

## 1.2 Pilot Symbol-Assisted Demodulation of Turbo-Coded Quadrature Amplitude Modulation in Doppler Fading Channels

High-order quadrature amplitude modulation requires channel coding to reduce the power requirements in wireless communications. Much research has been done on developing power and bandwidth efficient channel coding schemes for QAM. A well-established technique is trellis-coded modulation (TCM) proposed by Ungerboeck in 1982 [6] that uses set partitioning to map the convolutional coded bits into signal points such that the minimum Euclidean distance is maximized. TCM can obtain significant coding gains (3-6 dB) in additive white Gaussian noise channels without sacrificing either data rate or bandwidth.

With the invention of turbo codes by C. Berrou, A. Glavieux, and P. Thitimajshima [7] in 1993, which is a more powerful coding scheme than the convolutional code, researchers began to combine turbo codes with QAM. In [8], the parallel outputs of the parallel concatenated turbo encoder are directly mapped to QAM symbols and the best 8 and 16 state codes for 8-PSK, 16-QAM and 64-QAM are found for this particular structure. In [9], two parallel concatenated trellis encoders are connected by a group of interleavers and the outputs of the two trellis encoders are punctured alternately. In the receiver, symbol-by-symbol MAP decoders are used to decode the received symbols alternately and exchange the extrinsic information between each other. According to [8] and [9], both systems perform within 1 dB from the Shannon limit at certain BER ($10^{-7}$) with large interleaver size in additive white Gaussian noise channels.

Although TCM is a successful coding scheme in additive white Gaussian

noise channels, it was recently found that the best trellis codes in additive white Gaussian channels are often not the best in fading channels. According to [10], to minimize error probability in fading channels the code should be designed to maximize the Hamming distance (as measured by the number of modulated symbols). But in TCM, Ungerboeck's rule of set partitioning often leads to parallel branches, in which case the Hamming distance is only one and thus there is no coding diversity against fading [11] [12] [13]. Based on this discovery, some power and bandwidth will be given efficient schemes with separated coding and modulation [14], have been proposed for Rayleigh fading channels.

Another problem in wireless channels is to estimate the channel state information. Given the time-varying nature of the channel impulse response in multipath channels, one way to estimate the channel state information is to use a pilot tone [15] [16] [17]. The best known technique of pilot tone is transparent-tone-in-band (TTIB) in [15], [16] and [17]. Although it is a general solution, it requires relatively complex signal processing and results in an increased peak-to-average power ratio.

In pilot symbol-assisted modulation, the transmitter periodically inserts known symbols to be used by the receiver as references to estimate the channel state information. Compared with pilot tone, PSAM does not change the transmitted pulse shape or peak-to-average power ratio. Processing at the transmitter and receiver of PSAM is also simpler than that of TTIB. In [18], closed form expressions were derived for the BER of BPSK and QPSK. In [19], closed form BER performance was extended to M-QAM signals with estimated channel state information.

To further improve the performance of PSAM, Su [?] proposed iterative fil-

tering to perform the estimation of the channel state information (CSI) with the help of decoding process by feeding back the soft information from decoder to the channel estimator in a BPSK system. This scheme has a linear complexity and was shown to reduce effectively the performance lag caused by the channel estimation error in PSAM. However, due to the inherent drawback of the BPSK signal, the above system has limited power and bandwidth efficiency. To our best knowledge, no research effort has been made to apply this turbo coded scheme with iterative filtering to high-order QAM.

We propose a pilot symbol-assisted, turbo-coded quadrature amplitude modulation (QAM) scheme with iterative channel estimation in Doppler fading channels. We start with flat-fading channels and propose two schemes for iterative channel estimation. One is based on the threshold-controlled feedback. The other one is much simpler with linear complexity but has similar performance. Then we will extend our work to frequency-selective multipath channels using space-time coded Rake receiver. We will study the performance of the single user system under different transmit and receive diversity combinations.

## 1.3  Anti-Jamming Multicarrier Communication Systems

Multicarrier communication systems provide a simple solution to frequency-selective fading by dividing the transmitted data into a number of bit streams and transmitting them through different frequency subchannels. In multicarrier systems, the frequency response is flat or approximately constant within each subchannel but varies from one subchannel to another. Basics about multicarrier systems can be found in [20], [21] and [1].

In fading channels, the channel state information for all subchannels of multicarrier systems must be accurately estimated for coherent demodulation. Compared to the serial data system in which only a single channel gain need to be estimated at each symbol period, channel gains on each subchannels must be estimated simultaneously. In [22], Li proposed a robust channel estimator that makes full use of the time and frequency domain correlations of the channel frequency response for OFDM systems in rapid dispersive fading channels. In [23], pilot symbol-assisted channel estimation schemes with one-dimensional and two-dimensional Weiner filters were studied and compared. It was shown that the performance of two one-dimensional Wiener filters combined is similar to that of a two-dimensional Wiener filter in terms of mean square estimation error. In [24], an exact expression of the BER performance was derived for a multicarrier system using optimal pilot symbol-assisted, two-dimensional Wiener filters in an unknown time-variant, frequency-selective Rayleigh fading channel. However, this result was limited to the case where each subcarrier is binary modulated. No efforts were made in those papers to apply the iterative filtering technique to multicarrier communication systems for joint detection and decoding.

Because multicarrier signals are also wide band, we are tempted to study the anti-jamming capability of multicarrier signals. In the multicarrier modulation, multiple samples of jamming signals in both time and frequency directions can be used to estimate and cancel jamming signals. We consider two types of jamming signals – the partial-band tone jamming and the partial-time pulse jamming.

We start with detection and estimation of jamming signals in the additive white Gaussian noise (AWGN) channel. We propose to detect the presence of jamming signals by computing the eigenvalues of the autocorrelation matrix in all

subchannels and to estimate the jamming signal and cancel it from the received signal if detected. The receiver will then demodulate and decode the received signal as usual. To further improve the performance, we propose to reconstruct the data signal to help detect and estimate jamming signals iteratively and to use a correlation detector to generate soft decisions on the jamming state.

Next we will consider anti-jamming design in the multipath fading channel with Doppler spread. The key issue here is the estimation of the channel state information for coherent demodulation. We propose to use pilot symbol sequences specially designed for working in the jamming environment for the estimation of time-variant channel state information (CSI) at the receiver. We also propose to combine iterative channel estimation with iterative jamming detection and estimation to achieve better performance.

## 1.4 Power Control and Adaptive Modulation for OFDM with Transmit and Receive Diversity

One of the main problems in mobile communications is how to maximize the system throughput against frequency-selective multipath fading. With OFDM, the problem of maximizing the system throughput against the frequency-selective fading in a wireless channel can be achieved through power allocation and adaptive modulation among subchannels. When there is only a single cell, the optimization problem can be solved using water-pouring. In a multi-cell mobile communication environment, in order to increase the spectral efficiency with given

bandwidth one would tend to increase the frequency reuse, which, however, introduces severe cochannel interferences and makes the problem of maximizing the system throughput intractable.

In [25], Su proposed a distributed water-pouring algorithm (DWPA) for adaptive modulation which is executed independently by the cochannel interfering users. It was shown that the DWPA could effectively suppress cochannel interference and improve the system throughput. Since the optimization of a multi-cell system is complicated and computationally intensive, this heuristic distributed algorithm is more practical and much easier to implement. The idea was based on the fact that in many practical situations, a feedback channel with limited bandwidth from the receiver to the transmitter is usually available. Therefore channel state information can not only be obtained (estimated) at the receiver but is also available at the transmitter. Adaptive modulation can thus be used together with power control to improve the OFDM throughput for a given QoS (Quality of Service).

Another effective method to mitigate fading, especially deep slowly fading, is to use spatial diversity – multiple transmit and receive antennas. Transmit and receive antenna diversity has been an area of intensive research with the invention of trellis-based space-time codes by Tarokh, etc in [26]. Later, full-rate space-time block codes have also been [27], [28] proposed. Among them, Alamouti [28] proposed a simple transmit diversity technique. For our problem of interest, space-time coded OFDM systems have been explored by Agrawal, etc. [29] and Li [22].

In this part of our research, we first extend Su's distributed algorithm from single transmit and receive antenna to multiple antennas and combine it with

transmit diversity to mitigate fading and further improve the throughput, where multiple transmit antennas also cause an increase in the number of cochannel interfering sources. For simplicity, we will consider only the uplink communications in the dissertation, although the algorithm is applicable to both uplink and downlink communications. We will focus on the system with two transmit antennas on the mobile and one receive antenna on the base station. We will consider both selective diversity and equal power diversity on the transmitter side.

Then we will develop a centralized power control algorithm (CPCA) for different antenna combinations. In the case of multiple transmit antennas, the number of parameters to be controlled doubles and simply splitting the power evenly to two transmit antennas as in the space-time code usually does not give good performance.

Finally, we will study the performance of the system in the hostile jamming environments. The jammer randomly selects a subset of the OFDM subchannels and sends the jamming signals in those subchannels. Because both the DWPA and the CPCA allows the transmitter to remove subchannels that do not satisfy the service requirements and reallocate the power to the subchannels with better channel conditions – large channel gains, small cochannel interference and no jamming signals, we expect the system to be robust in the presence of strong jamming signals.

# Chapter 2

# Iterative Demodulation and Decoding of High-Order CPM Signals In Flat Fading Channels

Wireless communications require high data rate information transmission at low bit error rate (BER). CPM signals are suitable for wireless communications because of their high spectral efficiency and immunity to amplitude nonlinearity. But the BER performance of continuous phase modulation provided by current receivers is generally worse than that of the memoryless modulation like MPSK (minimal phase-shift keying). This is in part due to the correlation in signals introduced by the memory in continuous phase modulation, which is obvious in uncoded signals. In the case of coded CPM signals, however, the improper handling of the inherent memory in CPM signals by current CPM receivers is more to be blamed for the bad performance than the CPM memory itself. They either use differential detection or the Viterbi algorithm to demodulate CPM signals and send hard decisions to their channel decoders but their decoders do not send back information to help demodulate CPM signals and execute

demodulation and decoding iteratively.

Iterative demodulation and decoding has been a topic under intense research efforts since the introduction of turbo codes [7] and the so-called "turbo principle" [4]. The core of the iterative demodulation and decoding is soft decoding algorithms such as the soft output Viterbi algorithm (SOVA) [30], and the symbol-by-symbol *a posteriori* probability (APP) decoding algorithm [31] – also referred to as the MAP (maximum *a posteriori*) algorithm or the BCJR (L. R. Bahl, J. Cocke, F. Jelinek, and J. Raviv) algorithm. They let the demodulator and the channel decoder generate and exchange soft decisions reciprocally between each other with little information loss. Another key component in iterative demodulation and decoding is the pseudo-random interleaver, which decorrelates soft decisions of the demodulator (the decoder) so they are weakly correlated at the input to the decoder (the demodulator).

Recently, many researchers have successfully applied this idea to achieve large performance improvements in various communication systems. In [32], Narayanan and Stuber designed a coherent DPSK demodulator for additive white Gaussian noise (AWGN) channels and showed that large performance gains in BER can be achieved by exploiting the recursive nature of differential modulation. They treated the differential modulator as an inner encoder and applied iterative demodulation and decoding to coded DPSK signals. In [33], Moqvist and Aulin investigated serially concatenated continuous phase modulation with iterative decoding in the AWGN channel and derived transfer function bound for coded and interleaved MSK with a uniform interleaver. To demodulate DPSK or CPM signals by the APP algorithm in time-variant wireless channels, however, the receiver must have accurate channel state information, which can not

be known *a priori* and must be estimated in real time.

Pilot symbol-assisted modulation (PSAM) has proved to be an effective way of estimating channel state information in flat fading channels with low complexity, limited power and bandwidth loss. Although most of the research on PSAM has concentrated on linearly modulated signals, Ho and Kim [3] demonstrated a data dependent pilot encoding rules for continuous phase modulation with rational modulation indices and showed that, unlike differential detection, a CPM receiver with PSAM had no error floor in demodulating uncoded CPM signals in Doppler fading channels.

Another way to apply the APP algorithm to demodulate signals in time-variant channels is to use joint data detection and channel estimation. In [2] and [34], Hoeher and Lodge demonstrated using MPSK signals that joint data detection and channel estimation can be done accurately by incorporating linear prediction into trellis decoding. Significant performance gains can be achieved in this way at a price of expanding trellis states, the number of which grows with the size of the signal constellation to the power of the predictor length. For high-order modulation, the computational complexity quickly explodes. It has a light advantage in power and bandwidth efficiency over PSAM in that it does not need any pilot symbols.

In the first part of this chapter, we present a coherent, iterative demodulation and decoding system for high-order CPM signals. To track the time-varying channel state information (CSI) caused by the Doppler effect in mobile wireless channels, pilot symbols are inserted periodically in data streams to serve as references for channel estimation. Due to the inherent memory in continuous phase modulation, those pilot symbols are set to be data-dependent so that the

CPM phase trellis can be forced to some pre-defined reference state at certain time epochs. In addition, pilot symbols are used as parity check symbols in demodulating each pilot frame to help reduce decoding errors. A pseudo-random interleaver and a convolutional code is then combined with the phase trellis of the CPM signal to form a structure similar to that of serial concatenated convolutional codes so that the BER performance can be significantly improved by applying iterative demodulation and decoding. The proposed system uses pilot symbols to separate channel estimation from demodulation so it has low computational complexity compared with other joint detection and decoding systems.

To further improve the receiver performance, information is exchanged between the CPM demodulator, the convolutional decoder, and the channel estimator. First, the channel estimator uses the information from the CPM demodulator to construct an estimate of the phase trajectory of the transmitted signal and filters all received samples on this estimated phase trajectory to obtain a more accurate estimation of the CSI. Then the CPM demodulator combines this newly estimated CSI with the extrinsic information from the convolutional decoder to generate more reliable soft decisions, which is to be used as the input to the convolutional decoder. This process can be carried out iteratively to improve the BER performance. Although there may be some errors in reconstructing the phase trajectory which will cause an increase in channel estimation errors, the number of errors will decrease at high signal-to-noise ratio (SNR) and the accuracy of the estimated CSI will improve due to the increased sampling rate.

In the second part of this chapter, we consider a noncoherent, iterative demodulation and decoding system for high-order CPM signals. The trellis branch

metrics are calculated by using a linear predictor without explicitly estimating the channel state information for a particular symbol period. As in the coherent case, a pseudo-random interleaver and a convolutional code are then combined with the phase trellis of the CPM signal to apply iterative demodulation and decoding. Although both coherent and noncoherent CPM receivers can achieve large performance gains in BER, the noncoherent receiver avoids using pilot symbols so there is no power and bandwidth loss due to the insertion of pilot symbols. But since it has to enlarge the CPM trellis for linear prediction, its computation complexity is much higher than that of a coherent receiver.

This chapter is organized as follows. In Section 2.1, a brief description will be given on CPM signals and the channel model. In Section 2.2, we present iterative demodulation and decoding of CPM signals with PSAM. In Section 2.3, we propose to use iterative filtering to further improve the system performance by reducing channel estimation error. In Section 2.4, we consider multiple differential detection of CPM signals. Finally, Section 2.5 summarizes and concludes this chapter.

## 2.1 Signal and Channel Models

For simplicity, we consider only CPM signals with single modulation index in this chapter. The complex envelope of the baseband transmitted CPM signal is given by

$$x(t) = Ae^{j\phi(t,\underline{d}_k)}, \tag{2.1}$$

and

$$\phi(t, \underline{d}_k) = 2\pi h \sum_{l=0}^{k} d_l q(t - LT), \quad kT \leq t \leq (k+1)T, \tag{2.2}$$

where $d_l$ is the *lth* modulation symbol, $\underline{d}_k = [d_0, d_1, \cdots, d_k]^T$ is the entire transmitted sequence up to time $kT$. $h$ is the modulation index, and $T$ is the symbol period. The elements of $\underline{d}_k$ are assumed to be independent, identically distributed and form an $M$-ary set

$$\Omega_d = \{-(M-1), \cdots, -3, -1, 1, 3, \cdots, M-1\}. \tag{2.3}$$

The function $q(t)$ is the phase-smoothing response function. It is continuous, nondecreasing and satisfies

$$q(t) = \begin{cases} 0, & t \le 0; \\ \frac{1}{2}, & t \ge LT. \end{cases} \tag{2.4}$$

Here we consider $L$ as integers only. For $k \ge L$ and $kT \le t \le (k+1)T$,

$$\begin{aligned} \phi(t, \underline{d}_k) &= \pi h \sum_{l=0}^{k-L} d_l + 2\pi h \sum_{l=k-L+1}^{k} d_l q(t - LT) \\ &= \theta_k + 2\pi h \sum_{l=k-L+1}^{k} d_l q(t - LT), \end{aligned} \tag{2.5}$$

where

$$\theta_k = \pi h \sum_{l=0}^{k-L} d_l \ .$$

For rational modulation indices $h$, $\theta_k \bmod 2\pi$ forms a finite set $\Theta$. In particular, let $h = m/p$, where $m$ and $p$ are relatively prime integers. For $M$-ary CPM signals,

$$||\Theta|| = \begin{cases} pM^{L-1}, m \text{ is even} \\ 2pM^{L-1}, m \text{ is odd} \end{cases} \tag{2.6}$$

For example, consider 8-ary continuous phase-shift keying (CPFSK). $L = 1$, $M = 8$, $h = 1/8$.

$$\Theta = \left\{ 0, \frac{\pi}{8}, \frac{2\pi}{8}, \cdots, \frac{15\pi}{8} \right\} \tag{2.7}$$

20

0

π/8

2π/8

3π/8

4π/8

5π/8

6π/8

7π/8

8π/8

9π/8

10π/8

11π/8

12π/8

13π/8

14π/8

15π/8
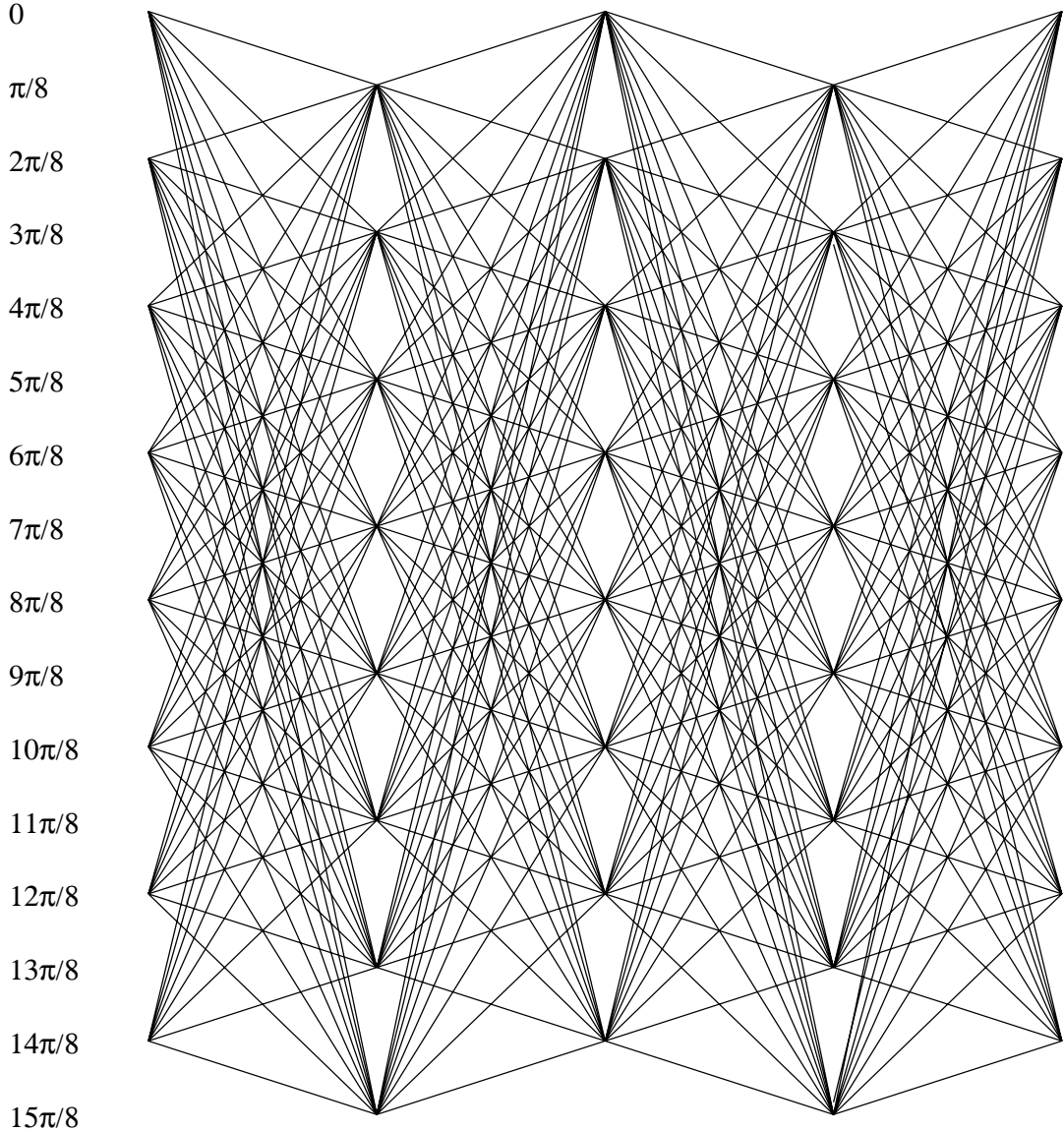
Figure 2.1: Phase trellis of 8-CPFSK signals

The phase trellis is shown in Fig. 2.1. There are a total of 16 states. One characteristics of this phase trellis is time-variant in the sense that the phase trajectories in the even-numbered symbol intervals are not time translates of those in the odd-numbered symbol intervals. To obtain a time-invariant phase trellis, Rimoldi [5] introduced the tilted-phase

$$\psi(t, \underline{d}_k) \quad = \quad \phi(t, \underline{d}_k) + \pi h(M-1)t/T$$

21

$$= 2\pi h \sum_{l=0}^{k-L} \frac{d_l + M - 1}{2} + 4\pi h \sum_{i=0}^{L-1} \frac{d_{k-i} + M - 1}{2} q(t - kT + iT)$$

$$+\pi h(M-1)(t-kT)/T - 2\pi h(M-1) \sum_{i=0}^{L-1} q(t - kT + iT)$$

$$+(L-1)(M-1)\pi h$$

$$= 2\pi h \sum_{l=0}^{k-L} u_l + 4\pi h \sum_{i=0}^{L-1} u_{k-i} q(t - kT + iT)$$

$$+\pi h(M-1)(t-kT)/T - 2\pi h(M-1) \sum_{i=0}^{L-1} q(t - kT + iT)$$

$$+(L-1)(M-1)\pi h, \ kT \le t \le (k+1)T \tag{2.8}$$

where $u_l = \frac{d_l + M - 1}{2}$. Let $\psi_k = 2\pi h \sum_{l=0}^{k-L} u_l$, then $\psi_k$ forms a new finite set $\Psi$. In the case of 8-ary CPFSK,

$$\Psi = \left\{ 0, \frac{\pi}{4}, \frac{2\pi}{4}, \cdots, \frac{7\pi}{4} \right\}. \tag{2.9}$$
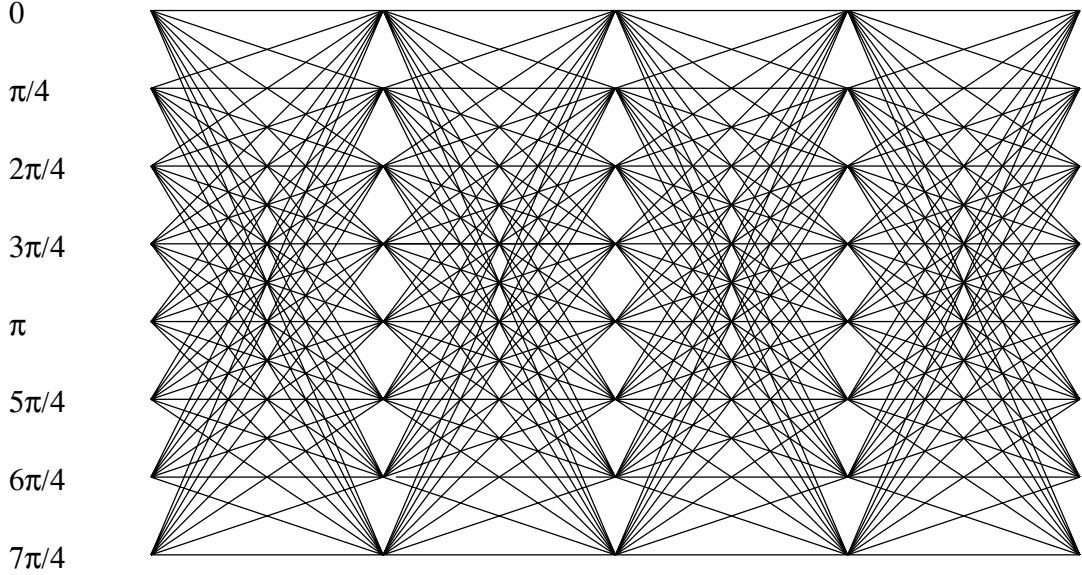


Figure 2.2: Titled-phase trellis of 8-CPFSK signals

The tilted-phase trellis is shown in Fig. 2.2. There are only 8 states in the tilted-phase trellis.

In both phase trellises, the phase sequence $\phi(t, \underline{d}_k) \bmod 2\pi$ or $\psi(t, \underline{d}_k) \bmod 2\pi$ is constrained to lie on a trellis. Hence CPM signals with rational modulation indices can be demodulated with either the Viterbi algorithm for hard decisions or the APP decoding algorithm for soft decisions. The tilted-phase trellis, however, is favored because it is time-invariant and has only half the number of states.

The transmitter modulates the baseband CPM signal to a specified carrier frequency and transmits it through the channel. It is assumed that at the beginning of the receiver, the signals are first down-converted to complex baseband and passed through an ideal anti-aliasing filter whose bandwidth is wide enough to pass all of the signal energy spread by the fading process. The baseband received signal can be written as

$$y(t) = c(t)x(t) + n(t), \tag{2.10}$$

where $n(t)$ is the zero-mean, additive white Gaussian noise with one-sided power spectral density $N_0$. The complex channel gain $c(t)$ incorporates both fading and frequency offset:

$$c(t) = \exp(j2\pi f_0 t)g(t) \tag{2.11}$$

where $f_0$ is the residual frequency offset, and $g(t)$ is the complex Gaussian fading process with variance $\sigma_g^2$ and Doppler spread $f_D$, and $c(t)$ represents the Rician fading with autocorrelation function [35]

$$R_c(\tau) = \sigma_c^2 \left( \frac{K_c}{1 + K_c} + \frac{1}{1 + K_c} J_0(2\pi f_D \tau) \right), \tag{2.12}$$

where $f_D$ is the Doppler frequency, $\sigma_c^2$ is the total power of $c(t)$, and $K_c$ is the ratio between the line-of-sight power and the scattered power. In this chapter, we are most interested in Rayleigh fading when there is no line-of-sight path, i.e., $K_c = 0.0$.
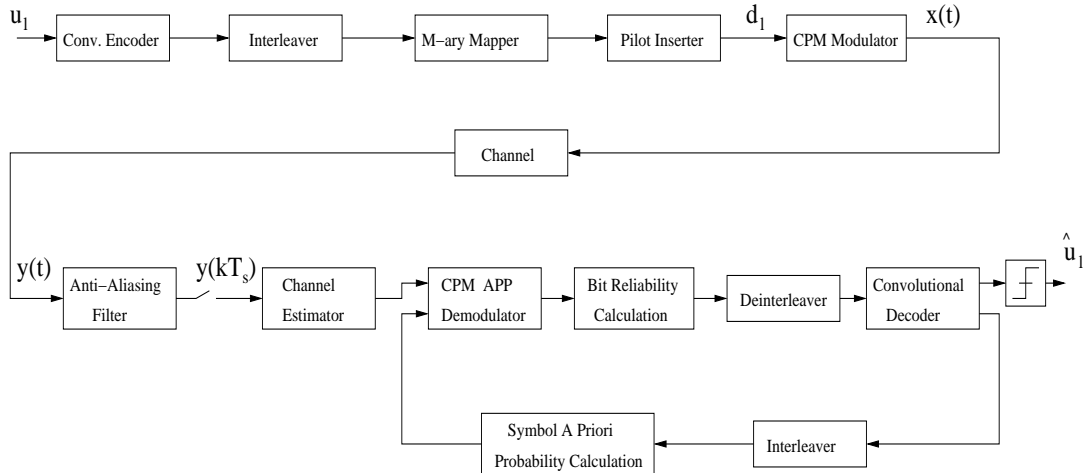
Figure 2.3: CPM system with iterative demodulation and decoding

The received signal is sampled at a frequency $f_s = N/T$. The output samples are denoted by

$$y(kT_s) = c(kT_s)x(kT_s) + n(kT_s), k = 0, 1, ...,\qquad(2.13)$$

where $T_s = 1/f_s$, $n(kT_s)'s$ are complex additive white Gaussian noise samples with a variance of $\sigma_n^2 = f_s N_0$. The samples $y(kT_s)'s$ are then iteratively processed by the channel estimator, the APP CPM demodulator, the channel deinterleaver and the convolutional decoder as shown in Fig. 2.3. Hereafter all of the modeling and analysis will be done using this discrete-time complex baseband model.

## 2.2 Iterative Demodulation and Decoding with PSAM

In this section, we present a detailed description of various aspects for the proposed iterative demodulation and decoding system with PSAM as shown in Fig. 2.3. We first briefly review the APP decoding algorithm. Then we describe rules for data-dependent pilot insertion, channel estimation using pilot references, and *a posteriori* probability conversion between nonbinary symbols

24

and binary bits. Iterative demodulation and decoding will be discussed before
numerical results are given at last.

### 2.2.1  *A Posteriori* Probability Decoding Algorithm

The APP decoding algorithm has also been referred to as the maximum *a pos-
teriori* (MAP) decoding algorithm or the BCJR algorithm [31] in the literature.
We will adhere to the name APP in this chapter unless it is necessary to be loyal
to referred works to avoid confusion. As shown in Fig. 2.3, the CPM receiver
contains two APP decoders. One is for CPM phase trellis, which is nonbinary
in general; the other for the convolutional code. Here we briefly review the APP
decoding algorithm [31], [36], [9] for the purpose of illustrating how to compute
*a posteriori* probability for trellis states.

Let the trellis state at time $kT$ be denoted by $S_k$, the input data symbols dur-
ing the period $[(k-1)T, kT)$ by $u_k \in \{0, 1, \cdots, M-1\}$ ($\forall d \in \Omega_d, \exists u_k$ such that $d =
2\, u_k - (M-1)$ and vice versa.), and output denoted by a vector corresponding
to $N$ samples per symbol period

$$
\underline{x}_k = \begin{bmatrix} x(kT + 0\, T_s) \\ x(kT + 1\, T_s) \\ \vdots \\ x(kT + (N-1)\, T_s) \end{bmatrix}. \tag{2.14}
$$

Let the received sequence corresponding to $\underline{x}_1^K = \underline{x}_1, \underline{x}_2, \cdots, \underline{x}_K$ be $\underline{y}_1^K = \underline{y}_1, \underline{y}_2,
\cdots, \underline{y}_K$. Define the branch transition probability $\gamma_k(s', s)$ and the extrinsic
branch transition probability $\gamma_k^{(e)}(s', s)$ as

$$
\gamma_k(s', s) \triangleq Pr\{\underline{y}_k | S_{k-1} = s';\ S_k = s\} \cdot Pr\{S_k = s | S_{k-1} = s'\},
$$

$$\gamma_k^{(e)}(s', s) \triangleq Pr\{\underline{y}_k | S_{k-1} = s'; S_k = s\}. \tag{2.15}$$

Suppose a symbol $m$ is the input to the trellis branch (s',s), then

$$Pr\{S_k = s | S_{k-1} = s'\} = Pr\{u_k = m\}, \tag{2.16}$$

which is the *a priori* probability for $u_k$. If we further define

$$\alpha_k(s) \triangleq Pr\{S_k = s; \underline{y}_1^k\},$$

$$\beta_k(s) \triangleq Pr\{\underline{y}_{k+1}^K | S_k = s\}.$$

Then for $k = 1, 2, \cdots, K$, $\alpha_k(s)$ can be calculated by a forward recursion

$$\alpha_k(s) = \sum_{s'} \alpha_{k-1}(s')\gamma_k(s', s). \tag{2.17}$$

And $\beta_k(s)$ can be calculated by a backward recursion

$$\beta_{k-1}(s') = \sum_{s} \beta_k(s)\gamma_k(s', s). \tag{2.18}$$

The *a posteriori* probability for the input symbol $Pr\{u_k = m | \underline{y}_1^K\}$ is determined
by

$$Pr\{u_k = m | \underline{y}_1^K\} = \frac{\sum_{(s',s) \in A_m} \alpha_{k-1}(s')\gamma_k(s', s)\beta_k(s)}{\sum_{m=0}^{M-1} \sum_{(s',s) \in A_m} \alpha_{k-1}(s')\gamma_k(s', s)\beta_k(s)}, \tag{2.19}$$

where the set $A_m = \{(s', s) : m$ is the input to the trellis branch$\}$. To reduce the
computational complexity in computing the *a posteriori* probability, the APP
algorithm often works in the log domain.

$$\begin{aligned}
&\log Pr\{u_k = m | \underline{y}_1^K\} \\
&= \log \frac{\sum_{(s',s) \in A_m} \alpha_{k-1}(s')\gamma_k(s', s)\beta_k(s)}{\sum_{m=0}^{M-1} \sum_{(s',s) \in A_m} \alpha_{k-1}(s')\gamma_k(s', s)\beta_k(s)}, \\
&= \log Pr\{u_k = m\} + \log \frac{\sum_{(s',s) \in A_m} \alpha_{k-1}(s')\gamma_k^{(e)}(s', s)\beta_k(s)}{\sum_{m=0}^{M-1} \sum_{(s',s) \in A_m} \alpha_{k-1}(s')\gamma_k^{(e)}(s', s)\beta_k(s)}.
\end{aligned}$$

The first term $\log Pr\{u_k = m\}$ is the *a priori* information and the second term

is the extrinsic information. In Section 2.3 we need to calculate the *a posteriori*

probability for the trellis state $Pr\{S_k = s | \underline{y}_1^K\}$ in order to construct an estimate

of the transmitter phase trajectory. This is determined by

$$Pr\{S_k = s | \underline{y}_1^K\} = \frac{\alpha_k(s) \cdot \beta_k(s)}{\sum_s \alpha_k(s) \cdot \beta_k(s)}. \tag{2.21}$$

## 2.2.2   Data Dependent Pilot Encoding

In the case of continuous phase modulation, pilot symbols have to be dependent

on the data symbols to force the CPM signal to return to a certain state known

to the receiver [3]. Consider first the phase of a full response CPM signal at time

$nT$

$$\phi_n = \pi h \sum_{l=1}^{n} d_l \bmod 2\pi, \ d_l \in \Omega_d, \ \forall \, l = 1, \cdots, n. \tag{2.22}$$

If $h = 1/M$ and $n$ is odd, then $\phi_n$ must be of the form

$$\phi_n = \frac{m}{M}\pi \bmod 2\pi, \quad m \in \Omega_d. \tag{2.23}$$

$\phi_{n+1}$ can be forced to zero by using a pilot symbol $d_{n+1} = -m, \ -m \in \Omega_d$.
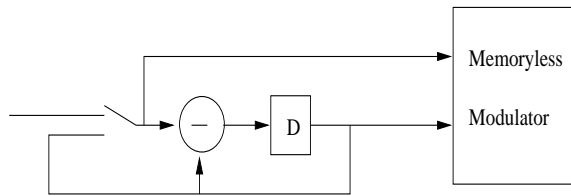


Figure 2.4: CPM modulator with pilot encoder

Here we would like to point out that the pilot encoding problem in CPM or

DPSK signals is the same as the trellis termination problem in the component

encoder of turbo codes. So the minimum number of pilot symbols required per pilot frame is the same as the memory size of the CPM phase encoder. According to [5], the CPM modulator can be decomposed into a continuous-phase encoder and a memoryless modulator. Thus we can integrate the pilot encoder into the CPM modulator as in Fig. 2.4, where the switch is turned to the feedback branch at the last symbol period of every pilot frame and the subtraction is mod $M$ operation. The generalization to the case of partial response signal or general rational modulation index is straightforward.

Due to the introduction of the pilot symbols, the non-binary CPM phase trellis is forced to zero state periodically within each packet. In this case, the forward and backward recursion in demodulating CPM signals with APP algorithm can be carried out within each pilot frame instead of the entire transmitted packet. So the CPM demodulator can be implemented in a parallel structure and the delay due to the APP demodulation can be greatly reduced. In addition, samples taken at the pilot symbol period serve as parity check in each pilot frame so that the pilot symbols also help reduce the decoding errors directly.

### 2.2.3 Channel Estimation

Since the phase of the CPM signal is forced to zero at pilot positions, the receiver can make use of this information to estimate the channel state information through Wiener filtering and interpolation. Perfect timing is assumed for sampling at the receiver. We also assume the channel gain is constant in each symbol period for slowly fading, therefore only one estimate is needed for all the samples within one symbol period. In the simulation we will further assume the receiver has a perfect knowledge of the SNR and optimal Wiener filters will be used for

estimating channel state information.

Let $P$ be the number of data symbols per pilot symbol. The pilot frame size is $(P+1)$. Since we have assumed that the channel state information remains constant within a symbol period, we also let $c_k = c(kT)$ for convenience. The estimation for channel gain $c_k$, $k = m(P+1) + n, n = 0, 1, \cdots, P$, using an $L_p$-tap linear filter can be written as

$$\hat{c}_k = \underline{h}_{p,n}^H \underline{y}_p(m), \tag{2.24}$$

where

$$\underline{y}_p(m) = \begin{bmatrix} y((m - \lceil L_p/2 \rceil + 1)(P+1)T) \\ y((m - \lceil L_p/2 \rceil + 2)(P+1)T) \\ \vdots \\ y((m + \lfloor L_p/2 \rfloor)(P+1)T) \end{bmatrix} \tag{2.25}$$

is the received vector of $L_p$ nearest pilot samples. Although there are multiple samples during each pilot symbol period, only the last sample – the sample taken at the position that the signal phase trellis is at zero state – can be used in the $\underline{y}$ vector. Other samples cannot be used for estimating channel state information at this stage because the receiver has no knowledge about them. According to [37], the $L_p$-tap filter coefficient vector $\underline{h}_{p,n}$ can be determined by

$$R_p \underline{h}_{p,n} = \underline{w}_{p,n}, \tag{2.26}$$

where

$$R_p = E[\underline{y}_p(m)\underline{y}_p^H(m)], \tag{2.27}$$

$$\underline{w}_{p,n} = E[c_k^* \underline{y}_p(m)]. \tag{2.28}$$

Here $\underline{w}_{p,n}$ depends on $n = k \bmod (P+1)$ and a total of $(P+1)$ filters are needed for the channel state information at all symbol positions in a pilot frame.

### 2.2.4  Symbol-To-Bit Reliability Values (*A Posteriori* Probability) Conversion

In converting *a posteriori* probabilities between $M$-ary symbols and binary bits, we assume perfect interleaving between the convolutional encoder and $M$-ary symbol mapping. So the $\log_2 M$ bits forming an $M$-ary symbol are mutually independent. Let $b_k$ represent the $k$th binary bits of an $M$-ary symbol $d \in \Omega_d$ and $m_k^{-1}(d)$ represent the binary value of bit $k$ corresponding to the symbol $d$. For simplicity, we use $P_a$ to represent the *a posteriori* probability. Then the conversion from symbol *a posteriori* probabilities to bit *a posteriori* probabilities can be carried out as follows:

$$P_a\{b_k = 0\} \quad = \sum_{\left\{n \in \Omega_d : \, m_k^{-1}(n) = 0\right\}} P_a\{d = n\}, \tag{2.29}$$

$$P_a\{b_k = 1\} \quad = \sum_{\left\{n \in \Omega_d : \, m_k^{-1}(n) = 1\right\}} P_a\{d = n\}. \tag{2.30}$$

And the conversion from bit *a posteriori* probabilities to symbol *a posteriori* probabilities can be carried out as

$$P_a\{d = n\} \quad = \prod_{k=0}^{\log_2 M - 1} P_a\{b_k = m_k^{-1}(n)\}. \tag{2.31}$$

### 2.2.5  Iterative Demodulation and Decoding

As mentioned above, the pilot encoder can be integrated into the CPM modulator with a phase trellis periodically forced to zero. We can interpret the CPM transmitter as a serial concatenated encoding system – the outer code is a binary convolutional code, the inner code a non-binary continuous phase encoder, and a random channel interleaver in between. So we can apply iterative

demodulation and decoding to the receiver and it consists of a non-binary APP demodulator, a symbol-to-bit *a posteriori* probability (reliability) converter, a deinterleaver, a convolutional decoder and a feedback path to generate symbol *a priori* information for the next iteration as shown in Fig. 2.3.

The *a priori* input of the CPM demodulator is initially set to zero when a new packet of data arrives. To apply the APP decoding algorithm described in Subsection 2.2.1 to the CPM demodulator, the branch transition probability $\gamma_k(s', s)$ must be calculated first. For a particular trellis branch $(s', s)$ ($s'$ and $s$ are the starting state and ending state respectively) at time k, the extrinsic branch transition probability can be written as

$$\gamma_k^{(e)}(s', s) = \text{constant} \cdot \exp\left\{ \frac{2E_s}{f_s N_0} Re\left[ \hat{c}_k^* \cdot < \underline{x}^H(s', s), \underline{y}_k > \right] \right\}, \qquad (2.32)$$

where $< \cdot, \cdot >$ denotes vector inner product and $H$ denotes Hermitian transpose of a matrix. $\underline{x}(s', s)$ is the vector of CPM output samples on the branch $(s', s)$. $\frac{E_s}{N_0}$ is the SNR per symbol. $Pr\{S_k = s | S_{k-1} = s'\}$ is equal to the *a priori* information $Pr\{d_k = i\}$ if $d_k = i$ is the input symbol to the branch $(s', s)$ and zero otherwise. With $\gamma_k(s', s)$, the symbol *a posteriori* probability $Pr\{d_k = i | \underline{y}_1^K\}$ and the extrinsic information can be calculated by a forward and a backward recursion using (2.17) and (2.18).

To reduce the computational complexity of the symbol-by-symbol APP decoder of the non-binary CPM phase trellis, a non-binary version of the MAX-LOG-MAP [38] algorithm is developed and used in the simulation. Note that the receiver does not need an explicit pilot remover because in the CPM demodulator, the extrinsic information is generated only for data symbols.

The extrinsic information on CPM symbols are then converted to the extrinsic information at bit level, deinterleaved and processed by an APP convo-

lutional decoder, which also uses the MAX-LOG-MAP algorithm. The extrinsic information of coded bits from the outer APP decoder is fed back to a channel interleaver, converted to the extrinsic information on CPM symbols, and used by the CPM demodulator as the *a priori* information in the next iteration. At the end of the last iteration, soft decisions on information bits generated by the outer APP decoder are used to generate hard decisions.

### 2.2.6 Numerical Results

The performance of the new scheme is assessed numerically for 8-ary continuous-phase frequency-shift keying (CPFSK), which is a full response continuous phase modulation. A coherent receiver with ideal channel state information is used as the benchmark. The Doppler spread normalized to the symbol rate, $f_D T$, is 0.01. The convolutional code used is the rate 1/2, constraint length 3, $(7_8, 5_8)$ nonsystematic code. The block size of the pseudo-random bit interleaver is 2160. The size of the pilot frame is 10, i.e., pilot insertion rate is one pilot every 9 data symbols. The modulation index for the 8-ary CPFSK is 1/8. Gray mapping is used to map every three bits in the data stream into an 8-ary symbol.

We first apply iterative demodulation and decoding to the coherent CPM receiver. The results for the Rayleigh fading channel ($K_c = -\infty$ dB) are shown in Fig. 2.5. It can be seen that the iterative receiver improves the BER performance significantly. At $10^{-4}$ BER, the gain in SNR of the iterative receiver over the noniterative receiver is about 3.5 dB with two iterations and more than 5.0 dB with eight iterations.

Shown in Fig. 2.6 are the simulation results of the iterative receiver with PSAM. The rightmost curve in Fig. 2.6 is the result of the PSAM receiver with
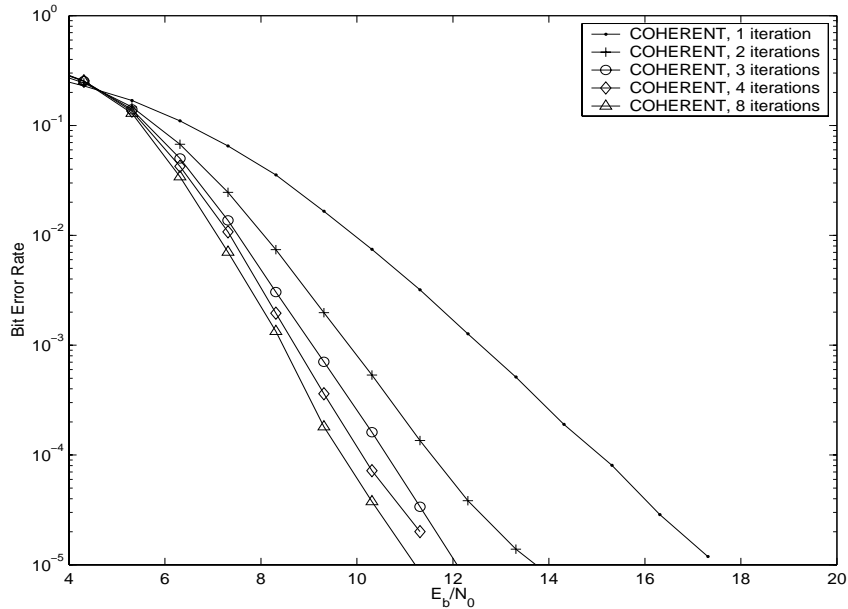
Figure 2.5: Performance of the coherent CPM receiver with iterative demodulation and decoding ($f_D T = 0.01$)

one iteration. It can be seen that after only two iterations, the PSAM receiver outperforms the noniterative coherent receiver at high SNR. With four iterations, it outperforms the noniterative coherent receiver by 2.5 dB at $10^{-4}$ BER. In addition, with four iterations, the PSAM receiver achieves almost the same performance as eight iterations. This means that there are only marginal benefits by simply increasing the number of iterations beyond four.

To study the potential performance improvement of the proposed system, we compare the iterative PSAM receiver with the iterative coherent receiver that has the ideal channel state information. Both results are also shown in Fig. 2.6. It can be seen that there exists a 2.7 dB performance gap between the coherent receiver and the PSAM receiver at $10^{-4}$ BER with eight iterations. This shows that further performance improvement can be obtained by reducing channel estimation errors with the help of iterative channel estimation. But since the
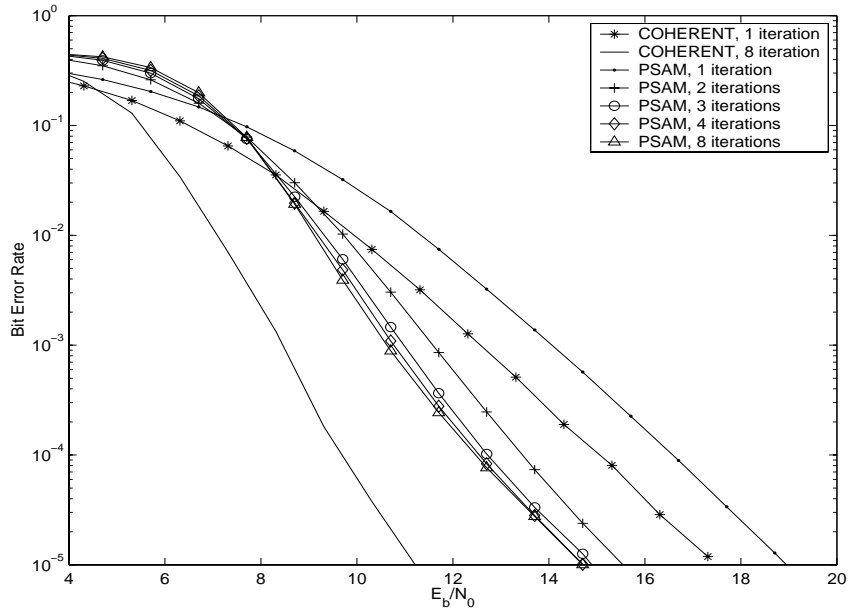
Figure 2.6: Performance of the PSAM receiver with iterative demodulation and decoding ($f_D T = 0.01$)

CPM signals are inherently differential, proper measures must be taken to reduce the error propagation. This problem will be addressed in the next section.

## 2.3  Use Iterative Filtering to Further Improve Performance

In order to further improve the BER performance, we use the iterative filtering technique to improve the channel estimation gradually. We first discuss methods for iterative filtering. Then we simulate and compare numerical results with those in the previous section.

### 2.3.1  Iterative Filtering

To apply iterative filtering to the proposed system, one would be tempted at first to send back the decoder output – soft or hard decisions about coded bits
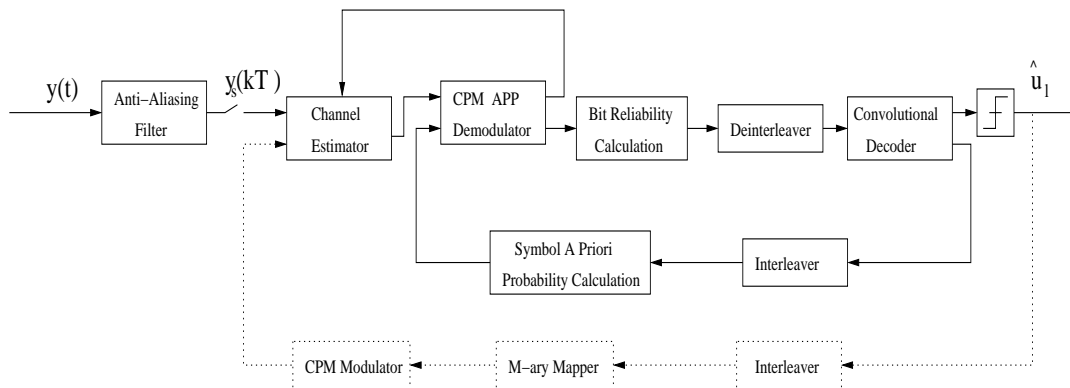
Figure 2.7: CPM receiver with iterative channel estimation

– directly to the channel estimator. However, because of the inherent memory in CPM modulation, if we try to reconstruct the transmitted signal by passing data symbols formed from the interleaved hard decisions of the decoder output through a CPM modulator as the dotted feedback in Fig. 2.7, we will run into severe error propagation problems. This is because the input to the CPM modulator must be integer symbols or hard decisions. When soft decisions are converted into hard decisions, important soft information on data symbols is lost.

To reduce error propagation, we must keep soft decisions in the feedback. This demands the elimination of the CPM modulator in feedback path. The question thus becomes how we can reconstruct the original CPM signals from soft decisions on the input data symbols as faithfully as possible.

Let the transfer function of a trellis encoder be denoted as $H(D)$. If we send a sequence $X(D)$ through this encoder, the output will be

$$Y(D) = X(D)H(D). \tag{2.33}$$

To recover $X(D)$ from the observation $Y(D)$, we can either pass $Y(D)$ through a trellis decoder for $H(D)$ or through another trellis encoder with transfer function

$1/H(D)$. This suggests that a trellis decoder for $H(D)$ functions in a way similar to a trellis encoder with transfer function $1/H(D)$. Likewise, a trellis decoder for $1/H(D)$ functions in a way similar to a trellis encoder with transfer function $H(D)$. Furthermore, if the trellis decoder uses a symbol-by-symbol soft decoder, then it functions similarly as a trellis encoder with $H(D)$ but still retains soft-in/soft-out property.

So in place of the CPM modulator in the feedback, we can use a symbol-by-symbol trellis decoder that can keep soft decisions and thus reduce error propagation. Specifically, we let $Y(D)$ represent the tilted-phase trellis [5] sequence of CPM signals. Imagine that $Y(D)$ is the input, $1/H(D)$ is the encoder, $X(D) = Y(D) \cdot 1/H(D)$ is the output in a transmitter and we try to estimate $Y(D)$ from the information we have on $X(D)$. But instead of having received samples from the signal generated from $X(D)$, we have the *a posteriori* probability of all the symbols in $X(D)$, which can be used directly as the branch transition probability $\gamma_k(s, s')$ in applying the APP decoding algorithm to $1/H(D)$. This is exactly the same problem as we have in the feedback – the *a posteriori* probability of the $X(D)$ sequence can be calculated by passing the *a posteriori* probability of coded bits from the convolutional decoder through the channel interleaver and converting them to symbol *a posteriori* probabilities. Furthermore, we can compute *a posteriori* estimates of CPM trellis states directly in the CPM demodulator by (2.21) and use them as the *a priori* information for $1/H(D)$ decoder. At the output of the $1/H(D)$ decoder, we use the states with maximum *a posteriori* probability to reconstruct the CPM phase trajectory (We have successfully implemented this idea in a convolutional coded DPSK system but the gain is similar to the method that we are going to discuss).

Although this represents a general solution to the error propagation problem, the complexity of the receiver increases with an extra APP decoder. Instead, to reduce the receiver complexity, we compute *a posteriori* estimates of CPM trellis states directly in the CPM demodulator by (2.21) and feed them back to the channel estimator as in Fig. 2.7.

After we obtain *a posteriori* estimates of CPM trellis states, we can reconstruct the CPM signal $\hat{x}(kT_s)$ in the most likely path for the use of iterative channel estimation. We have assumed that the channel gain is constant within a symbol period, so

$$
\begin{aligned}
y(kT) &= c(kT)x(kT) + n(kT), \\
y(kT + T_s) &= c(kT)x(kT + T_s) + n(kT + T_s), \\
&\vdots \\
y(kT + (N-1)T_s) &= c(kT)x(kT + (N-1)T_s) + n(kT + (N-1)T_s) \quad (2.34)
\end{aligned}
$$

Define

$$
z(kT) \triangleq \frac{1}{N} \sum_{n=0}^{N-1} y(kT+nT_s)/x(kT+nT_s) = c(kT) + \frac{1}{N} \sum_{n=0}^{N-1} n'(kT+nT_s), \quad (2.35)
$$

where

$$
n'(kT + nT_s) = n(kT + nT_s)/x(kT + nT_s). \quad (2.36)
$$

As $x(kT + nT_s)$ has constant amplitude for all $k$ and $n$, it is obvious that the new noise sequence $n'(kT + nT_s)$ is still additive white Gaussian. If there is no error in reconstructing $\hat{x}(kT_s)$, then $z(kT)$ is an observation of the channel gain $c_k$ distorted only by additive white Gaussian noise. Compared to the pilot sequence $\underline{y}(m)$, the SNR in the sequence $z(kT)$ is $10\log 10(N)$ dB higher. The estimation of channel gain $c_k$ using an $L_z$-tap linear filter is given by

$$
\hat{\hat{c}}_k = \underline{h}_z^H \underline{z}_k, \quad (2.37)
$$

37

where

$$\underline{z}_k = \begin{bmatrix} z((k - \lceil L_z/2 \rceil + 1)T) \\ z((k - \lceil L_z/2 \rceil + 2)T) \\ \vdots \\ z((k + \lfloor L_z/2 \rfloor)T) \end{bmatrix}. \tag{2.38}$$

The filter coefficient vector $\underline{h}_z$ can be determined by [37]

$$R_z \underline{h}_z = \underline{w}_z, \tag{2.39}$$

where

$$R_z = E\left[\underline{z}(k)\underline{z}^H(k)\right], \tag{2.40}$$

$$\underline{w}_z = E\left[c_k^* \underline{z}(k)\right]. \tag{2.41}$$

In the iterative filtering, not only the neighboring $L_z$ observations used to estimate the channel gain $c(kT)$ are more strongly correlated, but also the sequence $\{z(kT)\}$ has higher SNR provided that the number of errors in reconstructing $\hat{x}(kT)$ is small. As a result, both the channel estimation error and the BER can be reduced iteratively with limited additional complexity.

## 2.3.2  Numerical Results and Discussions

In this part, we use numerical methods to assess the performance of iterative channel estimation. The simulation parameters are the same as before unless specified. We simulate three receivers: the coherent receiver, with perfect channel state information; the PSAM receiver , with the channel state information estimated using only pilot-induced references (i.e., the PSAM system in Section 2.2); the PSAM-IF receiver, with channel state information estimated initially
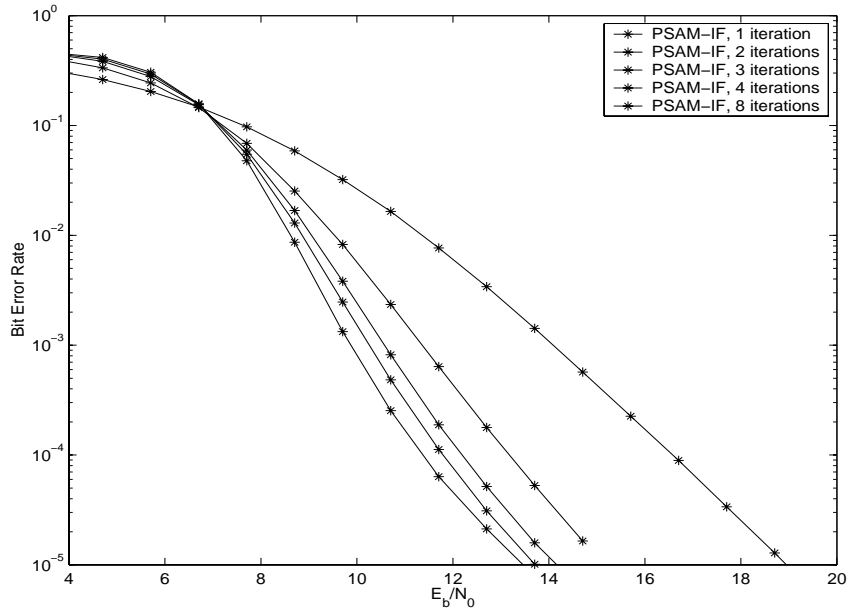
Figure 2.8: Performance of the PSAM-IF receiver on Rayleigh fading channels $(f_D T = 0.01)$

using pilot-induced references and iteratively on reconstructed CPM phase trajectories. All three receivers use eight iterations.

We first simulate the PSAM-IF receiver. The results are shown in Fig. 2.8. Compared with the PSAM receiver in Fig 2.6, the BER performance of the PSAM-IF receiver improves with the number of iterations, even beyond four iterations. Shown in Fig. 2.9 are the performance of the three receivers in the Rayleigh fading channel ($K_c = -\infty$ dB). We can see that at $10^{-4}$ BER, the improvement in SNR per information bit is about 0.9 dB from the PSAM receiver to the PSAM-IF receiver. This is remarkable considering that the PSAM receiver has already performed much better than the noniterative coherent receiver.

To learn more about the performance of the three receivers, we fix the pilot insertion rate and simulate them in different Doppler spreads. The results for 0.005 and 0.02 normalized Doppler spreads are shown in Fig. 2.10 and Fig. 2.11 respec-
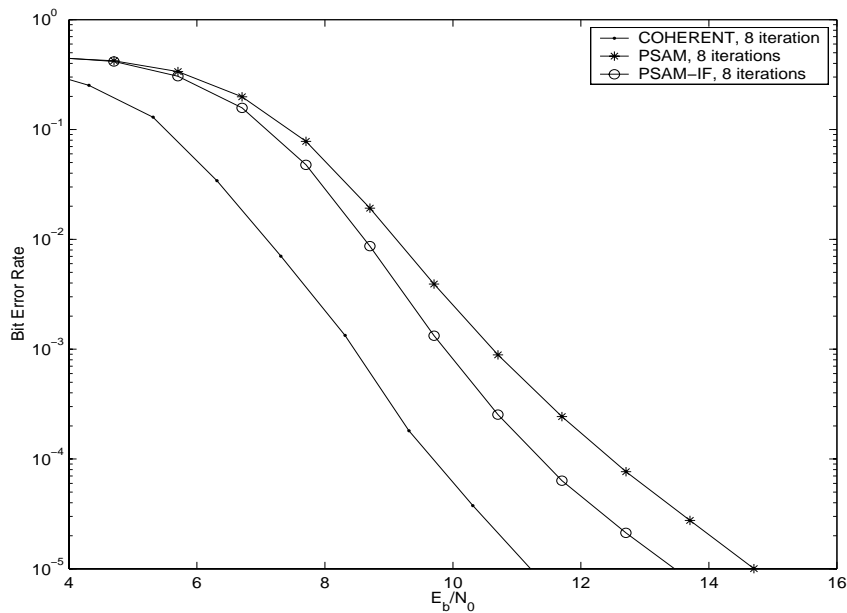
Figure 2.9: Performance of CPM receivers on Rayleigh fading channels ($f_D T = 0.01$)

tively. At 0.005 Doppler spread, the BER performance of the three receivers are very close. This is because both the PSAM receiver and the PSAM-IF receiver can obtain more accurate channel state information at a lower fading rate. But the coherent receiver performs much worse at 0.005 Doppler spread than that at 0.01 Doppler spread. This is because the slower the fading rate, the less the temporal diversity gain for the BER performance. For the same reason, we can see in Fig. 2.11 that at 0.02 Doppler spread, the coherent receiver performs the best. But the performance of the PSAM receiver and the PSAM-IF receiver are further away from that of the coherent receiver. The reason is that at high fading rate, channel estimation errors increase and degrade the BER performance more than at lower fading rates. The solution to this problem can be solved by increasing the ratio of pilot symbols over data symbols, although this implies a higher loss in data rate.
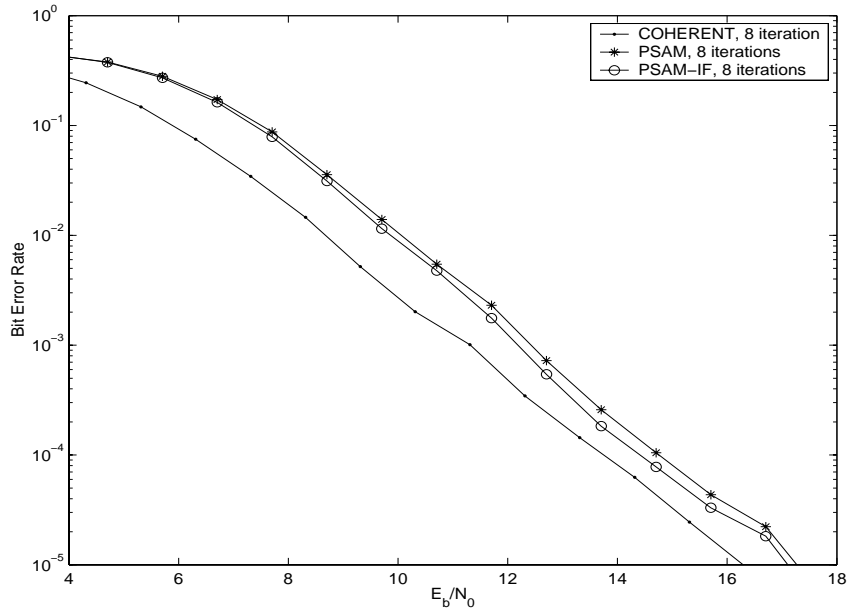
Figure 2.10: Performance of CPM receivers on Rayleigh fading channels ($f_D T = 0.005$)

Both the PSAM receiver and the PSAM-IF receiver provide low complexity solutions to joint channel estimation and coherent demodulation of CPM signals for wireless communications. Both are able to achieve significant gains in SNR by exploiting the inherent memory in CPM signals. With iteratively improved channel estimation, the PSAM-IF receiver is able to achieve better performance than the PSAM receiver for the Rayleigh fading channel. The disadvantage of both receivers include a ten percent loss in throughput due to the introduction of pilot symbols.

## 2.4   Multiple Differential Detection of CPM Signals

In this section, we present the noncoherent, iterative demodulation and decoding system with multiple differential detection. The system is as shown in Fig. 2.12.
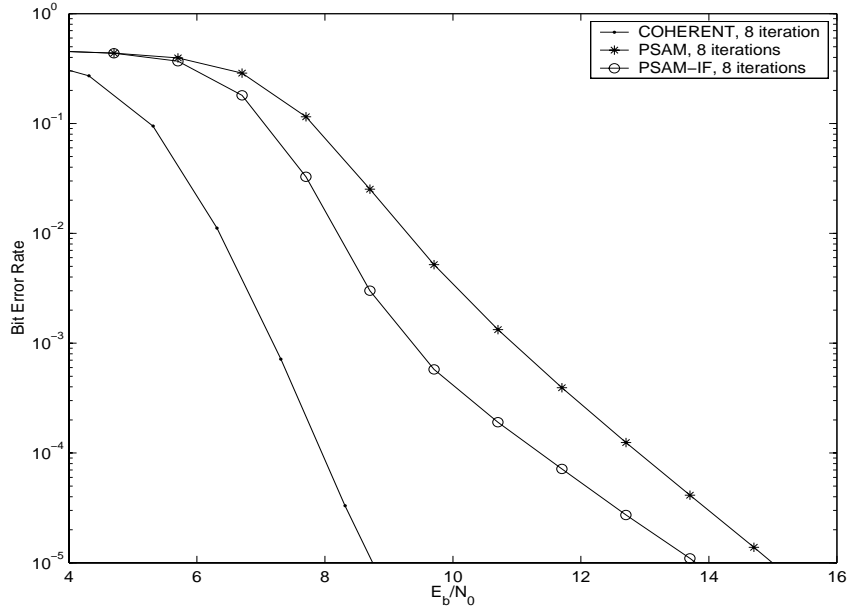
Figure 2.11: Performance of CPM receivers on Rayleigh fading channels ($f_D T = 0.02$)

Most of the components in Fig. 2.12, such as the pseudo-random interleaver, the APP convolutional decoder, etc., are the same as those in the coherent system shown in Fig. 2.3. What is different here is the CPM MDD demodulator, even though the CPM modulator is the same. We will focus on the description of multiple differential detection of CPM signals first. Then we will give the numerical results and compare them with those of the coherent, iterative receiver.

### 2.4.1   Multiple Differential Detection of CPM Signals

Let

$$\underline{y}_k = \begin{bmatrix} y(kT) \\ y(kT + T_s) \\ \vdots \\ y(kT + (N-1)T_s) \end{bmatrix}. \tag{2.42}$$
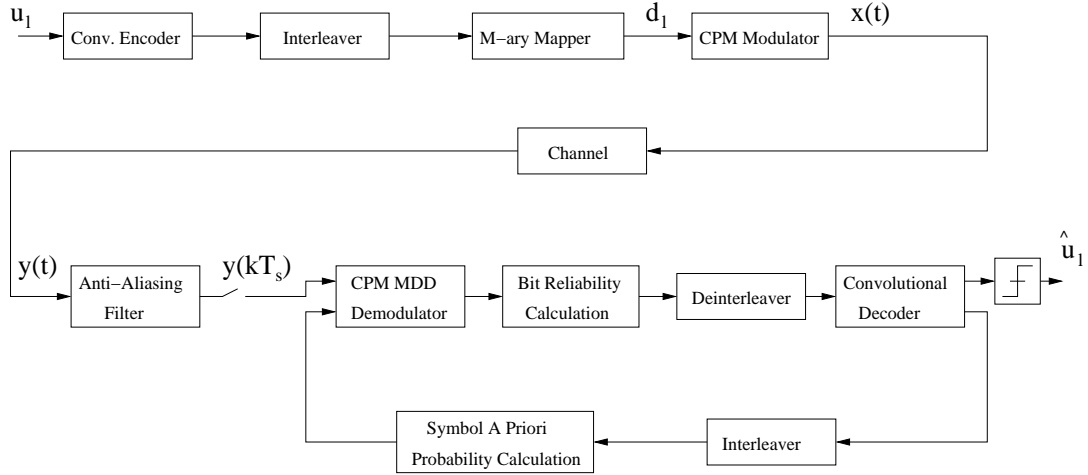
Figure 2.12: CPM system with multiple differential detection

In the case that the channel state information is given in the $k$th symbol period, the conditional probability of $\underline{y}_k$ on a particular trellis branch $(s', s)$ $(s', s \in \Theta)$ is given by

$$Pr\{\underline{y}_k | S_{k-1} = s'; \ S_k = s\} = \frac{1}{(2\pi\sigma^2)^N} \exp\left\{-\frac{||\underline{y}_k - c_k \underline{x}(s', s)||^2}{2\sigma^2}\right\}, \quad (2.43)$$

where $\underline{x}(s', s)$ is the vector of CPM output samples on the branch $(s', s)$. Then the branch transition metrics can be calculated with the knowledge of the *a priori* information $Pr\{U_k = u\}$. But in practice, the CSI is not available at the receiver and it must be estimated.

We have defined $\theta_k = \pi h \sum_{l=0}^{k-L} d_l$. Now let

$$\Theta_k = \{\theta_k, d_{k-L}, d_{k-L-1}, \cdots, d_{k-L-N_p+1}\}$$

be the new trellis state. And $\{\underline{x}_{k-L+1}, \underline{x}_{k-L}, \cdots, \underline{x}_{k-L-N_p+1}\}$ be the output samples of the trellis.

The channel state information $c_k$ on the newly defined trellis can be obtained

by applying a prediction filter

$$c_{k-L+1} = \frac{1}{N} \sum_{l=0}^{N_p-1} a_l \cdot \underline{x}_{k-L-l}^H \cdot \underline{y}_{k-L-l} \qquad (2.44)$$

where $a_l, l = 0, \cdots, N_p - 1$, are the predictor coefficients. The branch transition probability on the newly defined trellis branch $(s', s)$ at time $(k - L + 1)T$ can be written as

$$\begin{aligned} \gamma_{k-L+1}(s', s) &= \text{constant} \cdot Pr\{S_{k-L+1} = s | S_{k-L} = s'\} \\ &\cdot \exp\left[\frac{2E_s}{f_s N_0} Re\left(\hat{c}_{k-L+1}^* < \underline{x}^H(s', s), \underline{y}_{k-L+1} >\right)\right]. \quad (2.45) \end{aligned}$$

Then $\alpha_k(s)$, $\beta_k(s)$ and symbol-by-symbol decisions can be computed in the same way as before using the newly defined trellis $\Theta_k$.

## 2.4.2  Numerical Results and Discussions
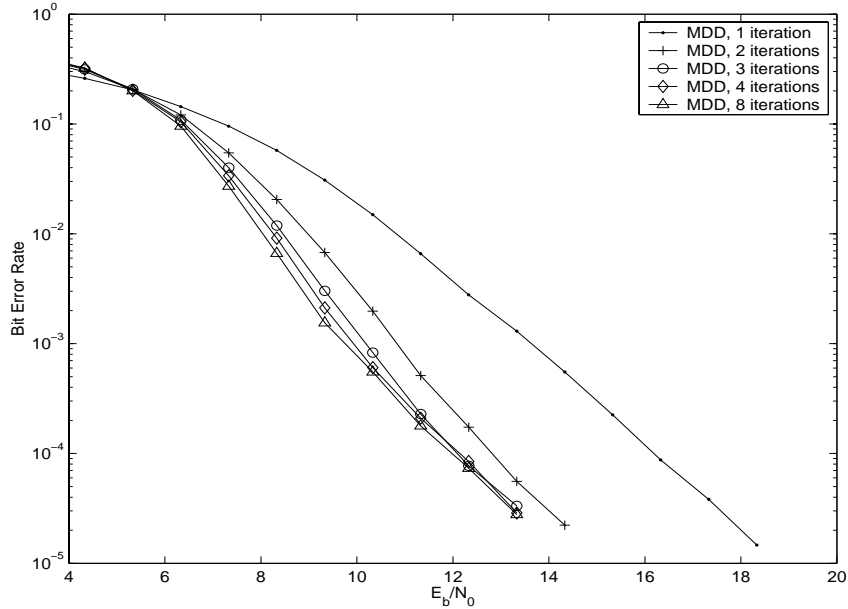


Figure 2.13: Performance of MDD CPM receiver with different number of iterations ($f_D T = 0.01$, predictor order $= 3$)
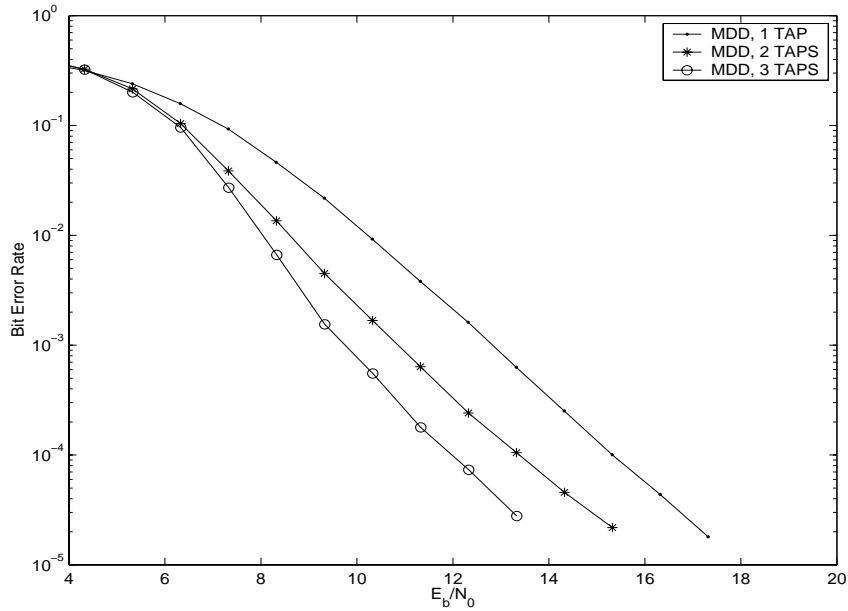
Figure 2.14: Performance of MDD CPM receiver with different predictor lengths ($f_D T = 0.01$, 8 iterations)

As in Section 2.2, we use 8−ary CPFSK to assess the performance of the non-coherent, iterative demodulation and decoding receiver. We will call it the MDD receiver for simplicity. The channel code and the pseudo-random interleaver are the same as in Section 2.2.

Shown in Fig. 2.13 are the results of the MDD receiver in the Rayleigh fading channel with normalized Doppler spread $f_D T = 0.01$. The order of linear predictor used in MDD is three. It can be seen that the iterative demodulation and decoding also improves the BER performance in the MDD receiver. But there is little gain in BER performance at high SNR after three iterations.

Shown in Fig. 2.14 are the results of the MDD receiver with different linear predictor lengths. Eight iterations are used. Due to high computational complexity and high memory requirements imposed by the MDD receiver, the maximum linear predictor length we can simulate in a Sun Ultra 10 computer
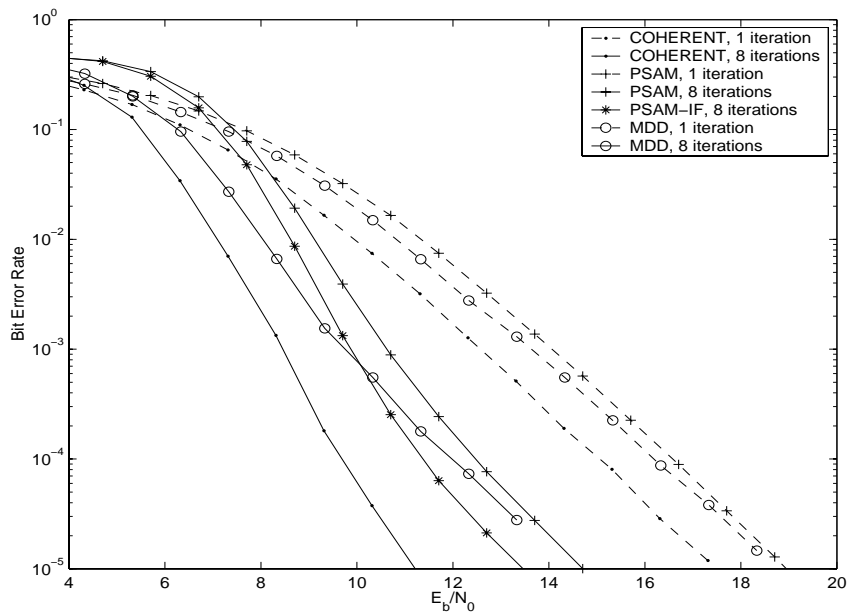
Figure 2.15: Performance of CPM receivers on Rayleigh fading channels ($f_D T = 0.01$)

is 3. It can be seen that the performance of the MDD receiver well depends on the length of the linear predictor. At $10^{-4}$ BER, the 3-tap linear predictor outperforms the 1-tap linear predictor by more than 3.0 dB and 2-tap linear predictor by more than 1.0 dB.

We compare the performance of the MDD receiver with those of the coherent receiver, the PSAM receiver, and the PSAM-IF receiver in Fig. 2.15. The order of the linear predictor used in the MDD receiver is three. At one iteration, it can be seen that the MDD receiver always performs better than the PSAM receiver but worse than the coherent receiver. At eight iterations, the MDD receiver performs better than the PSAM receiver but worse than the PSAM-IF receiver. At high SNR, the BER curve of the PSAM receiver descends faster and expects to match that of the MDD receiver eventually.

Compared with the PSAM receiver, the MDD receiver performs better under

a certain SNR with a predictor length of three. There is no power and bandwidth loss due to pilot symbols in the MDD receiver. Ideally, if the order of the linear predictor used in MDD receiver is sufficiently large, the MDD receiver can perform very close to the COHERENT receiver. Unfortunately, due to the limitations in the computing facility, especially computer memory, we were not able to simulate the cases with the linear predictor order larger than three. With the linear predictor order $N_p$ being set to three, the MDD CPM demodulator has $8 \cdot 8^{N_p} = 4092$ states (tilted-phase trellis) and the program needs about 200 mega-bytes in memory. While for the PSAM receiver, its CPM demodulators has only 8 states. High computational complexity and memory consumption is also the most severe disadvantage for the MDD receiver.

## 2.5   Conclusions

In this chapter, we have designed coherent and noncoherent iterative receivers for high-order CPM signals. All of them uses the CPM demodulator as inner decoder and have a structure similar to a serial concatenated convolutional decoder. For the coherent receiver, in addition to using pilot symbols as references for channel estimation, the PSAM receiver and the PSAM-IF receiver use them as parity check symbols within each pilot frame to help reduce the decoding error directly. Simulation results have shown significant improvement in BER performance for both PSAM and PSAM-IF receivers. Since the PSAM-IF receiver also uses the output of the CPM demodulator to reconstruct the CPM phase trajectories and iteratively estimate the channel state information on reconstructed trajectories, it has about 1.0 dB gain in SNR over the PSAM receiver at high SNR with

limited additional complexity.

The noncoherent MDD receiver that applies multiple-symbol differential detection in the CPM demodulator, also benefits from iterative processing. Therefore its BER performance is largely determined by the length of the linear predictor. But increasing the predictor length incurs huge increase in computational complexity and memory requirement. Therefore, one of our future works is to design reduced-state MDD demodulator using the techniques described in [39]. By balancing between the number of trellis states and the linear predictor length, we might achieve better performance under the same computational complexity and memory requirement.

Other ways to improve the performance include increasing interleaver size or using more powerful codes, although both will increase receiver complexity and decoding delay. At last, it should be pointed out that although the proposed system is designed for CPM signals, it applies to other differentially encoded signals like DPSK signals as well.

Chapter 3

# Pilot Symbol-Assisted Demodulation of Turbo-Coded Quadrature Amplitude Modulation in Doppler Fading Channels

Motivated by development in mobile and wireless communications, the problem of system design for reliable, high-speed data transmission over fading channels have received considerable interests in recent years. Various newly developed techniques have been combined together to combat fading and improve the system performance. In [40], pilot symbol-assisted modulation (PSAM) [18], [19], turbo codes [7], and joint iterative channel estimation and decoding, have been applied together for the demodulation of BPSK signals transmitted over Rayleigh fading channel. However, due to the inherent drawback of the BPSK signal, the above system has limited power and bandwidth efficiency.

Given the emerging interest in high-order modulation for speech and data transmission for mobile systems, we concentrate on the system design of transmitting QAM signals over Doppler fading channels. Among fading channels, two kinds of them are of particular interest to us. One is the flat-fading channel,

the other is the multipath fading channel, where multipath will cause frequency-selective fading.

In the flat fading channel, we investigate the application of iterative channel estimation [40] and decoding for turbo-coded M-QAM signals. Pilot symbols are inserted periodically in the encoded data stream for the estimation of the time-variant channel state information (CSI). The decoder uses this estimated CSI, together with the received data sequence, to generate soft decisions for each data symbol. These soft decisions are used to reconstruct data symbols, which together with the known pilot symbols are then filtered again to obtain improved estimation of the CSI.

We consider two schemes for iterative channel estimation in the flat fading channel. One is a threshold-controlled scheme that uses only the decisions whose reliability values are larger than a threshold value for data reconstruction and subsequent channel estimation. The other is an indiscriminating channel estimation scheme that reconstructs all data symbols for iterative channel estimation and allows a low complexity implementation.

In the multipath fading channel, the difficulties lie not only with the need to estimate multiple channel parameters for each symbol period, but also with different delays of multipath signals, which will result in intersymbol interference and thus destroy references provided by pilot symbols at the receiver side. To handle this problem, we consider turbo-coded QAM signals in a DS-CDMA system and use the Rake receiver to resolve multiple dominant transmission paths. Thus for each path, the fading can be considered to be flat so references provided by pilot symbols can be used to estimate the path gain for that path. Another widely used channel estimation scheme in DS-CDMA is to use a dedicated pilot

signal, which shares the same bandwidth but has its own spreading code. It is often called "PAD" (pilot-aided demodulation). We will consider both PSAM and PAD for channel estimation and compare their performances. For this part, similar work has been done for MPSK signals by Khairy in [41]. But he only considered receiver diversity in [41]. Besides, because of the model inaccuracy in his simulator, his results for PSAM are flawed (PAD uses only neighboring symbols and are more tolerant on model inaccuracy).

Since the rake receiver can exploit the diversity gain by coherently combining the received signals from multiple paths, we also consider diversity gain at the transmitter side. This can be achieved by using the space-time code proposed by Tarokh, etc. in [26], [29]. For simplicity, we consider only the space-time code proposed by Alamouti in [28]. Although similar work has been done by Lenardi [42], Schulz-Rittich [43], etc., our approach differentiates from their work in several aspects. First, although they have used space-time code, no other channel codes are considered. As a result, they didn't include the performance gain from iterative channel estimation, which is often more significant than the diversity gain. Second, they only used pilot symbols to estimate the channel state information so there is no comparison between PSAM and PAD. Therefore our approach here is much more comprehensive.

The outline of this chapter is as follows. In Section 3.1, we present the turbo-coded QAM with PSAM in flat-fading channels. We will first describe the proposed system. Then we will present the flat-fading channel and signal models, computation of log-likelihood ratio, soft decisions for turbo-coded bits, channel estimation with PSAM, and simulation results. In Section 3.2, the turbo-coded QAM with PSAM in multipath fading channels are studied. Conclusions will be

51

drawn in Section 3.3.

## 3.1   PSAM in Flat-Fading Channels
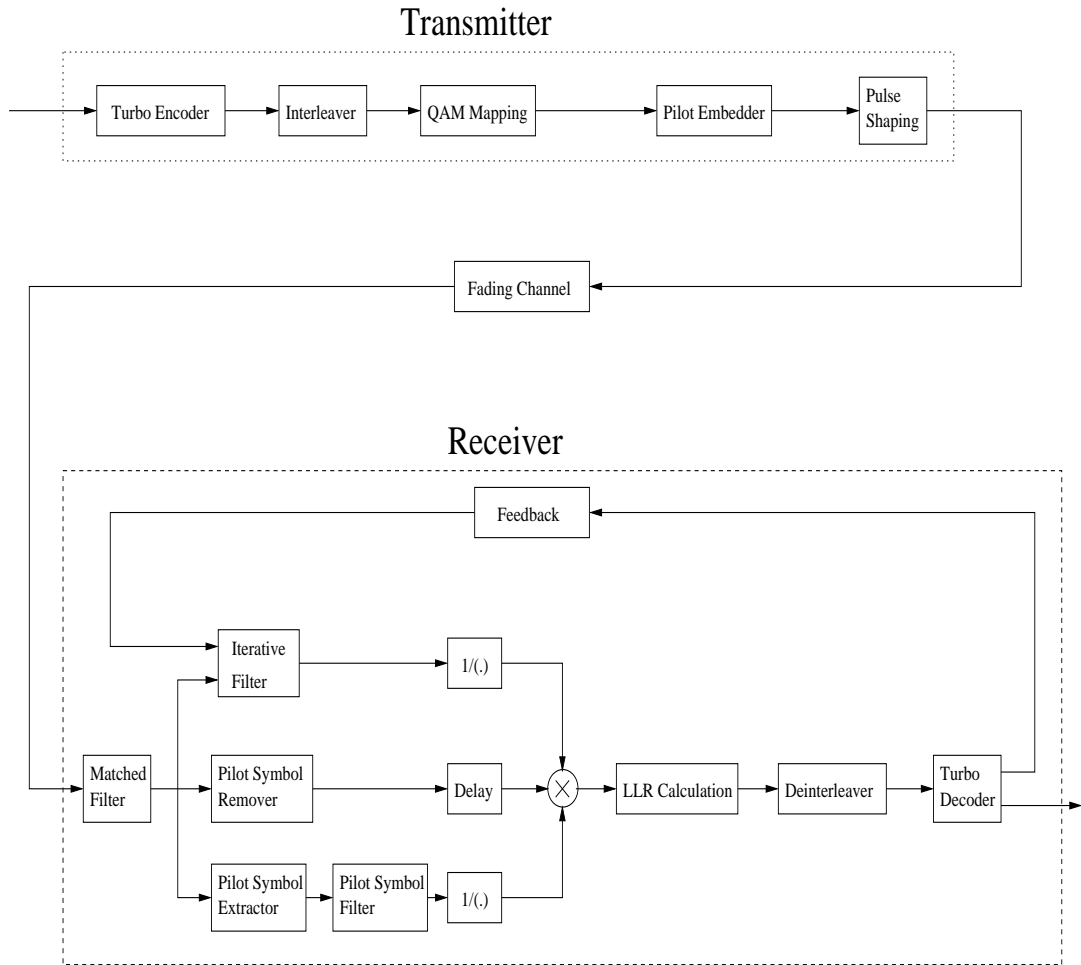
Transmitter



Figure 3.1: Transmitter and Receiver of Pilot Symbol-Assisted Demodulation
Turbo Coded QAM

The proposed PSAM turbo-coded QAM system is as shown in Fig. 3.1.
Transmitted signals go through turbo encoder, channel interleaver, QAM mapping, and pilot insertion before it is pulse-shaped and transmitted through the
flat-fading channel. At the receiver, QAM signals are first passed through a

matched filter. Here we assume perfect timing and synchronization for received signals and ignore the inter-symbol interference caused by the Doppler fading. The output of the matched filter are separated into the pilot stream – to be used for channel estimation, and the data stream. The data stream is delayed and compensated by the estimated channel state information before it is used for the calculation of log-likelihood ratio at bit level. The bit level log-likelihood ratio are then deinterleaved and sent to the turbo decoder and so completes the first iteration. From the second iteration, the output of the turbo decoder are fed back to reconstructed the transmitted data symbols, which are then used together with pilot symbols to obtain a more accurate channel estimation through an iterative filter. The rest is the same as the first iteration. And this processing can be carried on to the third iteration, the fourth iteration, $\cdots$, and so forth. In the rest of this section, we will first present the flat-fading channel and signal models, followed by the key components in the proposed PSAM system: log-likelihood ratio computation, soft decisions for information and coded bits, and iterative channel estimation. At last, we will evaluate the system performance using numerical methods.

### 3.1.1   Rayleigh Flat-Fading Channel and PSAM Signal Models

We assume the transmitted signal $s(t)$ has a complex envelope given by

$$s(t) = A \sum_{k=-\infty}^{\infty} b(k)p(t - kT) \tag{3.1}$$

where $T$ is the symbol duration, $b(k)$ is the $kth$ symbol for 16-QAM. $A$ is the amplitude factor and p(t) is a unit energy pulse:

$$\int_{-\infty}^{\infty} |p(t)|^2 \, dt = 1 \tag{3.2}$$

At the receiver, the fading channel output $r(t)$ is given by

$$r(t) = c(t)s(t) + n(t) \tag{3.3}$$

in which $n(t)$ is AWGN with power spectral density $N_0/2$ in both real and imaginary components. The complex channel gain $c(t)$ represents the Rician fading with autocorrelation function [35]

$$R_c(\tau) = \sigma_c^2 \left( \frac{K_c}{1 + K_c} + \frac{1}{1 + K_c} J_0(2\pi f_D \tau) \right), \tag{3.4}$$

where $J_0(\cdot)$ is the zeroth order Bessel function of the first kind, $f_D$ is the Doppler frequency, $\sigma_c^2$ is the total power of $c(t)$, and $K_c$ is the ratio between the line-of-sight power and the scattered power.

The receiver detects the pulses using a matched filter with impulse response $p^*(-t)/\sqrt{N_0}$ [18]. The symbol-spaced samples $r(k)$ of the matched filter output are given by

$$r(k) = h(k)s(k) + n(k) \tag{3.5}$$

where $h(k) = \frac{A\,c(k)}{\sqrt{N_0}}$ and the Gaussian noise samples $n(k)$ are white with unit variance.

In PSAM, known symbols are inserted periodically into the data symbol sequence once per $(M - 1)$ symbols. At the receiver, these symbols are filtered and interpolated to estimate channel gains associated with each data symbols. The optimum filter under a given signal-to-noise-ratio and Doppler spread is Wiener filter [18]. The receiver then scales and rotates a reference decision grid for QAM constellation with the estimate, and feeds the modified decision boundaries to the data branch. This modified decision boundaries are then used to generate logarithm likelihood ratios of four bits associated with each received 16-QAM data symbol, which will be discussed in detail in the next section.

## 3.1.2  Logarithm Likelihood Ratio (LLR) Calculation

For reasons stated in the introduction, a set of binary turbo encoder and decoder is used in the system. However, the symbols transmitted over the fading channel and received after matched filtering are 16-QAM symbols. This requires that an appropriate mapping from binary coded bits to 16-QAM symbols be used in the transmitter and that noise-corrupted data symbols be broken into their associated bit logarithm likelihood ratio at the receiver. As in [12], Gray mapping is used in the transmitter. Next we will deal with the calculation of bit logarithm likelihood ratio for 16-QAM signals.

Consider a sequence of information bits $b_1b_2b_3b_4...b_{4k-3}b_{4k-2}b_{4k-1}b_{4k}...$, a sequence of 16-QAM symbols $r(1), r(2), ..., r(k), ...$, and the following mapping.

| $b_{4k-3}b_{4k-2}$ | $X_k$ | $b_{4k-1}b_{4k}$ | $Y_k$ |
|---|---|---|---|
| 01 | -3 | 01 | -3 |
| 00 | -1 | 00 | -1 |
| 10 | +1 | 10 | +1 |
| 11 | +3 | 11 | +3 |

The bit logarithm likelihood ratio for 16-QAM signals is given by

$$\Lambda(b_{4k-i}) = K\, log \frac{Pr\{b(4k-i) = 1|r(k)\}}{Pr\{b(4k-i) = 0|r(k)\}}, \; \forall\, i = 0, 1, 2, 3, \tag{3.6}$$

where $K$ is a constant.

In the case of additive white Gaussian channel with no fading, according to [12], a good approximation of the LLR can be achieved using the following expressions:

$$\Lambda(b_{4k-3}) = X_k$$

$$\Lambda(b_{4k-2}) = |X_k| - 2$$

$$\Lambda(b_{4k-1}) = Y_k$$

$$\Lambda(b_{4k}) = |Y_k| - 2$$

Let $r(k) = X(k) + jY(k)$. In the case of Rayleigh fading channel, we need to scale and rotate the reference frame according to the channel gain before calculating the LLR. It is easy to prove that the following expressions hold, where $h(k)$ is the complex channel gain associated with symbol $(X_k, Y_k)$.

$$\Lambda(b_{4k-3}) = |h(k)|X_k^c$$

$$\Lambda(b_{4k-2}) = |h(k)|(|X_k^c| - 2)$$

$$\Lambda(b_{4k-1}) = |h(k)|Y_k^c$$

$$\Lambda(b_{4k}) = |h(k)|(|Y_k^c| - 2)$$

where

$$X_k^c + jY_k^c = (X_k + jY_k)/h(k)$$

### 3.1.3   Soft Decisions for Information and Coded Bits

A standard binary turbo decoder generates the soft decisions only for the information bits, the extrinsic part of which are to be used in the next iteration as a priori information. In this design, the soft decisions for the coded bits as well as information bits are needed for the iterative channel estimation. Let $u_k$ be the information bit associated with the transition from time $k - 1$ to $k$. Let $x_{k,1}, ..., x_{k,\nu}$ be the coded bits associated with the branch transition from time $k - 1$ to $k$. And let the trellis states at level $k - 1$ and at level $k$ be denoted by the integer $s'$ and $s$ respectively. Then for the information bit, the soft decision

can be calculated by

$$L(u_k) = log\frac{\sum_{\{(s',s):u_k=1\}} \alpha_{k-1}(s')\gamma_k(s',s)\beta_k(s)}{\sum_{\{(s',s):u_k=0\}} \alpha_{k-1}(s')\gamma_k(s',s)\beta_k(s)} \quad (3.7)$$

where

$$\gamma_k(s',s) = Pr(s|s')p(\underline{y}_k|s',s) \quad (3.8)$$

$\alpha_k(s)$ is yielded by the forward recursion

$$\alpha_k(s) = \sum_{s'} \alpha_{k-1}(s')\gamma_k(s',s) \quad (3.9)$$

$\beta_k(s)$ is yielded by the backward recursion

$$\beta_{k-1}(s) = \sum_{s'} \gamma_k(s,s')\beta_k(s') \quad (3.10)$$

For the coded bits $x_{k,1}, ..., x_{k,\nu}$, their soft decisions are given by

$$L(x_{k,i}) = log\frac{\sum_{\{(s',s):x_{k,i}=1\}} \alpha_{k-1}(s')\gamma_k(s',s)\beta_k(s)}{\sum_{\{(s',s):x_{k,i}=0\}} \alpha_{k-1}(s')\gamma_k(s',s)\beta_k(s)}, \quad \forall i = 1, 2, ..., \nu. \quad (3.11)$$

## 3.1.4   Iterative Channel Estimation

The idea behind iterative channel estimation is to reconstruct data symbols from the output of the channel decoder and use them together with pilot symbols to re-estimate the channel state information. When there are very few errors in data reconstruction, more accurate channel estimates can be obtained due to significantly increased sampling rate. We consider two approaches for iterative channel estimation. One aims to reduce error propagation and use a threshold-controlled feedback so that only those reconstructed symbols with high reliability values are used for iterative channel estimation. In this case, the taps and coefficients of iterative filters are determined by the reliability values of neighboring

symbols and must be computed for each symbol position. The other will simply reconstruct all data symbols and use a single iterative filter for all symbols.

We first consider the approach with threshold controlled feedback. The soft values of *a posteriori* probability generated by the turbo decoder reflects the extent that a particular bit can be trusted. The higher the value, the more reliable its corresponding hard decision. The role of the threshold controller is to decimate all the bits with a confidential level lower than the threshold and allow only the bits with a higher confidential level to pass through. Those bits will then be turned into hard decisions for reconstructing the 16-QAM symbols to be used for iterative channel estimation. Note that a symbol can only be reconstructed when all of its four bits pass through the threshold controller. Otherwise, no symbol will be formed in that symbol position. For pilot symbols, since they are known *a priori* to the receiver, they will always be included in the iterative channel estimation.

To estimate the channel state information $h(k)$. We consider a time window $\Omega_t(k) = \{k - L_W/2, \cdots, k - 1, k, k + 1, k + L_W/2\}$. Suppose there are $N_t$ pilot and reconstructed data symbols in this window: $s(k_1)$, $s(k_2)$, $\cdots$, $s(k_{N_t})$, $k_i \in \Omega_t(k)$. Let $\underline{r}(k) = [r(k_1), \cdots, r(k_{N_t})]^T$. The autocorrelation matrix $R(k) = \frac{1}{2} E[\underline{r}(k)\underline{r}^H(k)]$ and the cross-correlation vector $\underline{p}(k) = \frac{1}{2} E[\underline{r}(k)u^*(k)]$ for the calculation of iterative filter coefficients based on the estimated symbol value is given by,

$$
\begin{aligned}
& \frac{1}{2} E[r(k)r^*(l)] \\
= & \frac{1}{2} E[h(k)\hat{s}(k)\hat{s}^*(l)h^*(l)] + \frac{1}{2} E[n(k)n^*(l)] \\
= & \frac{1}{2} E[h(k)h^*(l)]\hat{s}(k)\hat{s}^*(l) + \delta_{k,l}
\end{aligned}
$$

$$= \frac{A^2}{2N_0} E[c(kT)c^*(lT)]\hat{s}(k)\hat{s}^*(l) + \delta_{k,l}$$

$$= \frac{A^2}{N_0} \sigma_g^2 J_0(2\pi f_D T(k-l))\hat{s}(k)\hat{s}^*(l) + \delta_{k,l},$$

$$\frac{1}{2} E[r(l)h^*(k)]$$

$$= \frac{1}{2} E[h(l)h^*(k)]\hat{s}(l)$$

$$= \frac{A^2}{2N_0} E[c(lT)c^*(kT)]\hat{s}(l)$$

$$= \frac{A^2}{N_0} \sigma_g^2 J_0(2\pi f_D T(l-k))\hat{s}(l), \tag{3.12}$$

where $\hat{s}(k), \hat{s}(l)$ are the data symbols formed in the feedback path. At this stage, we can calculate the Wiener filter coefficients directly by

$$\underline{w}(k) = R^{-1}\underline{p}(k) \tag{3.13}$$

Note here that both the dimension and the elements of the coefficient vector $\underline{w}(k)$ vary from symbol to symbol. To get the channel estimation of a specific symbol, we use the iterative filter

$$\hat{h}(k) = \underline{w}(k)\underline{r}(k), \tag{3.14}$$

The main problem of this threshold-controlled, iterative channel estimation scheme is that it requires matrix inversion at each symbol position, which sets the complexity to be polynomial. To reduce the complexity, we propose a simplified channel estimation scheme in the following.

We first select for each specific symbol the most reliable point out of the 16-QAM constellation, i.e.

$$\hat{s}(k) = \max_{i=1,...,16} Pr\{s(k) = q_i\}, \tag{3.15}$$

where $q_i, i = 1, ..., 16$ are 16-QAM constellation points. We then have

$$r(k) \approx h(k)\hat{s}(k) + n(k). \tag{3.16}$$

Divide both sides by $\hat{s}(k)$, we have

$$r'(k) \approx h(k) + n'(k), \tag{3.17}$$

where $r'(k) = r(k)/\hat{s}(k)$ and $n'(k) = n(k)/\hat{s}(k)$. Since $\hat{s}(k) = |\hat{s}(k)|e^{j\arg(\hat{s}(k))}$, this process is equivalent to a scaling of the amplitude of $r(k)$ by $|\frac{1}{\hat{s}(k)}|$ and a rotation of the phase of $r(k)$ by $-\arg(\hat{s}(k))$ .

Although the new noise term $n'(k)$ is no longer stationary Gaussian noise, we still treat it as if it were stationary Gaussian noise in the subsequent processing. To get the channel estimation of a specific symbol, we use the iterative filter

$$\hat{h}(k) = \underline{w}_a^H \underline{r}_a(k), \tag{3.18}$$

where $\underline{w}_a$ is a vector of iterative filter coefficients, $H$ stands for the matrix transpose and complex conjugate, and

$$\underline{r}_a(k) = \begin{bmatrix} r'(k - \frac{L_W}{2}) \\ \vdots \\ r'(k-1) \\ r'(k+1) \\ \vdots \\ r'(k + \frac{L_W}{2}) \end{bmatrix}. \tag{3.19}$$

With this updated version of channel estimation, the estimation error is given by

$$e(k) = h(k) - \hat{h}(k). \tag{3.20}$$

### 3.1.5   Simulation Results

In this section, we simulate the BER performance of the proposed system in a flat fading channel with a normalized fading rate, $f_D T$, of 0.01. The modulation is

16-QAM. The turbo code is a rate 1/2, (111, 101) code. The turbo interleaver is a pseudo-random interleaver of block size 1076 (in bit). The channel interleaver is also a pseudo-random interleaver of 2160 bits. With 16-QAM modulation, a packet has 540 data symbols. In the case of pilot symbol-assisted modulation, there are 55 pilot symbols. The pilot symbol filter has 20 taps. After the first iteration, the reconstructed data symbols from neighboring symbol positions are used for the purpose of iterative channel estimation, although some of them will be decimated by the threshold controller. The $L_w$ is equal to 20.
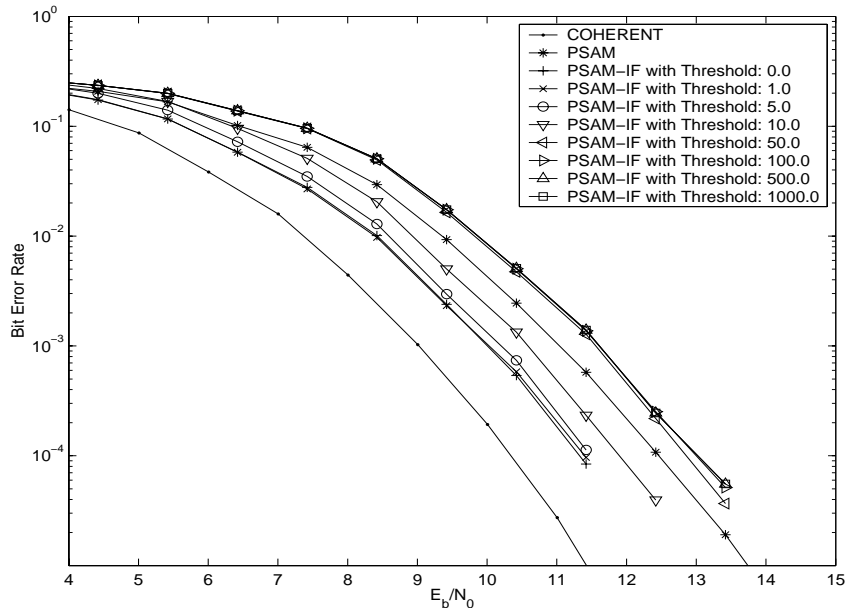


Figure 3.2: Bit Error Rate Performance of Turbo Coded QAM with Threshold-Controlled Iterative Channel Estimation

Shown in Fig. 3.2 are the simulation results of the threshold-controlled, iterative receiver in the flat fading channel. It can be seen that the smaller the threshold value, the better the BER performance. As the threshold value decreases from 1000 to 0, where the best BER performance is achieved, the required SNR decreases for more than 1.5 dB at a BER of $10^{-4}$. This means that dec-
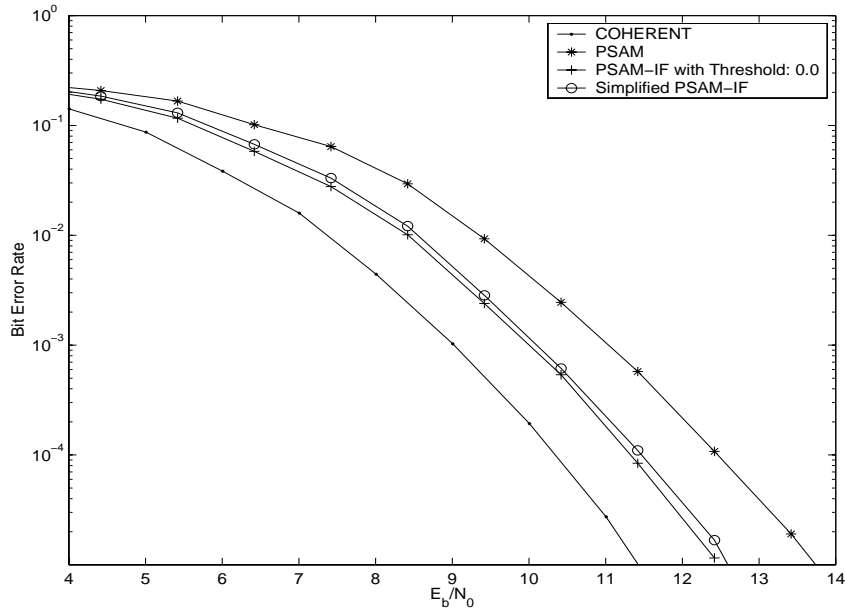
Figure 3.3: Bit Error Rate Performance of Turbo Coded QAM with Simplified Iterative Channel Estimation

imating the reconstructed symbols with low reliability values does not improve the BER performance, although it allows for removing some data symbols from iterative channel estimation without performance degradation at low threshold values. Furthermore, at high threshold values, the BER performance deteriorates because most of the data symbols are not used for channel estimation, which leads to higher estimation errors for the channel state information.

Also included in this figure are the performance results of receivers with perfect channel state information and with pilot symbol-assisted channel estimation only. In terms of SNR, the best threshold-controlled iterative receiver is about 1.1 dB better than the PSAM receiver without iterative channel estimation at a BER of $10^{-4}$. At this point, the SNR difference between the coherent receiver and the best threshold-controlled iterative receiver is only 1.0 dB.

Shown in Fig. 3.3 are the simulation results of the receiver with simplified

channel estimation. For comparison, we also include the results of the coherent receiver, the threshold-controlled iterative receiver and the PSAM receiver without iterative channel estimation. At the BER range that we are interested in, the SNR difference between the simplified receiver and the best threshold-controlled receiver is within 0.2 dB. Since the simplified receiver has only linear complexity, it is much favored for obvious practical reasons compared to the threshold-controlled receiver, which has polynomial complexity. Therefore, we will only consider the simplified scheme in the rest of this chapter.

## 3.2 Turbo-Coded QAM with PSAM and Transmit Diversity in Frequency-Selective Fading Channels
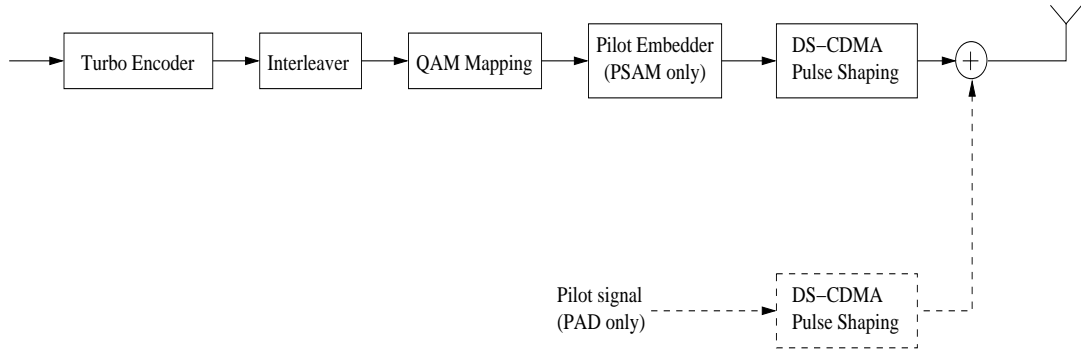


Figure 3.4: Transmitter of Turbo Coded DS-CDMA Signals

In this section, we consider turbo-coded quadrature amplitude modulation with PSAM and transmit diversity in multipath fading channels. The system is as shown in Fig. 3.6 and Fig. 3.7. As we will compare transmit diversity with receive diversity, we also show in Fig. 3.4 and Fig. 3.5 the diagrams for the transmitter and the Rake receiver without transmitter diversity. A number of users share the same channel using DS-CDMA. The transmitted signal of each
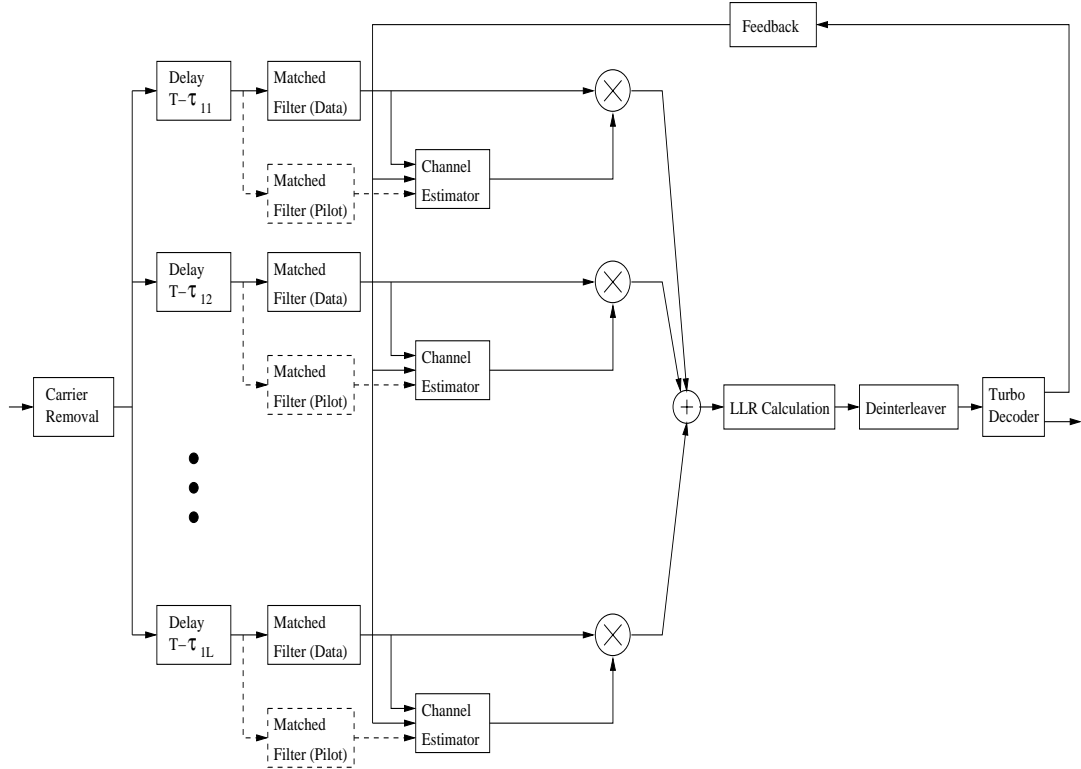
Figure 3.5: Rake Receiver of Turbo Coded DS-CDMA Signals

user will go through multiple transmission paths before it arrives at the receiver. Each path has different attenuation and delays. The fading on each path is flat in frequency and subject to Doppler shift. When there are multiple users in the system, their transmitted signals can either be demodulated with various single user detectors [1] or multiuser detectors proposed by [44], [45], etc. No matter what kind of detectors, the channel estimation with PSAM will remain the same. Without loss of generality, we will focus on the case that there is only one user in the system and consider single user detection with the correlation detector. It is straightforward to extend from single user case to multiple users. For comparison, we will also consider pilot-aided demodulation of multipath signals in DS-CDMA.
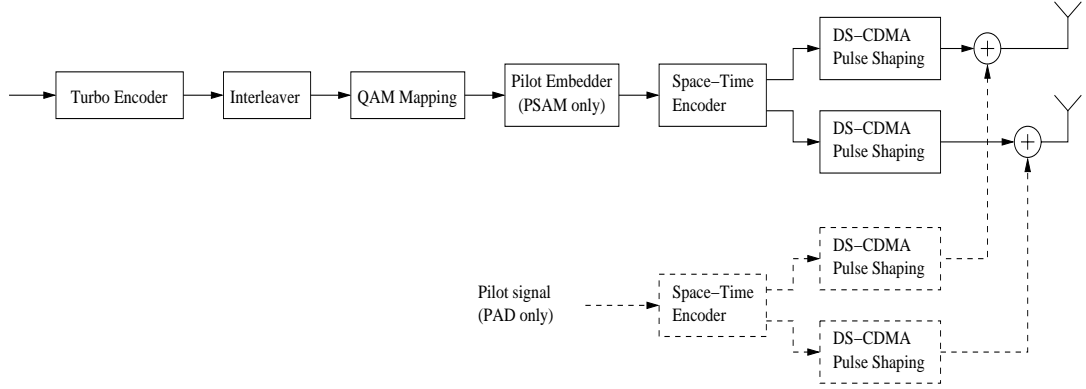
Figure 3.6: Transmitter of Turbo Coded DS-CDMA Signals with Transmitter Diversity

### 3.2.1 Multipath Channel and Signal Models

The transmitted signal for the $u$th antenna of a user in CDMA is given by

$$s_1^u(t) = A \sum_{k=-\infty}^{\infty} b_1^u(k) \, a_1(t - kT),\qquad(3.21)$$

where $b_1^u(k)$ is the space-time coded data symbol for the $u$th antenna, $a_1(t)$ is the spreading signal with a period $T = N\,T_c$. $T_c$ is the chip duration and $N$ is the number of chips in one symbol period. The spreading signal for the $i$th user is given by

$$a_i(t) = \sum_{j=1}^{N} a_{i,j} \, p(t - jT_c),\qquad(3.22)$$

where $p(t)$ is a unit energy pulse in the interval $0 \le t \le T_c$ and $a_{i,j}$ is a sequence of $N$ +1 and $-1$. The signal $s_1^u(t)$ is transmitted through a multipath channel. We assume a wide-sense stationary multipath fading channel model with $L$ uncorrelated paths. The channel impulse response for the $i$th user is given by

$$c_i^u(\tau, t) = \sum_{l=0}^{L} c_{il}^u(t) \, \delta(\tau - \tau_{il}),\qquad(3.23)$$
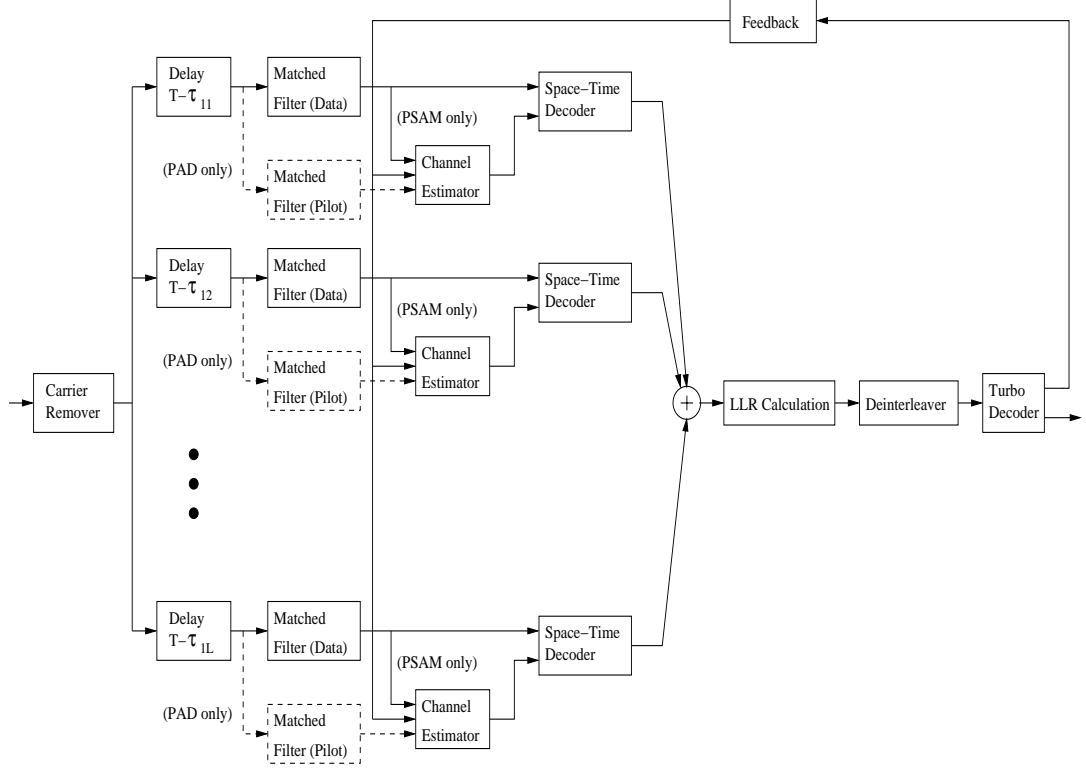
Figure 3.7: Rake Receiver of Turbo Coded DS-CDMA Signals with Transmitter Diversity

where $L$ is the number of resolvable paths for the Rake receiver. $c_{il}^u$ is the complex channel gain for the $l$th path for the $u$th transmit antenna of the $i$th user. Channel gains on different paths are i. i. d. random processes. The complex channel gain $c_{il}^u(t)$ represents the Rayleigh fading with autocorrelation function [35]

$$R_c(\tau) = E\left[|c_{il}^u(t)|^2\right] J_0(2\pi f_D \tau), \tag{3.24}$$

where $J_0(\cdot)$ is the zeroth order Bessel function of the first kind, and $f_D$ is the Doppler frequency.

The received signal is given by

$$r(t) = \sum_{u=1}^{N_u} \sum_{l=1}^{L} c_{1l}^u(t - \tau_{1l}) \, s_1^u(t - \tau_{1l})$$

$$+ \sum_{m=2}^{K_u} \sum_{u=1}^{N_u} \sum_{l=1}^{L} c_{ml}^{u}(t - \tau_{ml}) \, s_m^u(t - \tau_{ml}) + n(t), \qquad (3.25)$$

where $K_u$ is the number of total users in the CDMA system, $N_u$ is the number of transmit antennas, and $n(t)$ is the additive white Gaussian noise with two-sided power spectral density $N_0/2$. The signal is received by the Rake receiver shown in Fig. 3.7. The matched filters for the $i$th user have an impulse response $a_i(-t)/\sqrt{N_0}$. For convenience, we assume that $\tau_{11} = 0.0$ since it is the relative delay rather than the absolute delay that determines the level of multiuser interferences. The output of the first matched-filter of the first user, representing the first finger of the Rake receiver, is given by

$$\begin{aligned} r_{11}(k) &= \sum_{u=1}^{N_u} h_{11}^u(k) b_1^u(k) + \sum_{l=2}^{L} \sum_{u=1}^{N_u} h_{1l}^u(k) I_{1l}^u(k) \, \exp\{j\phi_{1l}^u(k)\} \\ &+ \sum_{m=2}^{K_u} \sum_{l=1}^{L} \sum_{u=1}^{N_u} h_{ml}^u(k) I_{ml}^u(k) \, \exp\{j\phi_{ml}^u(k)\} + n_{11}(k) \qquad (3.26) \end{aligned}$$

where $h_{11}^u(k) = \frac{A\, c_{11}^u(k)}{\sqrt{N_0}}$, $I_{ml}^u(k)$ is the interference from the $(u, l)$th path of $m$th user to the 1st finger of the 1st user's Rake receiver, and $n_{11}(k)$ is the AWGN with unit variance. In our case, we consider only one user in the DS-CDMA system. Hence the received signal for the 1st finger of the Rake receiver can be simplified to

$$r_{11}(k) = \sum_{u=1}^{N_u} h_{11}^u(k) b_1^u(k) + i_{11}(k), \qquad (3.27)$$

where

$$i_{11}(k) = \sum_{l=2}^{L} \sum_{u=1}^{N_u} h_{1l}^u(k) I_{1l}^u(k) \, \exp\{j\phi_{1l}^u(k)\} + n_{11}(k), \qquad (3.28)$$

The interference $I_{ml}^u(k)$ depends on the specific code used in the CDMA system. For a random signature sequence of length $N$, according to the approximation

67

in [46] and [47], $I_{ml}^u(k)$ can be approximated as additive white Gaussian noise, with its mean and power given by

$$E\left[I_{ml}^u(k)\right] = 0.0. \tag{3.29}$$

$$E\left[|I_{ml}^u(k)|^2\right] = \frac{2}{3N}E\left[|s_m^u(t)|^2\right]. \tag{3.30}$$

However, this approximation only applies for large $N$ values and multiples users. And since Gold sequences have excellent cross-correlation property and has been widely used in current DS-CDMA systems, we use Gold sequences so exact multipath interferences can be simulated.

### 3.2.2   Transmit Diversity

At time $k$ and $k+1$, the received signal at the matched filter output of the user 1's $l$th finger are given by

$$\begin{cases} r_{1l}(k) &= h_{1l}^1(k)b_1^1(k) + h_{1l}^2(k)b_1^2(k) + i_{1l}(k); \\ r_{1l}(k+1) &= h_{1l}^1(k+1)b_1^1(k+1) + h_{1l}^2(k+1)b_1^2(k+1) + i_{1l}(k). \end{cases} \tag{3.31}$$

To exploit the transmit diversity, we adopt Alamouti's [28] approach, which involves two transmit antennas, i.e., $N_u = 2$. Suppose there are symbols $b_1(k)$ and $b_2(k)$ to be transmitted at time $k$ and $k+1$ from the first user. To make use of the transmit diversity, at time $k$, $b_1(k)$ is transmitted through one of the antennas and $b_2(k)$ transmitted through the other antenna; at time $k+1$, $-b_2^*(k)$ and $b_1^*(k)$ are transmitted through two antennas. The received signals at time $k$ and $k+1$ are given by

$$\begin{cases} r_{1l}(k) &= h_{1l}^1(k)b_1(k) + h_{1l}^2(k)b_1(k+1) + i_{1l}(k); \\ r_{1l}(k+1) &= h_{1l}^1(k+1)\left(-b_1^*(k+1)\right) + h_{1l}^2(k+1)b_1^*(k) + i_{1l}(k+1). \end{cases} \tag{3.32}$$

68

In the slowly fading channel, there exists very strong correlation between path gains $h_{ml}^u(k)$ and $h_{ml}^u(k+1)$. Therefore we have $h_{ml}^u(k) \approx h_{ml}^u(k+1)$. So the above equations become

$$
\begin{cases}
r_{1l}(k) & = \; h_{1l}^1(k)b_1(k) + h_{1l}^2(k)b_1(k+1) + i_{1l}(k); \\
r_{1l}(k+1) & \approx \; h_{1l}^1(k)\left(-b_1^*(k+1)\right) + h_{1l}^2(k)b_1^*(k) + i_{1l}(k+1).
\end{cases}
\tag{3.33}
$$

When the channel state information is given, we can solve for $b_1(k)$ as follows,

$$
\begin{aligned}
\eta_{1l}(k) & = \; h_{1l}^{1*}(k)r_{1l}(k) + h_{1l}^2(k)r_{1l}^*(k+1) \\
& \approx \; h_{1l}^{1*}(k)\left[h_{1l}^1(k)b_1(k) + h_{1l}^2(k)b_1(k+1) + i_{1l}(k)\right] \\
& \quad + h_{1l}^2(k)\left[h_{1l}^{1*}(k)\left(-b_1(k+1)\right) + h_{1l}^{2*}(k)b_1(k) + i_{1l}^*(k+1)\right] \\
& = \; \left(|h_{1l}^1(k)|^2 + |h_{1l}^2(k)|^2\right)b_1(k) + h_{1l}^{1*}(k)i_{1l}(k) + h_{1l}^2(k)i_{1l}^*(k+1).
\end{aligned}
\tag{3.34}
$$

Similarly for $b_1(k+1)$, we have

$$
\begin{aligned}
\eta_{1l}(k+1) & = \; h_{1l}^{2*}(k)r_{1l}(k) - h_{1l}^1(k)r_{1l}^*(k+1) \\
& \approx \; h_{1l}^{2*}(k)\left[h_{1l}^1(k)b_1(k) + h_{1l}^2(k)b_1(k+1) + i_{1l}(k)\right] \\
& \quad - h_{1l}^1(k)\left[h_{1l}^{1*}(k)\left(-b_1(k+1)\right) + h_{1l}^{2*}(k)b_1(k) + i_{1l}^*(k+1)\right] \\
& = \; \left(|h_{1l}^1(k)|^2 + |h_{1l}^2(k)|^2\right)b_1(k+1) + h_{1l}^{2*}(k)i_{1l}(k) - h_{1l}^1(k)i_{1l}^*(k+1).
\end{aligned}
\tag{3.35}
$$

The Rake receiver then combines $\eta_{1l}(k)$ from $L$ fingers to form a decision variable $\sum_{l=1}^{L} \eta_{1l}(k)$ for the demodulation of $b_1(k)$. When there is perfect channel state information, $\sum_{l=1}^{L} \eta_{1l}(k)$ achieves a diversity order of $2L$.

### 3.2.3 Channel Estimation with PSAM and Transmit Diversity

To estimate the channel state information $h_{1l}^u(k)$, $u = 1, 2$, we need to send two pilot symbols, $b_1(k) = p1$ and $b_1(k+1) = p2$, at one time. So the received signals at time $k$ and $k+1$ can be written as

$$\begin{cases} r_{1l}(k) & = & h_{1l}^1(k)p_1 + h_{1l}^2(k)p_2 + i_{1l}(k); \\ r_{1l}(k+1) & \approx & h_{1l}^1(k)(-p_2^*) + h_{1l}^2(k)p_1^* + i_{1l}(k+1). \end{cases} \quad (3.36)$$

Let

$$\begin{cases} \xi_{1l}^1(k) = p_1^* r_{1l}(k) - p_2 r_{1l}(k+1); \\ \xi_{1l}^2(k) = p_2^* r_{1l}(k) + p_1 r_{1l}(k+1). \end{cases} \quad (3.37)$$

Substitute (3.36) into the above equations, we have

$$\begin{cases} \xi_{1l}^1(k) = (|p_1|^2 + |p_2|^2) h_{1l}^1(k) + p_1^* i_{1l}(k) - p_2 i_{1l}(k+1); \\ \xi_{1l}^2(k) = (|p_1|^2 + |p_2|^2) h_{1l}^2(k) + p_2^* i_{1l}(k) + p_1 i_{1l}(k+1). \end{cases} \quad (3.38)$$

$\xi_{1l}^1(k)$ and $\xi_{1l}^2(k)$ can be used to estimate the channel state information for the two paths from two transmit antennas to the $l$th finger of the Rake receiver. Then data signals are solved using these estimated channel state information and the output of all $L$ fingers are combined to form a decision variable. The processing after that is the same as Section 3.1, i.e., log-likelihood calculation, deinterleaving, and decoding. From the second iteration, the transmitted symbols are reconstructed from decoder output to iteratively estimate the channel state information.

### 3.2.4 Pilot-Aided Demodulation and Transmit Diversity

For comparison purpose, we also consider pilot-aided demodulation scheme. In this scheme, a pilot signal is transmitted simultaneously with the data signal.

The transmitted signal from the $u$th antenna of the 1st user is given by

$$s_1^u(t) = A \sum_{k=-\infty}^{\infty} \left[ A_p^u(k)\, a_{p_1}(t - kT) + b_1^u(k)\, a_1(t - kT) \right], \tag{3.39}$$

where $A_p^u(k)$ is the pilot value transmitted through antenna $u$, $a_{p_1}(t)$ is the pilot spreading code and is chosen to be nearly orthogonal to $a_1(t)$. All the other parameters are the same as in the PSAM scheme. In the single transmit antenna case, $A_p^1(k)$ can be any values known to the receiver. But in the case with transmit diversity, $A_p^u(k)$ must also be space-time coded in the same way as pilot symbols in the PSAM scheme in order to resolve distinct paths from two transmit antennas. The received signal can be written as

$$
\begin{aligned}
r(t) \;=\; & \sum_{u=1}^{N_u} \sum_{l=1}^{L} c_{1l}^u(t - \tau_{1l})\, s_1^u(t - \tau_{1l}) \\
& + \sum_{m=2}^{K_u} \sum_{u=1}^{N_u} \sum_{l=1}^{L} c_{ml}^u(t - \tau_{ml})\, s_m^u(t - \tau_{ml}) + n(t).
\end{aligned} \tag{3.40}
$$

As shown in Fig. 3.7, there are two branches in each finger of the PAD system. One is for data signals, the other is for pilot signals. In the data branch, the signal is first passed through a filter matched to $a_1(-t)/\sqrt{N_0}$. The output of this matched filter in the first finger of the first user is given by

$$
\begin{aligned}
r_{11}(k) \;=\; & \sum_{u=1}^{N_u} h_{11}^u(k) \left[ b_1^u(k) + I_{p1,1}(k) \right] + \sum_{l=2}^{L} \sum_{u=1}^{N_u} h_{1l}^u(k) I_{1l}^u(k)\, \exp\{j\phi_{1l}^u(k)\} \\
& + \sum_{m=2}^{K_u} \sum_{l=1}^{L} \sum_{u=1}^{N_u} h_{ml}^u(k) I_{ml}^u(k)\, \exp\{j\phi_{ml}^u(k)\} + n_{11}(k),
\end{aligned} \tag{3.41}
$$

where $h_{11}^u(k) = \frac{A\, c_{11}^u(k)}{\sqrt{N_0}}$, $I_{p1,1}(k)$ is the interference from the pilot signal to the data signal on the same path, and $n_{11}(k)$ is the AWGN with unit variance. Since we have assumed that each user's pilot and data code are nearly orthogonal, $I_{p1,1}(k) \approx 0.0$. $I_{ml}^u(k)$ is the total interference (including data and pilot) from

71

path $(u, l)$ of user $m$ to finger 1 of user 1's Rake receiver. In the pilot branch, the signal is passed through a filter matched to $a_{p_1}(-t)/\sqrt{N_0}$. The output of this matched filter in the first finger of the first user is given by

$$
\begin{aligned}
r_{11,p}(k) \;=\; & \sum_{u=1}^{N_u} h_{11}^u(k) \left[ A_p^u(k) + I_{1,1}^u(k) \right] + \sum_{l=2}^{L} \sum_{u=1}^{N_u} h_{1l}^u(k) I_{1l}^u(k) \, \exp\{j\phi_{1l}^u(k)\} \\
& + \sum_{m=2}^{K_u} \sum_{l=1}^{L} \sum_{u=1}^{N_u} h_{ml}^u(k) I_{ml}^u(k) \, \exp\{j\phi_{ml}^u(k)\} + n_{11,p}(k),
\end{aligned} \tag{3.42}
$$

where $I_{1,1}^u(k)$ is the interference from the data signal to the pilot signal on the same path. Again, we have $I_{1,1}^u(k) \approx 0.0$ due to near orthogonality between the user's pilot code and data code. In the case of one user, (3.41) can be simplified to

$$
r_{11}(k) \;=\; \sum_{u=1}^{N_u} h_{11}^u(k) b_1^u(k) + i_{11}(k), \tag{3.43}
$$

where

$$
i_{11}(k) = \sum_{l=2}^{L} \sum_{u=1}^{N_u} h_{1l}^u(k) I_{1l}^u(k) \, \exp\{j\phi_{1l}^u(k)\} + n_{11}(k). \tag{3.44}
$$

Under the same condition, (3.41) can be simplified to

$$
r_{11,p}(k) \;=\; \sum_{u=1}^{N_u} h_{11}^u(k) A_p^u(k) + i_{11,p}(k), \tag{3.45}
$$

where

$$
i_{11,p}(k) = \sum_{l=2}^{L} \sum_{u=1}^{N_u} h_{1l}^u(k) I_{1l}^u(k) \, \exp\{j\phi_{1l}^u(k)\} + n_{11,p}(k). \tag{3.46}
$$

Since $A_p^u(k)$ is known to the receiver, $r_{11,p}(k)$ can be used to estimate the channel state information $h_{11}^u(k)$. As mentioned before, $A_p^u(k)$ is also space-time coded, the estimation of the channel state information is the same as in the PSAM

scheme. Let $\{A_p(k)\}$ be the corresponding uncoded sequence of $\{A_p^u(k)\}$. Then the channel state information can be estimated from the following equations

$$
\begin{cases}
\xi_{1l,p}^1(k) &= \left(|A_p(k)|^2 + |A_p(k+1)|^2\right) h_{1l}^1(k) + A_p^*(k) i_{1l,p}(k) \\
&\quad - A_p(k+1) i_{1l,p}(k+1); \\
\xi_{1l,p}^2(k) &= \left(|A_p(k)|^2 + |A_p(k+1)|^2\right) h_{1l}^2(k) + A_p^*(k+1) i_{1l,p}(k) \\
&\quad + A_p(k) i_{1l,p}(k+1).
\end{cases}
\tag{3.47}
$$

The estimated CSI is then used to demodulate the transmitted data signal $b_1^u(k)$ from the received signal $r_{11}(k)$. The rest of the receiver processing – calculation of log-likelihood ratio, deinterleaving, and turbo decoding – is the same as the PSAM scheme described before in this chapter.

In the iterative channel estimation, the samples in the pilot branch and data branch of each Rake finger are combined to obtain a new estimate of the channel state information. In particular, if we assume a perfect feedback from the turbo decoder, we can reconstruct the transmitted data sequence $\{\hat{b}_1^u(k)\}$. By resolving $h_{11}^u(k)$ from (3.43), we have

$$
\begin{cases}
\xi_{1l}^1(k) &= \left(|\hat{b}_1(k)|^2 + |\hat{b}_1(k+1)|^2\right) h_{1l}^1(k) + \hat{b}_1^*(k) i_{1l}(k) \\
&\quad - \hat{b}_1(k+1) i_{1l}(k+1); \\
\xi_{1l}^2(k) &= \left(|\hat{b}_1(k)|^2 + |\hat{b}_1(k+1)|^2\right) h_{1l}^2(k) + \hat{b}_1^*(k+1) i_{1l}(k) \\
&\quad + \hat{b}_1(k) i_{1l}(k+1).
\end{cases}
\tag{3.48}
$$

We can combine (3.47) and (3.48) to form a new sequence with maximal SNR for iterative channel estimation

$$
\begin{cases}
\zeta_{1l}^1(k) = \sqrt{1 - r_p}\, \xi_{1l}^1(k) + \sqrt{r_p}\, \xi_{1l,p}^1(k); \\
\zeta_{1l}^2(k) = \sqrt{1 - r_p}\, \xi_{1l}^2(k) + \sqrt{r_p}\, \xi_{1l,p}^2(k),
\end{cases}
\tag{3.49}
$$

where $r_p$ is the ratio of the average pilot energy over the total energy (including both pilot and data signals) per symbol. Therefore $\{\zeta_{1l}^1(k)\}$ can be used to

estimate the channel state information for path $(1, l), l = 1, 2, \cdots, L$ and $\{\zeta_{1l}^1(k)\}$ for path $(2, l)$, $l = 1, 2, \cdots, L$.

### 3.2.5   Simulation Results
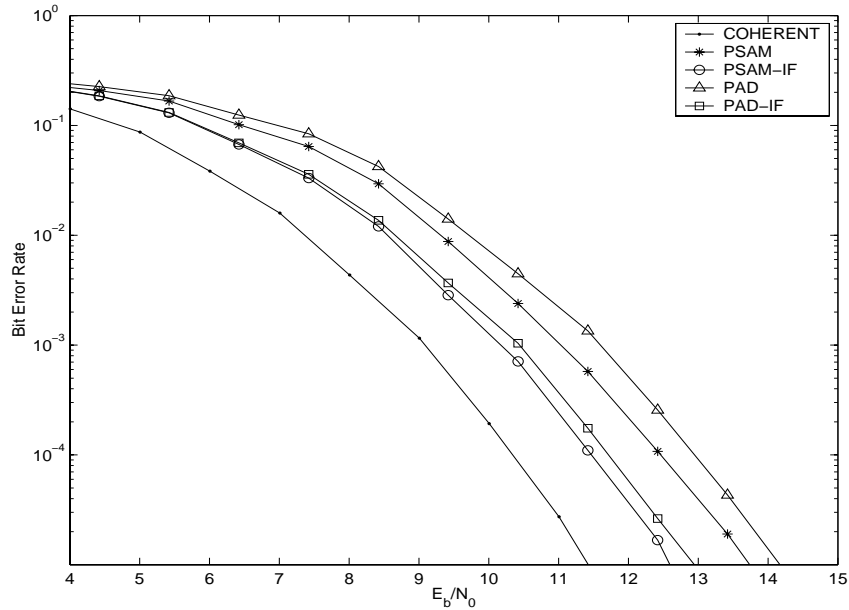


Figure 3.8: Bit Error Rate Performance of Turbo Coded QAM: 1 TX antenna, L = 1

Simulation results are shown in Fig. 3.8 – 3.17. At the transmitter side, we have simulated $1 - 2$ transmit antennas; at the receiver side, we have simulated $1, 2, 3, 4, 6, 8$ fingers separately. We assume that all transmission paths are mutually independent, subject to the same Doppler frequency, and have the same statistics: mean, variance. For each case, we simulated 5 receivers: CO-HERENT, PSAM, PSAM with iterative filtering (PSAM-IF), PAD, PAD with iterative filtering (PAD-IF). In the case of one transmit antenna, one pilot symbols are inserted every ten data symbols; while in the case of two transmission antennas, two pilot symbols are inserted every ten data symbols. We also add
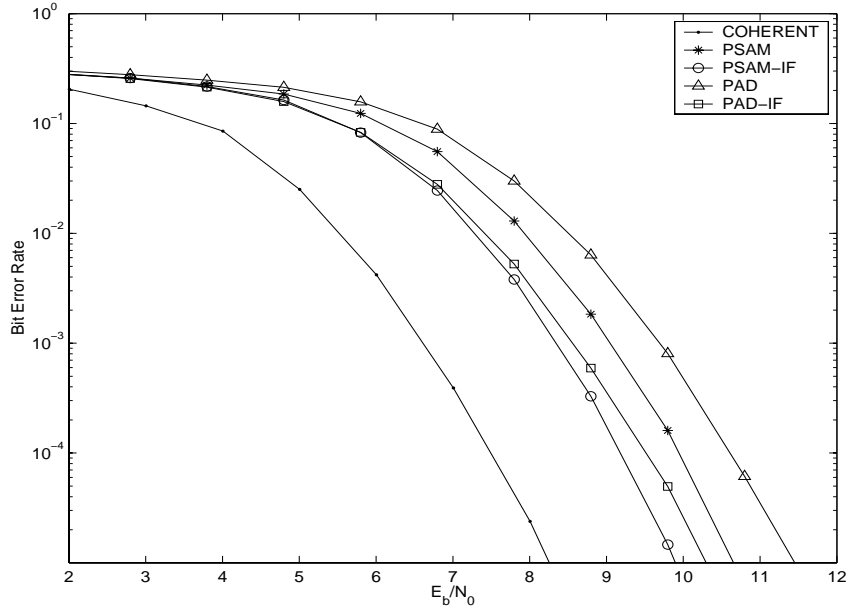
Figure 3.9: Bit Error Rate Performance of Turbo Coded QAM: 2 TX antenna, $L = 1$

one additional pair of pilot symbols so there are pilot symbols at the beginning and at the end of a packet. For PAD, we adjust the power ratio of the pilot signal over the data signal so the pilot signal consumes the same amount of power as pilot symbols in PSAM. The spreading sequences are Gold sequences from [48]. For the pilot signal, the spreading sequence is

$$0, 0, 0, 0, 1, 0, 1, 0, 1, 0, 1, 1, 1, 1, 0, 0, 0, 0, 1, 0, 1, 0, 0, 0, 0, 1, 1, 0, 0, 0, 1.$$

For the data signal, the spreading sequence is

$$1, 1, 0, 1, 1, 1, 1, 0, 1, 1, 0, 0, 1, 0, 1, 1, 1, 1, 1, 0, 0, 0, 0, 1, 1, 1, 1, 0, 0, 1, 1.$$

The sequence length or processing gain is 31. And the rest of simulation parameters are the same as the previous section unless otherwise specified.
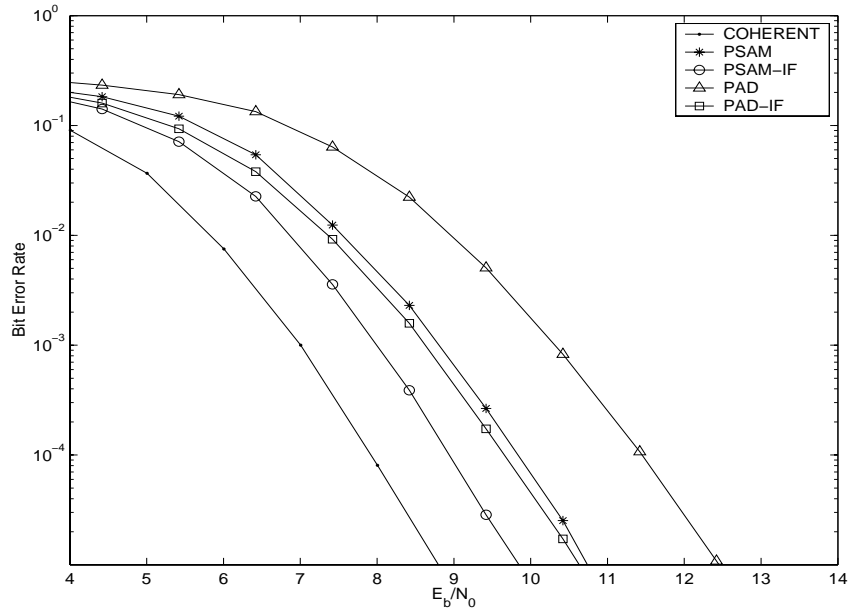
Figure 3.10: Bit Error Rate Performance of Turbo Coded QAM: 1 TX antenna, $L = 2$
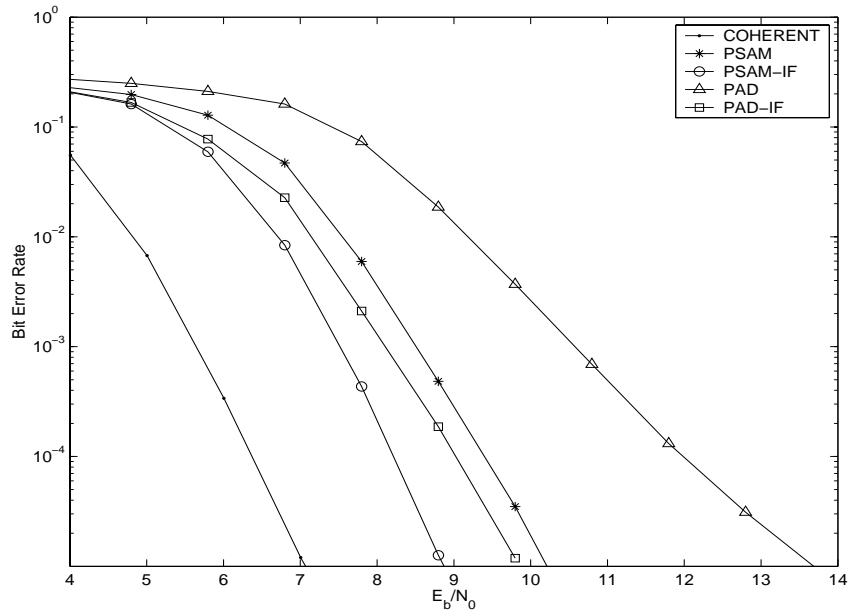


Figure 3.11: Bit Error Rate Performance of Turbo Coded QAM: 2 TX antenna, $L = 2$
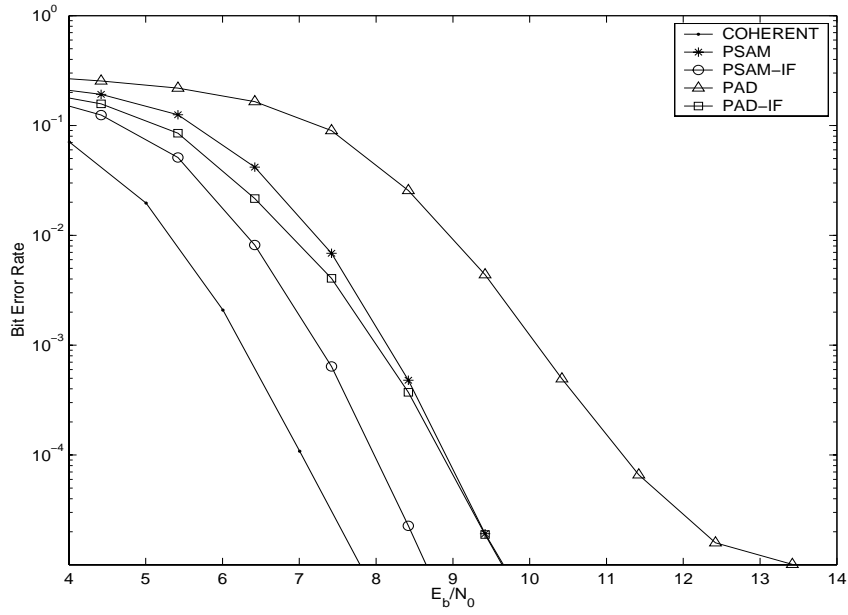
Figure 3.12: Bit Error Rate Performance of Turbo Coded QAM: 1 TX antenna, L = 3
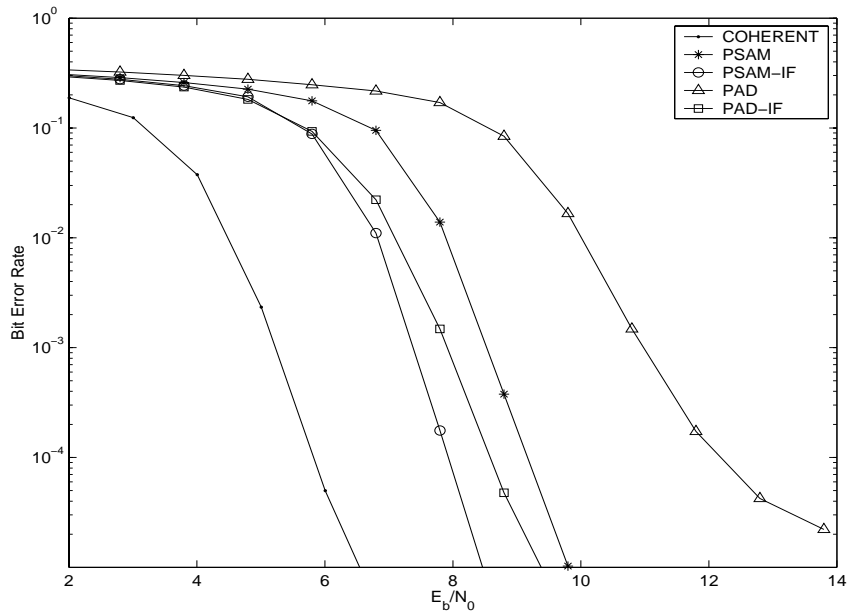


Figure 3.13: Bit Error Rate Performance of Turbo Coded QAM: 2 TX antenna, L = 3
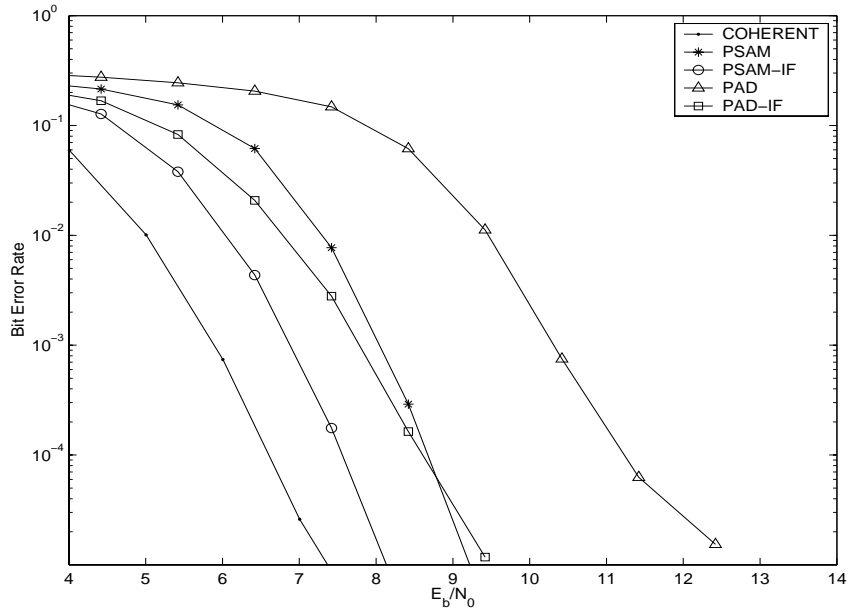
Figure 3.14: Bit Error Rate Performance of Turbo Coded QAM: 1 TX antenna, $L = 4$
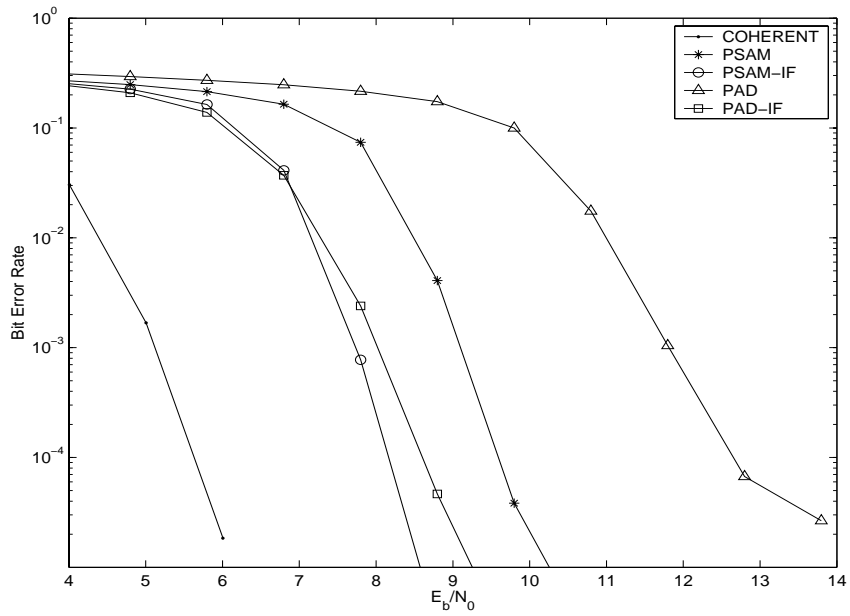


Figure 3.15: Bit Error Rate Performance of Turbo Coded QAM: 2 TX antenna, $L = 4$
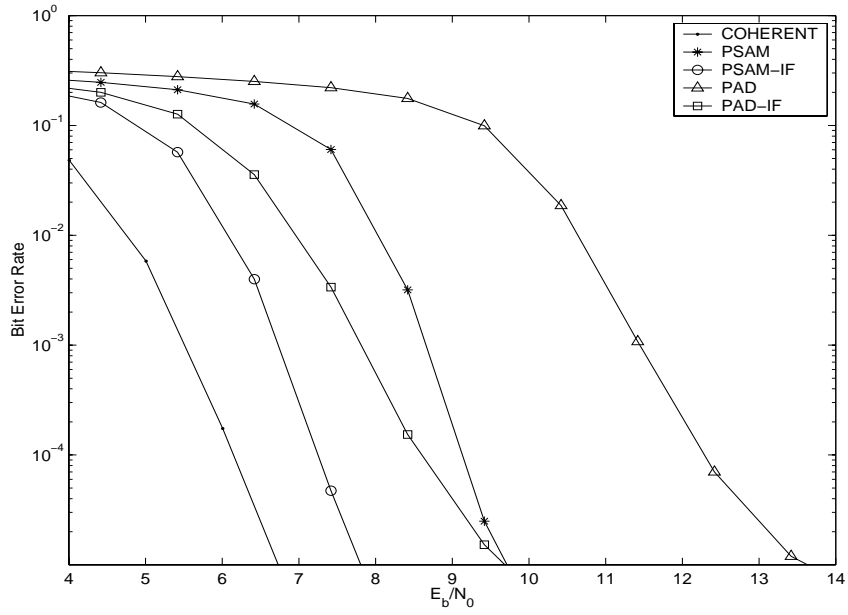
Figure 3.16: Bit Error Rate Performance of Turbo Coded QAM: 1 TX antenna,

L = 6
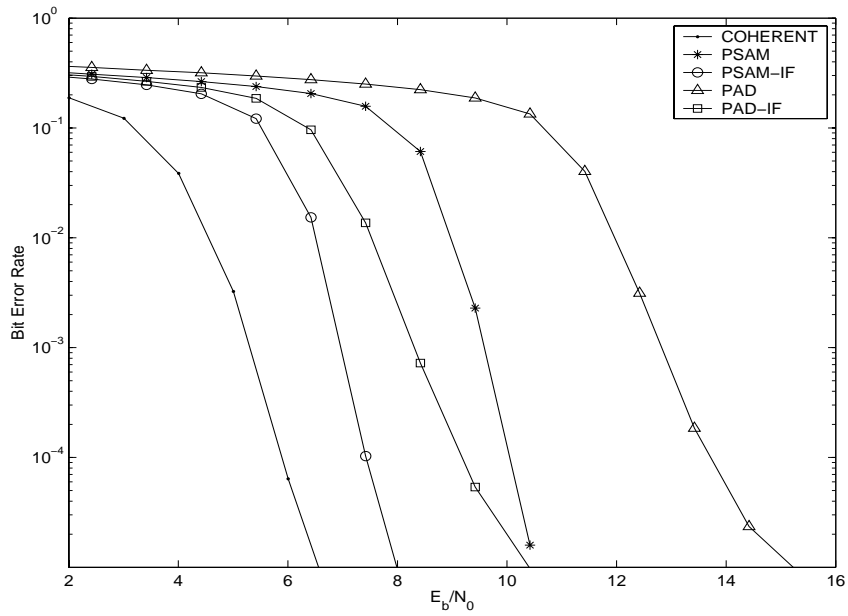


Figure 3.17: Bit Error Rate Performance of Turbo Coded QAM: 1 TX antenna,

L = 8

From all these figures, we can see that PSAM performs better than PAD in call cases. PSAM's advantage become more obvious as the number of paths goes high. In Fig. 3.8 where there is only one transmission path, the difference between PSAM and PAD in SNR at $10^{-4}$ BER is only about 0.3 dB, while in Fig. 3.15 and Fig. 3.17, where there are a total of eight transmission paths, the difference is more than 3.0 dB. This is because the initial channel estimation is very poor in PAD due to low SNR in pilot channel. As the number of paths increases, multipath interference increases and further reduces the SNR in pilot channel.

Another observation is that iterative channel estimation always provided remarkable performance improvement. The improvement becomes larger with the number of paths. In the case of single transmit antenna, the gain provided by iterative channel estimation for PSAM increases from about 1.0 dB at $10^{-4}$ BER when there is only one transmission path to more than 2.0 dB when there are eight transmission paths; for PAD, the gain ranges from about 1.2 dB to more than 3.0 dB. When there are transmit diversity, we observe the same trend but the gain is not as large for PSAM.

As the number of paths increases, the performance of PSAM, PSAM-IF, PAD, and PAD-IF all improves initially, reaches peak at some point, and then starts to degrade. For single transmission antenna, their performance reaches peak when $L = 4$; for two transmit antennas, it happens when $L = 3$. The reason is that when the number of paths increases, so does the order of diversity. But with further increase, the channel estimation error will increase due to the reduced signal power and increased multipath interference at each path; on the other hand, the gain provided by the increase in diversity order will be less

obvious as can be seen in the BER of COHERENT receiver in Fig. 3.16 – 3.17. At a certain point, the channel estimation error will more than offset the diversity gain when the number of paths increases.

The space-time code provides remarkable gains in BER performance only when the number of paths to the Rake receiver per transmit antenna is small. When $L = 1$, transmit diversity provides significant gain for all receivers. It is larger compared to the results of receive diversity in Fig. 3.10 even though the diversity orders are the same. This is because with transmit diversity, diversity is achieved by resolving signals from two parallel paths so the additional paths created by the additional transmit antenna do not introduce multipath interference. While in the case of receive diversity, multiple paths interfere with each other in the form of multipath interference. Although Gold sequences have excellent cross-correlation property, their auto-correlation property are not as good as maximal length sequences. As a result, Gold sequences are more vulnerable to multipath interference than maximal length sequences.

When $L$ is large, except the COHERENT receiver, in which the channel state information are assumed to be perfectly known, the performance of all other receivers actually deteriorates, especially for PAD. The reason is that distributing the transmission power over more paths degrades the SNR and subsequently degrades the channel estimation. In the case when there are multiple transmission paths between any pair of transmit and receive antennas, the system may achieve better performance by concentrating the power in one transmit antenna.

## 3.3 Conclusions

In this chapter, we have proposed joint iterative channel estimation and decoding systems for turbo-coded pilot symbol-assisted QAM systems over Doppler fading channels. We have considered both the flat-fading channel and the multipath channel. In the flat-fading channel, our focus is on how to design low complexity, power and bandwidth efficient, joint detection and decoding schemes for pilot symbol-assisted modulation. We have considered two schemes based on data reconstruction and iterative channel estimation. The first is a threshold-controlled iterative channel estimation scheme in which decisions from the channel decoder are selected for data reconstruction by their reliability values. We have simulated the scheme using a range of threshold values and determined that the best result is achieved at very low threshold values. To reduce the polynomial complexity of the threshold-controlled scheme, we propose another simplified joint detection and decoding scheme that have similar performance with only linear complexity.

In the multipath channel, our focus is on the comparison between pilot symbol-assisted demodulation and pilot-aided demodulation under various transmit and receive diversity scenarios. From the simulation results, some conclusions can be drawn. First, iterative channel estimation always provides remarkable performance improvement. Second, space-time code should only be used when $L$ is small; the system can achieve better performance by using only one transmit antenna when there are multiple transmission paths available. Third, as the number of paths increases, the performance of PSAM, PSAM-IF, PAD, and PAD-IF all improves initially, reaches peak at some point, and then starts to degrade. Fourth, PSAM always performs better than PAD, and PSAM-IF performs better than PAD-IF at medium or higher normalized Doppler frequency.

Although we have only simulated PSAM, PSAM-IF , PAD, PAD-IF under fixed complexity, the results would also be in favor of PSAM and PSAM-IF if we use the same pilot energy, i.e., using a larger window for PAD so that the pilot energy in this window is the same as the energy of pilot symbols used in PSAM. Because in this case, the complexity of the PAD will be much higher due to larger number of filter taps. When the normalized Doppler frequency is smaller than 0.001, however, the PAD filter can be replaced by a simple integrator. In this case, PAD and PAD-IF will have similar performance to PSAM and PSAM-IF with comparable complexity. So we conclude that while PSAM and PSAM-IF perform similarly to PAD and PAD-IF respectively at low normalized Doppler frequency (smaller than 0.001), PSAM and PSAM-IF are better choices for DS-CDMA systems at medium (0.005) or higher normalized Doppler frequency.

# Chapter 4

# Anti-Jamming Multicarrier Communication Systems

In this chapter, we investigate the anti-jamming design of frequency-hopped multicarrier communication systems. Multicarrier modulation is a form of frequency-division multiplexed (FDM) group-band. It divides the transmitted data into $B$ bit streams to modulate $B$ frequency carriers. The modulated carriers are summed for transmission, and must be separated at the receiver before demodulation. According to [21], there are three methods used for this separation: FDM filtering, overlapping staggered quadrature amplitude modulation (SQAM), and QAM with the sinc function, which has the advantage that both the transmitter and the receiver can be implemented using Fast Fourier Transform (FFT) techniques.

We consider two types of jamming signals – partial-band tone jamming and partial-time pulse jamming. Due to lack of separation between neighboring carriers, both the second and the third method are vulnerable to partial-band tone jamming because one jamming tone will not only jam the signal in the subchannel that the tone falls in, it will also jam neighboring subchannels. When there

are multiple jamming tones, they mix with each other, rendering the estimation and cancellation of jamming signals virtually impossible. So we only consider multicarrier modulation with FDM filtering. The design for partial-time pulse jamming, however, is not subject to this limit and is applicable to general multicarrier systems.

Most of the anti-jamming designs for communication systems rely on spread-spectrum techniques such as DS-CDMA or frequency-hopping. In DS-CDMA, the main focus has been on exploiting the processing gain to reduce the performance loss caused by the jamming; in frequency-hopping, the focus has been on avoiding the jamming signal by transmitting the data signal in the bandwidth free of jamming.

For multicarrier systems, anti-jamming design has received little attention in literature so far. In [49], a special complex sequence – complex quadratic sequence is proposed as the frequency-spreading sequence for multicarrier spread spectrum (MC-SS) modulation scheme. The resulting MC-SS signal has constant envelope in both time and frequency domains. The presence of the jamming signal is determined by monitoring the power level, which requires both the knowledge of the data signal power and the jamming signal power. Another shortcoming is that this detection scheme is not suitable for the fading channel, in which the instantaneous received power of both the data signal and the jamming signal could vary greatly. They also made no effort in estimating the jamming frequency and canceling the jamming signal.

Our design, however, is much more efficient and challenging. First, instead of frequency spreading, all multicarrier subchannels except pilot subchannels are used for data transmission so our system has much higher single user throughput.

For a single user, $B$ data symbols are transmitted in one symbol period in our system while only one symbol is transmitted in their system. Second, our scheme is to detect, estimate and cancel jamming signals in both time and frequency directions in both the AWGN and the fading channels, which is much more challenging than simple detection in the AWGN channel. Third, the central carrier frequency of our multicarrier signal hops from one band to another so that the deliberate jammer have to spread the jamming power over the entire frequency-hopped bandwidth. Therefore, only a small portion of the subchannels will be jammed at the same time. This, however, poses additional difficulty for jamming detection and estimation as the receiver only has limited observation period for the jamming period.

We start with detection and estimation of jamming signals in the additive white Gaussian noise (AWGN) channel. Upon receiving the data signal distorted by the jamming, the receiver first detects the presence of jamming signals by computing the eigenvalue spread of the autocorrelation matrix in all subchannels. If the receiver determines that a particular subchannel has been jammed, it will go ahead to estimate the jamming signal and cancel it from the received signal. The receiver will then demodulate and decode the received signal as without jamming signals. To further improve the performance, the receiver feedback the information from the decoder output and make use of the reconstructed data signal to enhance jamming detection and estimation. From the second iteration, the receiver uses a correlation detector to generate soft decisions on the jamming state so the performance can be further improved.

As for the problem of frequency estimation, there have been a rich dedicated literature in the area of signal processing. They range from classical methods like

periodogram, maximum entropy, linear regression [50], etc., to subspace-based super resolution algorithm, such as MUSIC (MUltiple SIgnal Classification) [51] and ESPRIT (Estimation of Signal Parameters Via Rotational Invariance Techniques) [52], etc. We choose the ESPRIT algorithm due to its high resolution and ease of computation. More information on frequency estimation methods can be found in [51] and [53].

Next we will move on to the multipath fading channel with Doppler spread. After the detection, estimation and subsequent cancellation of jamming signals, the receiver must estimate the channel state information for coherent demodulation. For this purpose, pilot symbols are inserted periodically in the encoded data stream for the estimation of time-variant channel state information (CSI) at the receiver. An important issue is that the pilot symbol sequence must be specially designed in a jamming environment so that its characteristics is different from that of the jamming signal. Because pilot symbols provide crucial references for the channel estimation and demodulation, it is also required that pilot symbol sequences are robust to jamming cancellation processing.

Compared to the serial data system in which only a single channel gain needs to be estimated at each symbol period, the channel gain of all subchannels must be estimated simultaneously in the multicarrier system for coherent demodulation. The decoder uses this estimated channel state information, together with the received data sequence, to generate soft decisions for each data symbol. These soft decisions are then feedback so they can be used in the iterative detection and estimation of jamming signals as well as in the iterative processing of channel state information and most importantly, data signals.

Since partial-time pulse jamming is a dual problem of partial-band tone jam-

ming, so we will use partial-band tone jamming to illustrate the anti-jamming design for the most part of the chapter. The outline of this chapter is as follows. Section 4.1 describes multicarrier signals, multipath fading channel, and jamming signal models. Section 4.2 presents anti-jamming design against partial-band tone jamming signals in both AWGN and fading channels. Section 4.3 is dedicated to the subsequent processing after jamming signal estimation and cancellation – iterative demodulation and decoding of MPSK signals with pilot symbol-assisted modulation. Simulation results are presented and discussed in Section 4.4. Finally, we conclude this chapter in Section 4.5.

## 4.1  Signal, Channel and Jamming Models

In this section, we model the multicarrier signals, the channel and the jamming signals. We start with the multicarrier signal. Then we move on to the fading channel model. Although we also consider the AWGN channel in this chapter, we will not discuss it specifically due to its simplicity. At last, we present two types of jamming models: partial-band tone jamming and partial-time pulse jamming.

### 4.1.1  Signal Model

According to [54], the transmitted signal in subcarrier $b$ is given by

$$
\begin{aligned}
x_b(t) \ = \ & \sum_{l=-\infty}^{+\infty} \xi(b,l)s(t-lT)\cos 2\pi f_b t \\
& - \sum_{l=-\infty}^{+\infty} \eta(b,l)s(t-lT)\sin 2\pi f_b t
\end{aligned}
\tag{4.1}
$$

where $\xi(b,l)$ and $\eta(b,l)$ are real and imaginary parts of the $l$th transmitted symbol in an MPSK constellation. $T$ is the symbol period, $l$ is discrete time index, and $f_b = f_0 + Wb$ is the carrier frequency of the $b$th subchannel, $W$ is the frequency separation between two carriers. $s(t)$, $t \in [0, T]$ is the shaping pulse and $s(t) = 0$, $t \notin [0, T]$. The energy of $s(t)$ is normalized to 1, i.e.,

$$\int_0^T s^2(t) = 1. \tag{4.2}$$

The receiver uses a matched filter $h(t) = s(T - t)$, $0 \le t \le T$ at each carrier to demodulate the signal. If we ignore the signal components from other carriers, the output of the matched filter in carrier $b$ due to the data signal is given by

$$
\begin{aligned}
\Re\{y_s(b,(l+1)T)\} &= \int_{lT}^{(l+1)T} \Re\{2\,x_b(\tau)\exp(-i2\pi f_b\tau)\}h((l+1)T - \tau)\,d\tau \\
&= \int_{lT}^{(l+1)T} \sum_{k=-\infty}^{\infty} \xi(b,k)s(\tau - kT)s(\tau - lT)\,d\tau \\
&= \xi(b,l)\int_{lT}^{(l+1)T} s^2(\tau - lT)\,d\tau \\
&= \xi(b,l)\int_0^T s^2(t)\,dt \\
&= \xi(b,l), \tag{4.3} \\
\Im\{y_s(b,(l+1)T)\} &= \int_{lT}^{(l+1)T} \Im\{2\,x_b(\tau)\exp(-i2\pi f_b\tau)\}h((l+1)T - \tau)\,d\tau \\
&= \eta(b,l). \tag{4.4}
\end{aligned}
$$

In the AWGN channel, the channel gain is constant throughout the entire bandwidth. In the multipath fading channel, we assume that the channel gain is flat in each subchannel of the multicarrier system but frequency-selective from one subchannel to another. In the frequency-domain, the received data symbol of $b$th subchannel at time $l$ can be written as

$$Y(b,l) = H(b,l)X(b,l) + N(b,l), \tag{4.5}$$

where $X(b,l) = \xi(b,l) + i\,\eta(b,l)$ is the transmitted data symbol in subchannel $b$ at time $l$; $H(b,l)$ is the complex channel gain of data signals in $b$th subchannel at time $l$; $N(b,l)$ is an additive white Gaussian noise with power spectrum density $N_0$.

In the presence of jamming, the received signal in the frequency domain is given by

$$Y(b,l) = H(b,l)X(b,l) + H^J(b,l)I(b,l)J(b,l) + N(b,l), \qquad (4.6)$$

where $I(b,l)$ is the indicator function of the jamming signal; $J(b,l)$ is the received jamming signal; $H^J(b,l)$ is the complex channel gain of jamming signals in $b$th subchannel at time $lT$.

## 4.1.2  Rayleigh Fading Channel Model

The complex baseband representation of a multipath channel impulse response can be written as

$$h(t,\tau) = \sum_p c_p(t)\delta(\tau - \tau_p), \qquad (4.7)$$

where $p$ is the index of the multiple propagation path; $\tau_p$ is the delay of the $p$th path; and $c_p(t)$ is the complex amplitude of the $p$th path which incorporates the propagation loss, shadowing effect, and the phase rotation caused by the delay $\tau_p$. In most of wireless channels, the attenuation and phase of one path are uncorrelated with those of another path; and $c_p(t)$'s can be modeled as wide-sense stationary complex Gaussian stochastic processes. We assume that all the paths have identical correlation function except their differences in power level. Thus,

$$E[c_p(t + \Delta t)c_p^*(t)] = \sigma_p^2 \phi_t(\Delta t), \qquad (4.8)$$

90

where $\sigma_p^2$ is the average power of the $p$th path and $\phi_t(\Delta t)$ is the time-domain correlation function. Let $H(t, f)$ be the frequency response of the time-varying channel impulse response $h(t, \tau)$:

$$
\begin{aligned}
H(t, f) &= \int_{-\infty}^{\infty} h(t, \tau) e^{-j2\pi f \tau} d\tau \\
&= \sum_p c_p(t) e^{-j2\pi f \tau_p}.
\end{aligned} \tag{4.9}
$$

The space-time, space-frequency correlation function of the multipath channel can be written as

$$
\begin{aligned}
\phi(\Delta t, \Delta f) &= E[H(t + \Delta t, f + \Delta f)H^*(t, f)] \\
&= \phi_t(\Delta t)\phi_f(\Delta f), \tag{4.10}
\end{aligned}
$$

where $\phi_f(\Delta f) = \sum_p \sigma_p^2 e^{-j2\pi \Delta f \tau_p}$. So the space-time, space-frequency correlation can be separated into a time-domain correlation $\phi_t(\Delta t)$ and a frequency-domain correlation $\phi_f(\Delta f)$. The frequency-domain correlation is dependent on the multipath delay profile, while the time-domain correlation is dependent on the vehicle speed and the carrier frequency.

### 4.1.3 Jamming Models

*Partial-Band Tone Jamming*   The partial-band tone jamming signal is given by

$$
\begin{aligned}
j_t(t) &= \sum_b A_t(b) \cos\left[2\pi(f_b + \Delta f_b)t + \phi_b\right] \\
&= \sum_b A_t(b) \cos\left(2\pi\Delta f_b t + \phi_b\right) \cos 2\pi f_b t \\
&\quad - \sum_b A_t(b) \sin\left(2\pi\Delta f_b t + \phi_b\right) \sin 2\pi f_b t \tag{4.11}
\end{aligned}
$$

where $-\frac{W}{2} \leq \Delta f_b \leq \frac{W}{2}$ is the frequency difference between the jamming tone and the $b$th carrier. $\phi_b$ is the initial phase. $A_t(b) \in \{0, A_t\}$, where $A_t$ is the

amplitude of the jamming tone. Here we assume that all the jamming tones have the same power.

We also assume that the frequency separation between two jamming tones is larger than that between two neighboring carriers, which is a reasonable one because in order to effectively jam a frequency-hopped multicarrier system, the jammer has to spread the jamming tones over the entire bandwidth so the frequency separation between two jamming tones cannot be small. Under this assumption, there is at most one jamming tone in each subchannel.

Suppose there is a jamming tone with frequency $f_b + \Delta f_b$, $\Delta f_b \in [-\frac{W}{2}, \frac{W}{2}]$, the output of the matched filters due to the multi-tone jamming signal can be written as

$$
\begin{aligned}
y_t(b, (l+1)T) &= \int_{lT}^{(l+1)T} 2\, j_b(\tau) \exp(-i2\pi f_b \tau) h((l+1)T - \tau)\, d\tau \\
&= \int_{lT}^{(l+1)T} A_t \exp\left[-i(2\pi\Delta f_b \tau + \phi_b)\right] h((l+1)T - \tau)\, d\tau \\
&= \int_{lT}^{(l+1)T} A_t \exp\left(-i\phi_b\right) \exp\left(-i2\pi\Delta f_b \tau\right) s(\tau - lT)\, d\tau \\
&= A_t \exp\left\{-i[2\pi\Delta f_b lT + \phi_b]\right\} \int_0^T s(t) \exp\left(-i2\pi\Delta f_b t\right)\, dt \\
&= A_t \exp\left\{-i[\omega_b l + \phi_b]\right\} S(\Delta f_b) \tag{4.12}
\end{aligned}
$$

where $\omega_b = 2\pi\Delta f_b T$. Because the frequency sub-bands are completely separated by filters, there are no jamming signals leaking from other sub-bands. Define $A_1(b) \triangleq A_t\, S(\Delta f_b)$. The frequency-domain received signal in the AWGN channel can be written as

$$
J(b, l) = y_t(b, (l+1)T) = A_1(b) \exp\{-i[\omega_b l + \phi_b]\}. \tag{4.13}
$$

In fading channels, the received jamming signal becomes $H^J(b, l) J(b, l)$, where

$H^J(b, l)$ is the channel gain for the jamming signal. Here we assume that the data channel and the jamming channel have the same statistics.

*Partial-Time Pulse Jamming*   The partial-time pulse jamming signal is given by

$$j_p(t) = \sum_{k=-\infty}^{\infty} A_p\, \delta(t - t_k), \tag{4.14}$$

We assume that the pulse jamming signal covers the entire frequency-hopped bandwidth and that the pulse is sufficiently short in time so that its frequency spectrum is constant over all multicarrier subchannels. We also assume that the time interval between two neighboring pulses are greater than the symbol period, i.e., $|t_l - t_{l+1}| > T$, $\forall l$ so that there is at most one jamming pulse within each symbol period. We further model the jamming state in a symbol period as a Bernoulli random variable, i.e., with probability $\alpha$, the pulse jammer transmits a single pulse with a power $P_J T/\alpha = A_p^2$ in a symbol period.

Suppose $lT \leq t_l \leq (l+1)T$, the output of the matched filter due to the pulse jamming signal can be written as

$$
\begin{aligned}
y_p(b, (l+1)T) &= \int_{lT}^{(l+1)T} 2\, j_p(t) \exp\left(-i2\pi f_b \tau\right) h((l+1)T - \tau)\, d\tau \\
&= \int_{lT}^{(l+1)T} 2 \sum_{k=-\infty}^{\infty} A_p\, \delta(\tau - t_k) \exp\left(-i2\pi f_b \tau\right) s(\tau - lT) d\tau \\
&= \int_{lT}^{(l+1)T} 2\, A_p\, \delta(\tau - t_l) \exp\left(-i2\pi f_b \tau\right) s(\tau - lT) d\tau \\
&= 2\, A_p \exp\left(-i2\pi f_b t_l\right) s(t_l - lT) \\
&= 2\, A_p \exp\left\{-i2\pi [f_0 + Wb] t_l\right\} s(t_l - lT) \\
&= 2\, A_p \exp\left\{-i[2\pi W t_l b + 2\pi f_0 t_l]\right\} s(t_l - lT) \\
&= 2\, A_p s(t_l - lT) \exp\left\{-i[\omega_l b + \phi_l]\right\}, \tag{4.15}
\end{aligned}
$$

93

where $\omega_l = 2\pi W t_l$ and $\phi_l = 2\pi f_0 t_l$. Define $A_2(l) \overset{\Delta}{=} 2A_p s(t_l - lT)$. In the additive white Gaussian channel with a unit channel gain, the received jamming signal is simply

$$J(b,l) = y_p(b,(l+1)T) = A_2(l) \exp\left\{-i[\omega_l b + \phi_l]\right\}. \tag{4.16}$$

The received pulse jamming signal becomes $H^J(b,l)J(b,l)$ in fading channels. As we have seen, partial-time pulse jamming is a dual problem of partial-band tone jamming, so we will use partial-band tone jamming to illustrate the anti-jamming design in the rest of the chapter.

## 4.2 Jamming Detection, Estimation and Cancellation in AWGN and Fading Channels

In this section, we consider detection and estimation of partial-band tone jamming signals for each subchannel. We first study the problem in the AWGN channel. Then we move to the fading channel.

### 4.2.1 Detection of Jamming Signals in the AWGN Channel

We first consider the multi-tone jamming in the AWGN channel. For $l = 0, \cdots, L-1$,

$$I^t(b) = 0 : Y(b,l) = X(b,l) + N(b,l),$$

$$I^t(b) = 1 : Y(b,l) = X(b,l) + A_1(b)\exp(-i\omega_b l)\exp(-i\phi_b) + N(b,l), \tag{4.17}$$

where

$$I^t(b) \in \{0,1\},$$

$$\omega_b, \phi_b \in [0, 2\pi],$$

$$X(b,l) \in \left\{ \exp\left(i\frac{\pi}{M}\right), \exp\left(i\frac{3\pi}{M}\right), \cdots, \exp\left(i\frac{(2M-1)\pi}{M}\right) \right\}.$$

For simplicity, we assume that the shaping pulse has a flat spectrum within the subchannel, i.e., $S(\Delta f_b) = $ constant. Under this assumption, $A_1(b) = A_1$. We define the jamming-to-signal ratio as

$$J/S \triangleq \frac{\alpha A_1^2}{E\left[|H(b,l)X(b,l)|^2\right]} = \frac{\alpha A_1^2}{E\left[|H(b,l)|^2\right] E\left[|X(b,l)|^2\right]}. \tag{4.18}$$

*Optimal Detection* For any matrix element $V(b,l)$, let $\underline{V}^t(b) = [V(b,0), \cdots, V(b, L-1)]^T$. Define

$$\Theta \triangleq \left[I^t(b), \underline{X}^t(b), \omega_b, \phi_b\right]^T. \tag{4.19}$$

The parameter set $\Gamma = \{0,1\} \times S^L \times [0, 2\pi]^2$. Let $\underline{x}_0^t, \cdots, \underline{x}_{M^L-1}^t$ represent $M^L$ $M$-ary sequence of length $L$. For convenience, we make the following definitions

$$\Gamma_{0,0} = \left\{ \Theta \in \Gamma | I^t(b) = 0, \underline{X}^t(b) = \underline{x}_0^t \right\},$$

$$\vdots$$

$$\Gamma_{0,M^L-1} = \left\{ \Theta \in \Gamma | I^t(b) = 0, \underline{X}^t(b) = \underline{x}_{M^L-1}^t \right\},$$

$$\Gamma_{1,0} = \left\{ \Theta \in \Gamma | I^t(b) = 1, \underline{X}^t(b) = \underline{x}_0^t \right\},$$

$$\vdots$$

$$\Gamma_{1,M^L-1} = \left\{ \Theta \in \Gamma | I^t(b) = 1, \underline{X}^t(b) = \underline{x}_{M^L-1}^t \right\}. \tag{4.20}$$

Because $N(b,0), \cdots, N(b, L-1)$ are i. i. d. Gaussian random variables with $N(b,l) \sim \mathcal{N}(0, 2\sigma^2)$, $l = 0, \cdots, L-1$. For $\Theta \in \Gamma_{0,i}$, the conditional probability $p(\underline{Y}^t(b) = \underline{y}^t(b) | \Theta \in \Gamma_{0,i})$ is given by

$$p(\underline{Y}^t(b) = \underline{y}^t(b) | \Theta \in \Gamma_{0,i}) = \frac{1}{(2\pi\sigma^2)^L} \exp\left\{ -\frac{||\underline{y}^t(b) - \underline{x}_i^t||}{2\sigma^2} \right\}. \tag{4.21}$$

We assume that the initial phase $\phi_b$ is uniformly distributed in $[0, 2\pi]$ and that $\Delta f_b$ is uniformly distributed in $[-\frac{W}{2}, \frac{W}{2}]$. Hence $\omega_b$ is also uniformly distributed in $[-\pi, \pi]$, or equivalently, in $[0, 2\pi]$. For $\Theta \in \Gamma_{1,i}$, the conditional probability $p(\underline{Y}^t(b) = \underline{y}^t(b) | \Theta \in \Gamma_{1,i})$ is given by

$$p(\underline{Y}^t(b) = \underline{y}^t(b) | \Theta \in \Gamma_{1,i}) =$$
$$\frac{1}{4\pi^2} \int_0^{2\pi} \int_0^{2\pi} \frac{1}{(2\pi\sigma^2)^L} \exp\left\{ -\frac{||\underline{y}^t(b) - \underline{x}_i^t - A_1 \exp(-i\underline{\omega}_b) \exp(-i\phi_b)||}{2\sigma^2} \right\} d\omega_b d\phi_b,$$

(4.22)

where

$$\underline{\omega}_b = [0, \omega_b, \cdots, (L-1)\omega_b]^T.$$

(4.23)

The jamming state $I^t(b)$ can be detected by

$$
\begin{aligned}
L_{t,1} &= \frac{P\{I^t(b) = 1 | \underline{Y}^t(b) = \underline{y}^t(b)\}}{P\{I^t(b) = 0 | \underline{Y}^t(b) = \underline{y}^t(b)\}} \\
&= \frac{P\{\underline{Y}^t(b) = \underline{y}^t(b) | I^t(b) = 1\} P\{I^t(b) = 1\}}{P\{\underline{Y}^t(b) = \underline{y}^t(b) | I^t(b) = 0\} P\{I^t(b) = 0\}} \\
&= \frac{\sum_{\underline{x}_i^t} P\{\underline{Y}^t(b) = \underline{y}^t(b), \underline{X}^t(b) = \underline{x}_i^t | I^t(b) = 1\} P\{I^t(b) = 1\}}{\sum_{\underline{x}_i^t} P\{\underline{Y}^t(b) = \underline{y}^t(b), \underline{X}^t(b) = \underline{x}_i^t | I^t(b) = 0\} P\{I^t(b) = 0\}} \\
&= \frac{\sum_{\underline{x}_i^t} P\{\underline{Y}^t(b) = \underline{y}^t(b) | \underline{X}^t(b) = \underline{x}_i^t, I^t(b) = 1\} P\{\underline{X}^t(b) = \underline{x}_i^t\} P\{I^t(b) = 1\}}{\sum_{\underline{x}_i^t} P\{\underline{Y}^t(b) = \underline{y}^t(b) | \underline{X}^t(b) = \underline{x}_i^t, I^t(b) = 0\} P\{\underline{X}^t(b) = \underline{x}_i^t\} P\{I^t(b) = 0\}}
\end{aligned}
$$

(4.24)

Since $P\{\underline{X}^t(b) = \underline{x}_i^t\} = 1/M_L$, $\forall i$, we have

$$
\begin{aligned}
L_{t,1} &= \frac{P\{I^t(b) = 1 | \underline{Y}^t(b) = \underline{y}^t(b)\}}{P\{I^t(b) = 0 | \underline{Y}^t(b) = \underline{y}^t(b)\}} \\
&= \frac{\sum_{i=0}^{M^L-1} P\{\underline{Y}^t(b) = \underline{y}^t(b) | \Theta \in \Gamma_{1,i}\} P\{I^t(b) = 1\}}{\sum_{i=0}^{M^L-1} P\{\underline{Y}^t(b) = \underline{y}^t(b) | \Theta \in \Gamma_{0,i}\} P\{I^t(b) = 0\}} \gtrless 1.
\end{aligned}
$$

(4.25)

Although $L_{t,1}$ is the optimal detection of the multi-tone jamming in subchannel $b$, its computational complexity increases exponentially with respect to the number

of symbols $L$. So we have to consider suboptimal detection algorithms with lower complexity.

*Detection Based on Eigenvalue Spread*   Consider an $M + 1$ element array of received samples

$$\underline{Y}_b(l) = [Y(b, l), \cdots, Y(b, l + M)]^T \tag{4.26}$$

The correlation matrix is

$$R = E[\underline{Y}_b(l) \, \underline{Y}_b^H(l)]$$
$$= \underline{s}_1 \, A_1^2 \, \underline{s}_1^H + (1 + 2\sigma^2) \, I, \tag{4.27}$$

where $\underline{s}_1 = [1, \exp(-i\omega_b), \cdots, \exp(-i\omega_b M)]^T$ and $I$ is the $(M + 1) \times (M + 1)$ identity matrix. Using eigenvalue decomposition, $R = Q\Lambda Q^H$, where $Q$ is an unitary matrix and

$$\Lambda = \begin{bmatrix} \lambda_1 & & & \\ & \lambda_2 & & \\ & & \ddots & \\ & & & \lambda_{M+1} \end{bmatrix} \tag{4.28}$$

is a diagonal matrix whose diagonal elements are the eigenvalues of the matrix $R$. By sorting, we can let $\lambda_1 \geq \lambda_2 \geq \cdots \geq \lambda_{M+1}$. Since $R = \underline{s}_1 \, A_1^2 \, \underline{s}_1^H + (1 + 2\sigma^2) \, I$, $Q\underline{s}_1 \, A_1^2 \, \underline{s}_1^H Q^H$ is also a diagonal matrix. Because $\underline{s}_1 \, A_1^2 \, \underline{s}_1^H$ is a rank one matrix, it has only one nonzero eigenvalue $\gamma_1$. So we have

$$\lambda_1 = \gamma_1 + 1 + 2\sigma^2,$$
$$\lambda_2 = 1 + 2\sigma^2,$$
$$\vdots$$

97

$$\lambda_{M+1} = 1 + 2\sigma^2. \tag{4.29}$$

When there is no jamming signal, $\gamma_1 = 0$; when there is one jamming signal, $\gamma_1 = MA_1^2$. Therefore we can detect the presence of the jamming signal by observing $r = \lambda_1/\lambda_2 \lesseqgtr \eta$. When the jamming power is not known, the $\eta$ is set to be 10. We use the covariance method of data windowing in estimating the matrix $R$ and $M$ is set to one in the simulation since we have assumed that there is at most one jamming tone in each subchannel.

## 4.2.2   Estimation of Jamming Signals in the AWGN Channel

After the receiver has determined that a particular subchannel has jamming signals using the detection schemes, the jamming parameters – amplitude and phase – must be estimated in order to cancel the jamming signal.

*Differential Frequency Estimation*   When the jamming signal has much stronger power than both the data signal and the background noise, we can ignore the data signal and the background noise in estimating the angle $\phi(b)$ using differential frequency estimation,

$$\frac{1}{L-1} \sum_{l=0}^{L-2} \frac{Y(b,l)}{Y(b,l+1)} \approx \frac{1}{L-1} \sum_{l=0}^{L-2} \exp(i\omega_b) = \exp(i\omega_b). \tag{4.30}$$

So $\omega_b$ can be estimated by

$$\hat{\omega}_b \approx \angle \left[ \frac{1}{L-1} \sum_{l=0}^{L-2} \frac{Y(b,l)}{Y(b,l+1)} \right] = \angle \left[ \sum_{l=0}^{L-2} \frac{Y(b,l)}{Y(b,l+1)} \right]. \tag{4.31}$$

To estimate $J(b,l)$, since

$$J(b,l) = A_1 \exp\{-i[\omega_b l + \phi_b]\} = A_1 \exp[-i\omega_b l] \cdot \exp[-i\phi_b], \tag{4.32}$$

we only need to estimate $A_J^t(b) = A_1 \exp(-i\phi_b)$, which is given by

$$\hat{A}_J^t(b) \approx \frac{1}{L} \sum_{l=1}^{L} Y(b,l) \exp[-i\hat{\omega}_b l]. \tag{4.33}$$

After canceling the jamming signal, there will be added noise due to the jamming cancellation. If we ignore the frequency estimation error, the power of this additional noise is equal to $(E|X(b,l)|^2 + 2\sigma^2)/L$.

*ESPRIT* The ESPRIT algorithm [52] is a high-resolution signal parameter estimation method that can be applied to the problem of estimating sinusoids in noise. Although the MUSIC algorithm [51] has smaller estimation variance, it requires huge cost in computation searching over parameter space. We choose the ESPRIT algorithm because of its high resolution compared to other frequency estimation method and its ease of computation compared to the MUSIC algorithm. For ease of reference, we include the algorithm in the following.

The ESPRIT algorithm:

- Compute $[R]_{MM \times MM}$ as defined in (4.27).

- Solve generalized eigenvalue decomposition, $RE = \Sigma_n E \Lambda$, where

$$[E]_{MM \times MM} = [\underline{e}_1, \cdots, \underline{e}_{MM}]$$

  and $[\Sigma_n]_{MM \times MM}$ is the noise covariance matrix.

- Form $E_s = \Sigma_n[\underline{e}_1, \cdots, \underline{e}_d] = \begin{bmatrix} [E_x]_{\frac{MM}{2} \times d} \\ [E_y]_{\frac{MM}{2} \times d} \end{bmatrix}$ and let $E_{xy} = [E_x \ E_y]$.

- Compute eigenvalue decomposition, $E_{xy}^H E_{xy} = E \Lambda E^H$ and divide the matrix $E$ into four submatrices as follows

$$E = \begin{bmatrix} [E_{11}]_{d \times d} & [E_{12}]_{d \times d} \\ [E_{21}]_{d \times d} & [E_{22}]_{d \times d} \end{bmatrix}.$$

99

- $\hat{\omega}_b = -E_{12}E_{22}^{-1}$ .

Note here $\Sigma_n$ is an identity matrix because both the data signal and the AWGN are uncorrelated. Hence the generalized eigenvalue decomposition is actually eigenvalue decomposition in the normal sense. Although it involves eigenvalue decomposition, the ESPRIT algorithm is still very simple because we only need to work with $2 \times 2$ matrices, i.e., $MM = 2$. For more information on the algorithm, please refer to [52].

### 4.2.3 Detection and Estimation of Jamming Signals in the Fading Channel

In fading channels, the received signal can be written as

$$Y(b,l) = H(b,l)X(b,l) + I^t(b)H^J(b,l)A_1\exp\{-i[\omega_b l + \phi_b]\} + N(b,l). \quad (4.34)$$

Due to correlated channel state information, the detection of the jamming state becomes more complicated in the fading channel. As a result, the detection scheme in (4.25) is too complicated for practical purpose. But we can still use the eigenvalue-based detection method to detect the presence of the jamming signal.

In slowly fading channel, $H^J(b,l)$ changes slowly so we can still use differential estimation or the ESPRIT algorithm to estimate $\omega_b$. But then we need to estimate

$$\mathcal{J}^t(b,l) = H^J(b,l)J(b,l)\exp\{i\omega_b\} = H^J(b,l)A_1\exp(-i\phi_b)$$

instead of $A_1\exp(-i\phi_b)$. Let

$$Z(b,l) \;=\; \exp(i\hat{\omega}_b l)Y(b,l)$$

$$= H^J(b,l)A_1\exp(-i\phi_b) + H(b,l)X(b,l)\exp(i\hat{\omega}_b l)$$

$$+N(b,l)\exp(i\hat{\omega}_b l)$$

$$= \mathcal{J}^t(b,l) + H(b,l)X(b,l)\exp(i\hat{\omega}_b l) + N(b,l)\exp(i\hat{\omega}_b l). \quad (4.35)$$

Then the receiver can make use of the *a priori* knowledge of the channel statistics to estimate $\mathcal{J}^t(b,l) = H^J(b,l)A_1\exp(i\omega_b)$ with Wiener filters. After canceling the jamming signal, there will be added noise due to the cancellation. If we ignore the error in frequency estimation, the power of this additional noise can be calculated by

$$E|e(b,l)|^2 = A_1^2(1 - \underline{w}_o^H R \underline{w}_o) \quad (4.36)$$

where $e(b,l) = J(b,l) - \hat{J}(b,l)$, $R$ is the autocorrelation matrix of the channel statistics, and $\underline{w}_o$ is the optimal Wiener filter coefficient vector. The actual noise power will be larger due to the error in frequency estimation.

## 4.2.4   Iterative Detection and Estimation of Jamming Signals

The receiver first detects, estimates and cancels the jamming signal from received samples and then proceeds to demodulate and decode multicarrier signals, completing the first iteration of processing. After that, the receiver tries to reconstruct the received data signal component based on the decoder output and feeds it back to the beginning of the receiver. Thus a new iteration starts.

In the new iteration, the jamming estimator first removes the reconstructed data signal from received samples and then re-estimates the jamming signal. This time, the jamming estimation benefits from the reduced noise level – noises to the estimation of the jamming signal include data signals and the AWGN.

Although the jamming detector based on the eigenvalue spread can also

benefit from the feedback information, we choose to use a different jamming detector because the original detector can only provide hard decisions on the jamming state. The new detector is a correlation detector that computes the cross-correlation of the jamming estimator output between the first iteration and subsequent iterations.

Let $\hat{J}_{(i)}(b,l)$ be the jamming output in the $i$th iteration. Note that when $i \geq 2$, the $\hat{J}_{(i)}(b,l)$ is free of noise due to the data signal when there is no error in data reconstruction. So we can detect the presence of the jamming tone by computing

$$\rho(b) = \frac{\sum_{l=0}^{L-1} \hat{J}_{(i)}(b,l)\hat{J}_{(1)}^*(b,l)}{\sqrt{\sum_{l=0}^{L-1} |\hat{J}_{(i)}(b,l)|^2 \sum_{l=0}^{L-1} |\hat{J}_{(1)}(b,l)|^2}}, \; i \geq 2. \tag{4.37}$$

$\rho(b)$ provides soft decisions on the jamming state. Because negative values of $\rho$ are meaningless in this case, we can limit $\rho$ to $[0,1]$ by using

$$\rho = \max(\rho, 0). \tag{4.38}$$

## 4.3 Iterative Demodulation and Decoding

Jamming estimation and cancellation is only part of the multicarrier receiver design. In this part, we discuss other key components in the multicarrier receiver working in the fading channels – joint detection and decoding of the convolutional coded multicarrier communication system. We will not discuss specifically about the design for the AWGN channel as it is a special case of the design for the fading channel. The transmitter includes a channel (convolutional) encoder, a channel interleaver, a serial-to-parallel converter, MPSK mapping, and multicarrier modulation. Pilot symbols are transmitted through dedicated subchannels. The receiver structure is shown in Fig. 4.1, Fig. 4.2, Fig. 4.3. Apart from
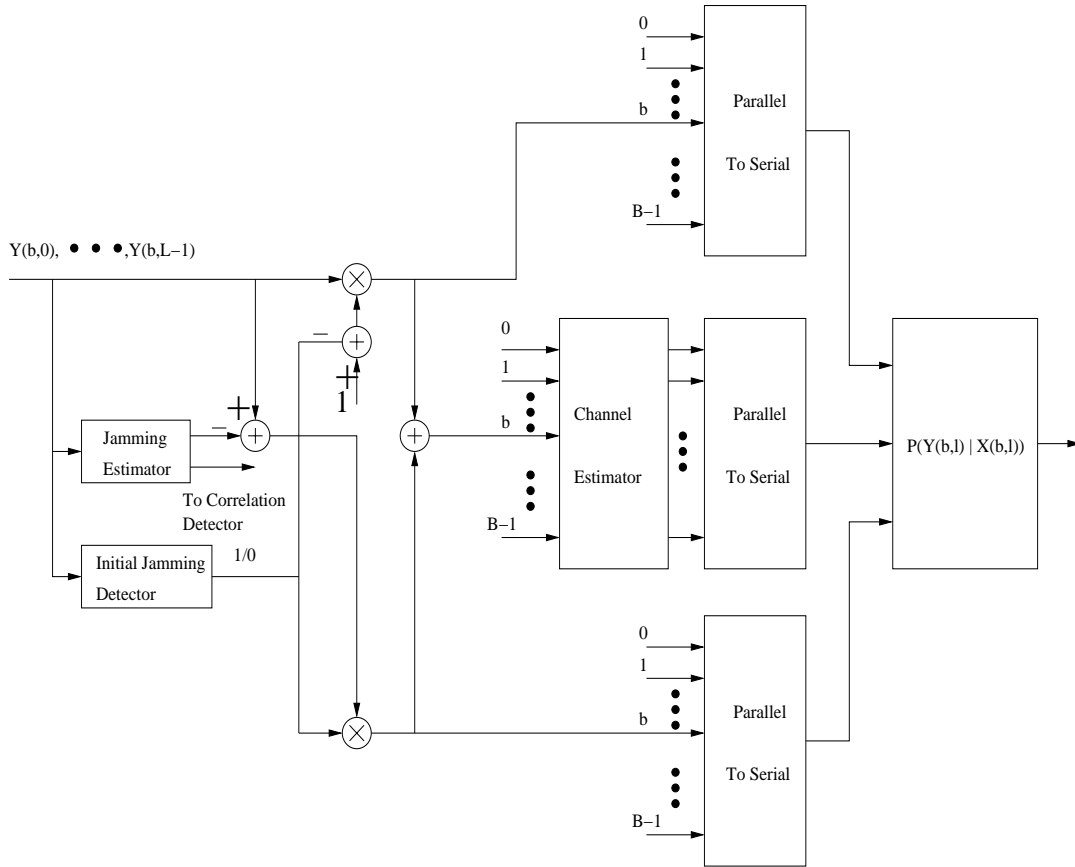
Figure 4.1: Multicarrier Receiver Part I – Jamming Detection, Estimation, and Cancellation for the First Iteration

the jamming estimation and cancellation discussed in Section 4.2, the receiver also includes computing $P(Y(b,l)|X(b,l))$, channel estimation, parallel-to-serial conversion, bit reliability calculation, channel deinterleaving, channel (convolutional) decoding and data feedback.

The role of bit reliability calculation is to convert symbol reliabilities to bit reliabilities. The main purpose of the feedback path is to reconstruct data symbols for channel estimation. We will not elaborate on these two parts in order to save space. For more information, please refer to Chapter 2 and [55]. Instead, we will concentrate on multicarrier signal demodulation with jamming, design
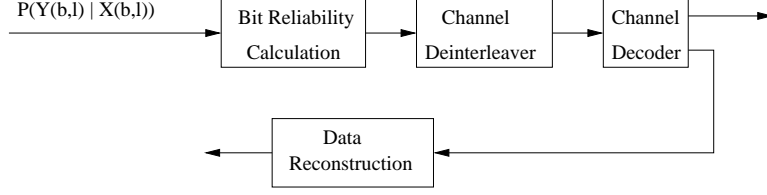
Figure 4.2: Multicarrier System Diagram Part II – Decoding and Data Reconstruction

of pilot symbol sequence, channel estimation and iterative channel estimation.

### 4.3.1 Multicarrier Signal Demodulation with Jamming

The received multicarrier signal with partial-time tone jamming can be represented by

$$Y(b,l) = H(b,l)X(b,l) + I^t(b)H^J(b,l)J(b,l) + N(b,l) \qquad (4.39)$$

In order to demodulate the received signal, the receiver need to compute the conditional probability $P(Y(b,l)|X(b,l))$

$$\begin{aligned}
&P(Y(b,l)|X(b,l) = x) \\
=\ &P(Y(b,l), I^t(b) = 0|X(b,l) = x) + P(Y(b,l), I^t(b) = 1|X(b,l) = x) \\
=\ &P(Y(b,l)|X(b,l) = x, I^t(b) = 0)P(I^t(b) = 0) \\
&+ P(Y(b,l)|X(b,l) = x, I^t(b) = 1)P(I^t(b) = 1). \qquad (4.40)
\end{aligned}$$

As we don't have the *a priori* information on $I^t(b)$, we use the decisions made by the jammer detectors in place of the probability $P(I^t(b) = i)$.

### 4.3.2 Design of Pilot Symbol Sequence

In frequency-selective, time-variant channel, references must be provided to the receiver for coherent demodulation. For this purpose, we use dedicated carriers
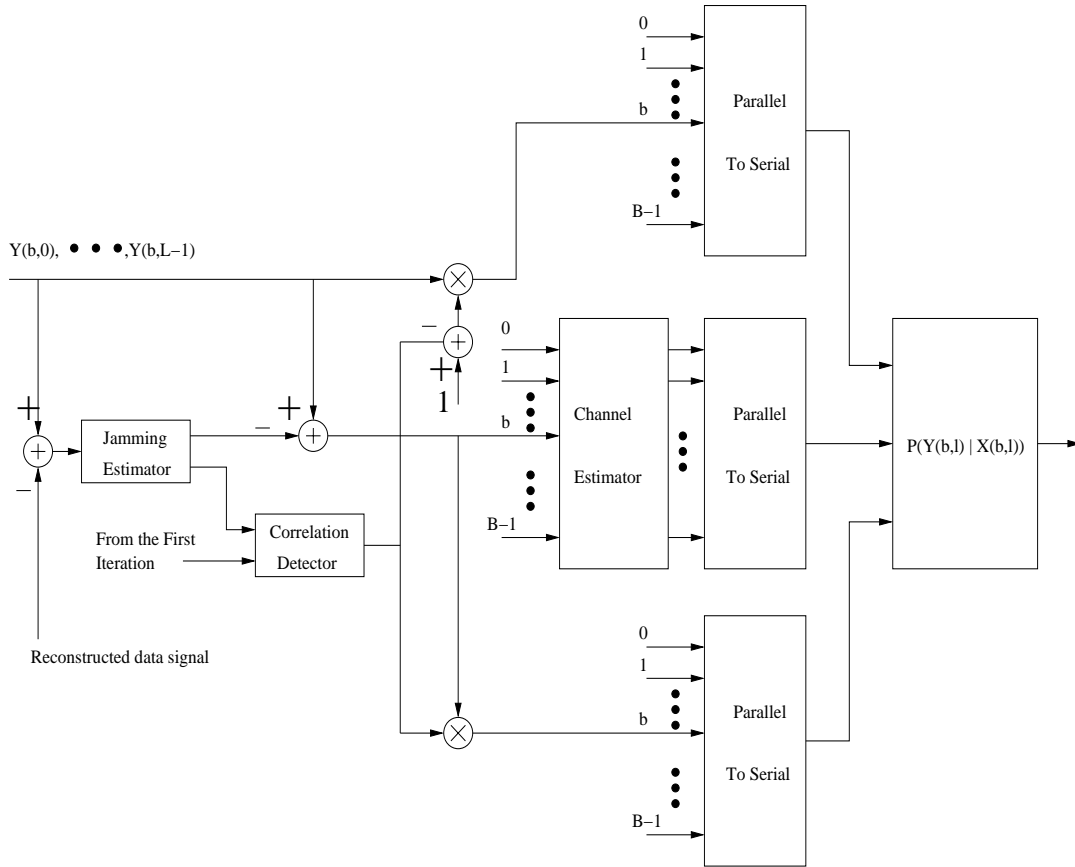
Figure 4.3: Multicarrier System Diagram Part III – Jamming Detection, Estimation, and Cancellation for the Second and Subsequent Iterations

to transmit pilot symbol sequence so that the channel state information in the data carriers can be estimated by interpolation.

The anti-jamming design presented in Section 4.2 has two requirements for pilot sequence. First, the sequence should avoid any repeated patterns so that it will not be mistaken for the jamming signal by the eigenvalue-based jamming detector. For instance, a constant sequence is no different than a jamming signal whose frequency coincides with one of the carrier frequencies. Second, the pilot sequence should have a white spectrum so that even if the jamming detector make a false alarm error in the pilot channel, the jamming estimation and can-

cellation process will cause little distortion by removing one particular frequency component or a continuum of frequency components within a narrowband.

To satisfy the first requirement, the sequence should be randomized so that its power is distributed evenly in all the dimensions of eigenspace. Fortunately, this kind of sequences also automatically satisfy the second requirement because the Fourier transform is unitary. Specifically, we take a symbol from the signal constellation and multiply it by a random sequence of $\pm 1$. This random $\pm 1$ sequence can be found by computing the eigenvalue spread, i.e., the ratio of the two eigenvalues of its $2 \times 2$ autocorrelation matrix and searching for the sequence that has a ratio closest to one. For a period of 40 symbols, we have found the following sequence to be used in the simulation:

$$-1, 1, -1, 1, -1, 1, 1, 1, -1, -1, 1, -1, -1, -1, 1, 1, 1, -1, 1, -1,$$

$$-1, 1, 1, -1, -1, -1, 1, -1, -1, -1, 1, 1, 1, 1, 1, 1, -1, -1, -1, 1.$$

The eigenvalue spread of the $2 \times 2$ autocorrelation matrix of this sequence is $20/19$, which is the best for this length.

### 4.3.3 Channel Estimation for Multicarrier

For convenience, we present the rest of the receiver as if there were no jamming signals. We assume that the multipath fading is flat in each subchannel of multicarrier but frequency-selective from one subchannel to another. Therefore, the received data symbol of $b$th subchannel at time $lT$ can be written as

$$Y(b, l) = H(b, l)X(b, l) + N(b, l), \tag{4.41}$$

where $H(b, l)$ is the complex channel gain of $b$th subchannel at time $lT$, and $N(b, l)$ is an additive white Gaussian noise with power spectrum density $N_0$.

Let $\mathcal{P} = \{(b,l) : X(b,l)$ be pilot symbol$\}$. The problem is to estimate the two-dimensional wide-sense stationary stochastic process $H(b,l)$ given observation $\{Y(b,l), (b,l) \in \mathcal{P}\}$. The mean square error is defined as

$$J = E\left|\hat{H}(b,l) - H(b,l)\right|^2. \tag{4.42}$$

Because both $H(b,l)$ and $Y(b,l)$ are Gaussian stochastic processes, the optimum estimator in the mean square sense is the linear minimum mean-square error (MMSE) estimator. Thus

$$\hat{H}(b,l) = \sum_{(b',l')\in\mathcal{P}} w_o(b,l,b',l')Y(b',l'), \tag{4.43}$$

where optimum Wiener filter coefficients $w_o(b,l,b',l')$ can be determined by the orthogonality principle

$$E[(H(b,l) - \hat{H}(b,l))Y^*(b',l')] = 0, \tag{4.44}$$

where $*$ represents complex conjugate. In the simulation, we use dedicated subchannels for transmitting pilot symbols. In this case, the two dimensional channel estimation problem can be simplified to one dimensional filtering in the frequency domain.

After the channel state information has been estimated, the multicarrier receiver uses this information to calculate the reliability value for each data bit. These reliability values are then passed through a channel decoder, the output of which are feedback to the channel estimator.

## 4.3.4  Iterative Channel Estimation

The iterative filters use the received pilot symbols and the reconstructed data symbols to obtain more accurate estimation of the channel state information.
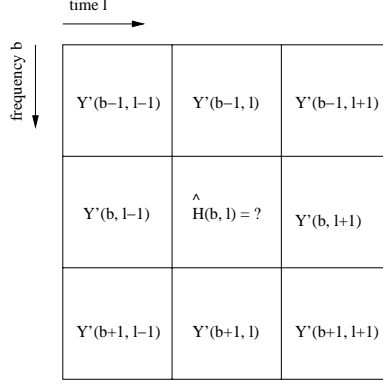
Figure 4.4: Iterative Channel Estimation Using Both Reconstructed Data Symbols and Pilot Symbols

Once we have reconstructed the data symbols $\hat{X}(b,l)$'s as in [55], we have

$$Y(b,l) \approx H(b,l)\hat{X}(b,l) + N(b,l), \tag{4.45}$$

Divide both sides by $\hat{X}(b,l)$,

$$Y'(b,l) \approx H(b,l) + N'(b,l), \tag{4.46}$$

where $Y'(b,l) = Y(b,l)/\hat{X}(b,l)$ and $N'(b,l) = N(b,l)/\hat{X}(b,l)$. Because $N'(b,l)$ is uncorrelated Gaussian noise, we can use (4.43) and (4.44) with $Y(b,l)$ replaced by $Y'(b,l)$ to estimate CSI. To obtain the estimation of the CSI at a data position $(b,l)$, we use eight neighboring $Y'(b',l') \in \{Y'(b+bb,l+ll),\ bb,ll \in \{-1,0,1\},\ bb^2 + ll^2 \neq 0\}$ to estimate $H(b,l)$ as shown in Fig. 4.4.

In Fig. 4.3, independent of the jamming state, the corresponding output of the jamming estimator are removed from all received samples used for iterative channel estimation. This is because in the second and subsequent iterations, the input to the jamming estimator on the subchannels without jamming contains only the additive white noise and some decoding errors. Therefore the output of the narrowband jamming estimator corresponding to those subchannels are of very low power level and can be ignored.

## 4.4   Simulation Results
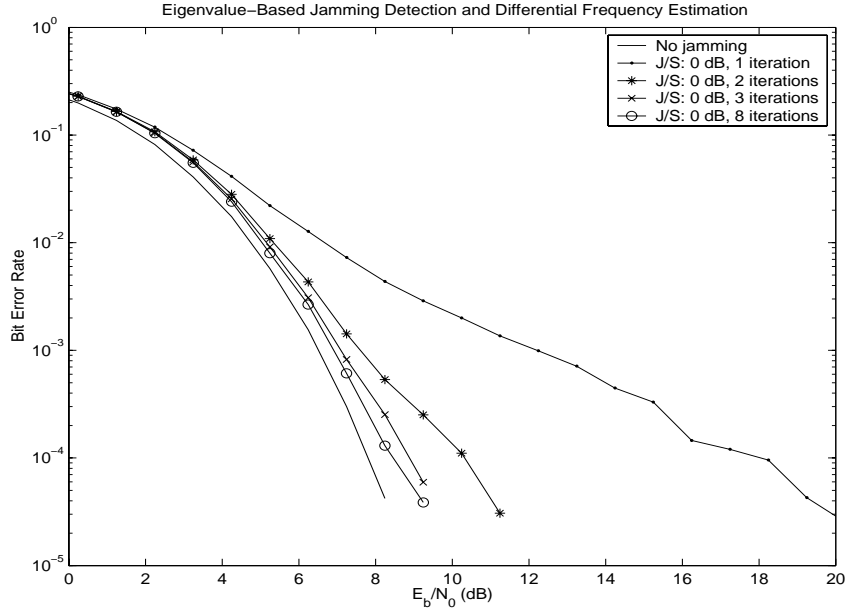


Figure 4.5: Number of Iterations on the Performance of Differential Frequency Estimation

In the simulation, we further assume the channel has a uniform Doppler power spectrum (with $f_D = 20.83\,Hz$ being the one-sided maximum Doppler frequency) and uniform delay spectrum (with $\tau_m = 10\,\mu s$ being the one-sided maximum echo delay). The carrier spacing is $4.1667\,kHz$. This corresponds to a normalized Doppler fading of 0.005 and a normalized delay spread of 1/24.

The scheme was investigated for blocks with a 40-symbol period and 25 subchannels for data signals. The entire transmission bandwidth hops to another range between two blocks. In the fading channel, six more subchannels are dedicated to the transmission of pilot symbols, i.e., one pilot subchannel in every 6 subchannels. For each received data blocks, the initial channel estimator uses 5-tap one dimensional filters in frequency domain. And the iterative filtering
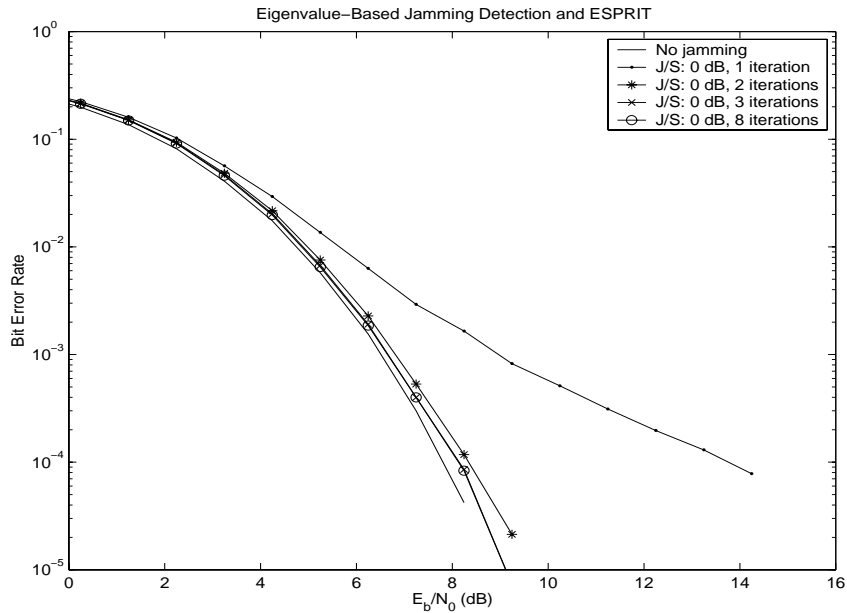
Figure 4.6: Number of Iterations on the Performance of Eigenvalue-Based Jamming Detection and ESPRIT

uses an 8-tap two dimensional filter. We use 40-tap linear filters to estimate the jamming signals.

We use 8-PSK modulation for each subchannel. Gray mapping is used for the mapping of 8-PSK symbols. The convolutional code is rate $1/2$, $(7,5)$ non-systematic convolutional code with constraint length 3. The channel interleaver is a pseudo-random interleaver of 3000 bits. The number of iterations is 3 unless otherwise specified.

For the jamming signal, as the partial-time pulse jamming is the dual problem of the partial-band tone jamming, we only simulate the multi-tone jamming. The probability that a particular subchannel is jammed is set to 0.1. As we have assumed, there is at most one jamming tone within a subchannel.

We first study the effect of iterative jamming detection and estimation on the system performance. We simulate the BER using 1, 2, 3, 8 iterations. Fig. 4.5

Figure 4.7: Performance of Iterative Jamming Detection and Estimation in the AWGN channel: J/S = -10 dB

shows the result for differential jamming frequency estimation. Fig. 4.6 shows the result for ESPRIT. In both cases, the performance improvement due to the iterative processing is obvious, especially between the first and the second iteration. After the third iteration, further iterative processing only provides marginal gain in Fig. 4.5 when differential estimation is used and no discernible gain in Fig. 4.6 when the ESPRIT algorithm is used. For this reason, three iterations are used for the rest of the simulation.

We then vary the jamming-to-signal power ratio and simulate the system performance. The simulated $J/S$ ratios are $-10$, $-5$, 0, 5, 10 dB. The results are shown in Fig. 4.7 – 4.11. For each figure, we simulate four cases: no jamming signals, iterative processing with differential frequency estimation, iterative processing with the ESPRIT algorithm, and the case without anti-jamming design. Although not shown here, we have also simulated the BER when $J/S = 20 \; dB$
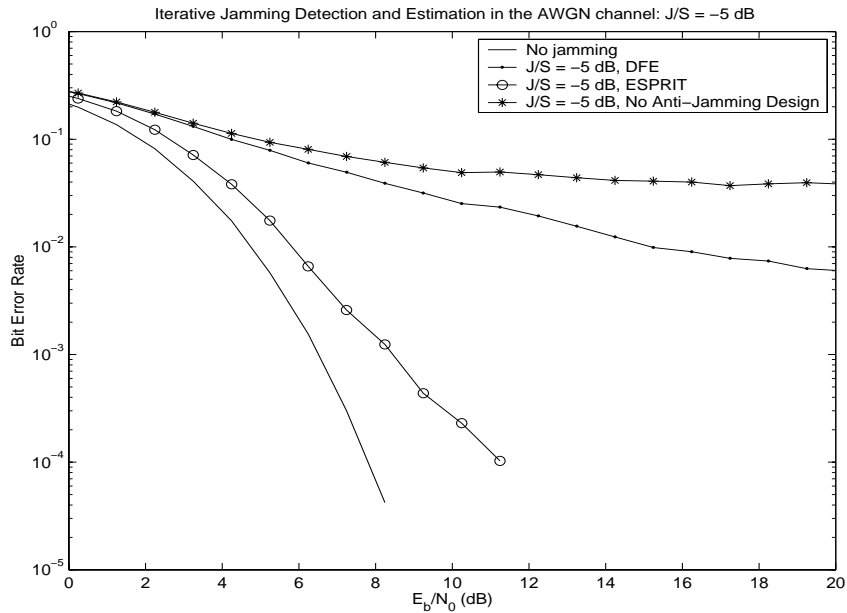
Figure 4.8: Performance of Iterative Jamming Detection and Estimation in the AWGN channel: J/S = -5 dB

and $J/S = 30 \ dB$. The results are the same as in Fig. 4.11 corresponding to $J/S = 10 \ dB$.

It can be seen clearly that iterative processing can effectively suppress the multi-tone jamming signals for a wide range of J/S values. The reason that it performs better at high $J/S$ values is because that the receiver can obtain more accurate estimates of jamming frequencies. In fact, the most difficult case for the receiver happens around $J/S = -5 \ dB$. At this point, the jamming signal mixes well with the data signal – it is sufficiently strong to affect the data signal while it is not strong enough for reliable detection and robust estimation. This is the very reason that we make use of soft decisions on the jamming state.

The ESPRIT algorithm also shows a clear advantage over differential frequency estimation at this point. While the latter has high error floor at $J/S = -5 \ dB$, the former is only about 1.0 dB worse than the case without jamming

112
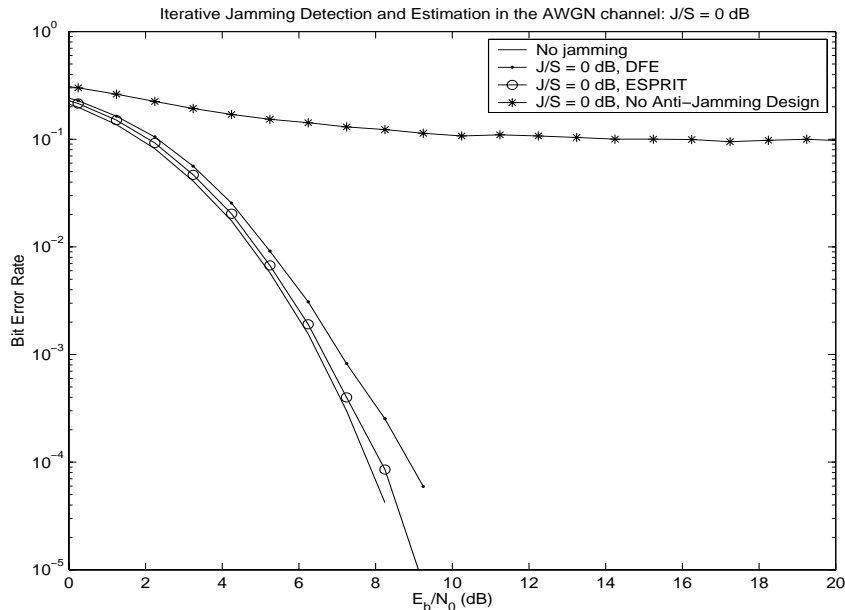
Figure 4.9: Performance of Iterative Jamming Detection and Estimation in the AWGN channel: $J/S = 0$ dB

at $10^{-3}$ bit error rate. When $J/S$ goes higher, the difference between the two vanishes.

It appears counterintuitive that the BER performance remains unchanged after the $J/S$ value increases to a certain level. In fact, as jamming power increases, both the jamming state detection error and the frequency estimation error decrease substantially. If we ignore the frequency estimation error and assume perfect jamming state detection at high $J/S$ values, the additional noise level caused by the jamming cancellation is $(E[|H(b,l)X(b,l)|^2] + 2\sigma^2])/L$ for the first iteration and $(E[|H(b,l)X(b,l) - \hat{H}(b,l)\hat{X}(b,l)|^2] + 2\sigma^2])/L$ for the second and subsequent iterations. Since the power of the noise due to jamming cancellation is independent of the jamming power, it is not unreasonable that the BER performance at high $J/S$ values does not deteriorate when the jamming power increases.
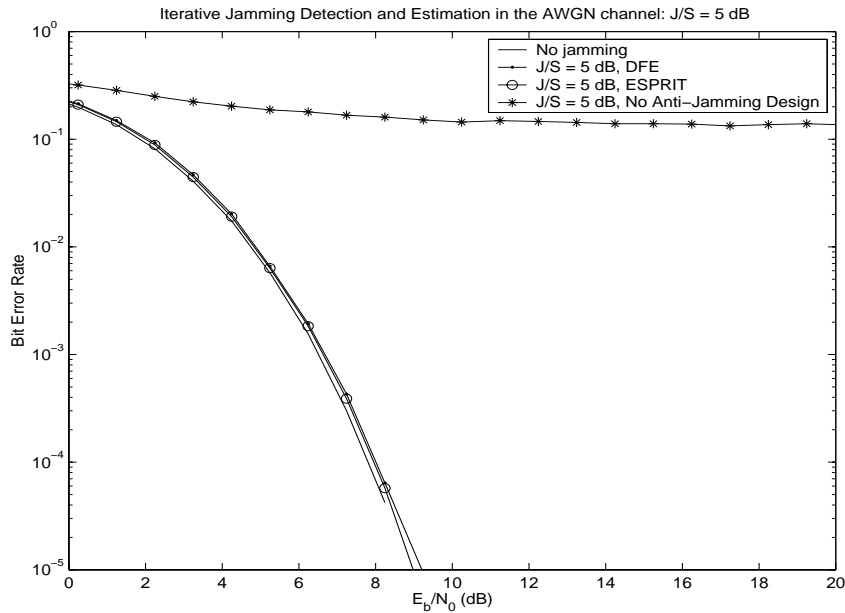
Figure 4.10: Performance of Iterative Jamming Detection and Estimation in the AWGN channel: J/S = 5 dB

Shown in Fig. 4.12 – 4.13 are the simulation results in the fading channel. Fig. 4.12 contains the results of differential frequency estimation. Fig. 4.13 contains the results of the ESPRIT algorithm. For reference, we have also included the performance of the coherent receiver and the PSAM-IF receiver without jamming.

Although iterative jamming estimation and cancellation can still suppress the multi-tone jamming signal for a wide range of $J/S$ values, it displays error floors at high signal-to-noise ratio. This is not unexpected because unlike the AWGN channel, the channel state information in the fading channel is frequency-selective and time-varying so it has to be estimated for coherent demodulation. Although we have designed the pilot sequence that are robust to multi-tone jamming signals, it can not avoid the residual noise as a result of jamming cancellation. This residual noise is much larger in the fading channel because
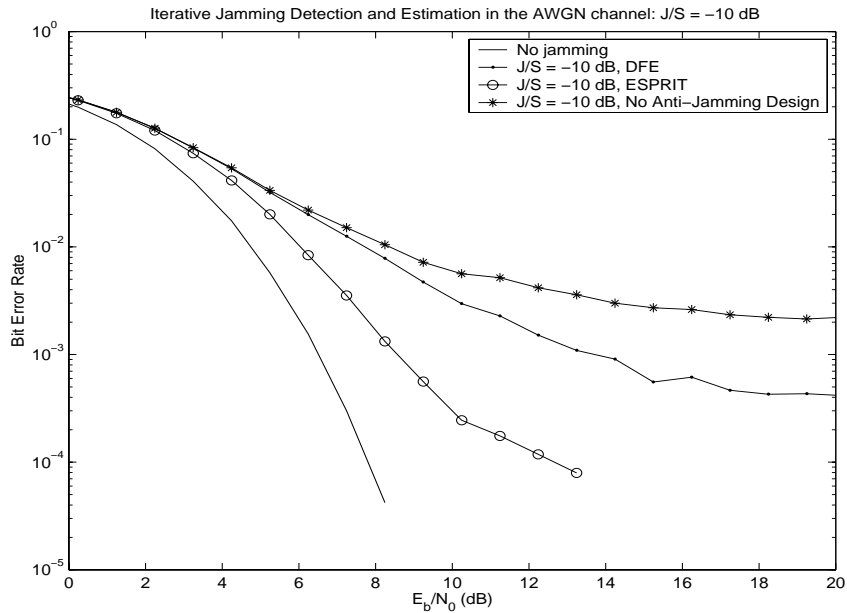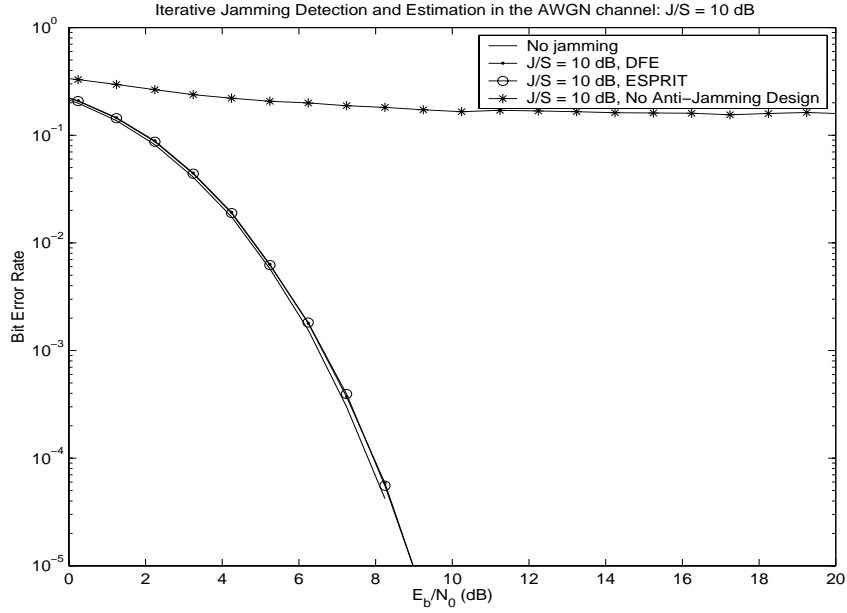
Figure 4.11: Performance of Iterative Jamming Detection and Estimation in the AWGN channel: $J/S = 10$ dB

the multi-tone jamming signals are spread by the Doppler fading. The fading also causes the amplitude of both the data signal and the jamming signal to vary, causing more detection errors. For the same reason, unlike the AWGN channel, the BER performance begins to decrease after $J/S = 10 \ dB$ in the fading channel.

The advantage of the ESPRIT algorithm, however, is more prominent in the fading channel. It is generally better than differential frequency estimation – its error floors are one magnitude lower than those of differential frequency estimation throughout the simulated $J/S$ range.
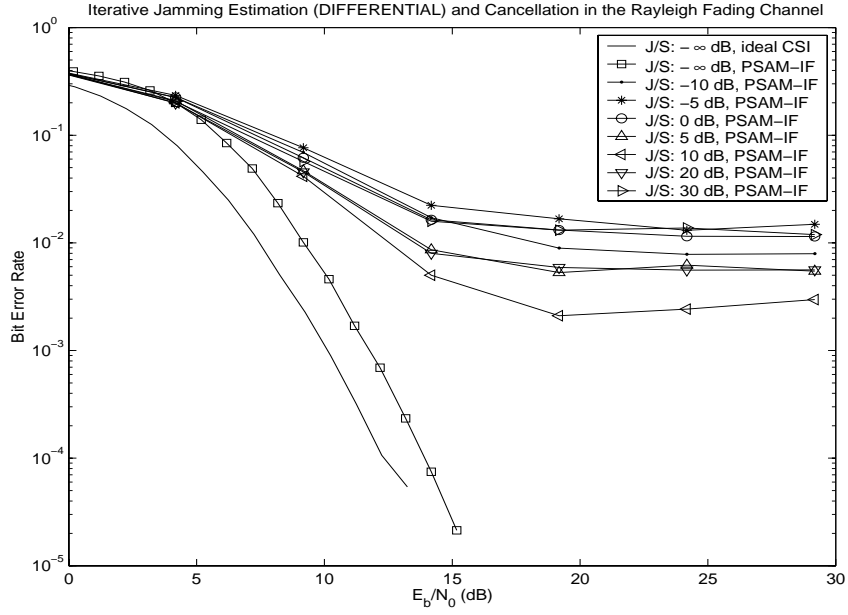
Figure 4.12: Performance of Iterative Jamming Detection and Estimation (Differential) in Fading Channels
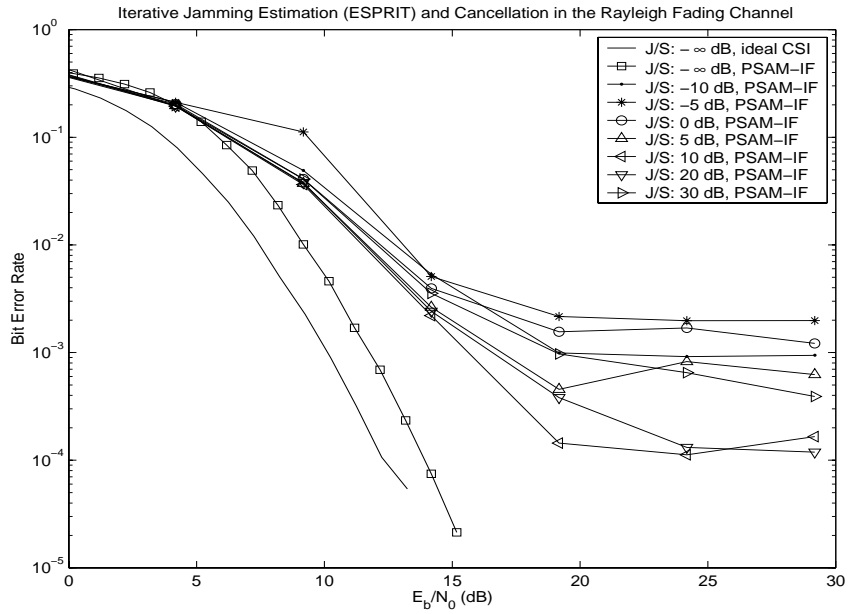


Figure 4.13: Performance of Iterative Jamming Detection and Estimation (ESPRIT) in Fading Channels

Although we have not simulated partial-time pulse jamming, we expect similar results from our anti-jamming design with little adaptation. For partial-time pulse jamming, jamming detection, estimation, and cancellation are performed across multiple carriers during a symbol period; while for partial-band tone jamming, they are performed over multiple symbol periods in a subchannel. Specifically, for the AWGN channel, if we assume $s(t) = $ constant, $t \in [0, T]$ and consider anti-jamming design for partial-time pulse jamming with 25 symbol periods, 40 data carriers, we will obtain the same results as those for partial-band tone jamming with 40 symbol periods, 25 data carriers. For fading channels, the duality is complicated by fading in time and frequency directions and by pilot symbols. Still, there exists a strict duality between partial-band tone jamming and partial-time pulse jamming if, in addition to the duality conditions for the AWGN channel, we insert pilot symbols periodically in each carrier as in a single carrier transmission for partial-time pulse jamming, exchange the values of normalized Doppler and delay spread, and adjust the channel interleaver so that a bit that constitutes the symbol $X(b, l)$ for partial-band tone jamming will be a corresponding bit of the symbol $X(l, b)$ for partial-time pulse jamming.

## 4.5   Conclusions

In this chapter, we have studied anti-jamming system design for multicarrier communications. We have considered two types of jamming signals – the partial-band tone jamming and the partial-time pulse jamming. The design of the anti-jamming system is illustrated by using the multi-tone jamming. Specifically, we have considered two types of detection schemes.  One is the eigenvalue-based

jamming detection, which generates hard decisions on jamming state for initial detection; the other is the correlation-based iterative detection, which generates soft decisions on jamming state for subsequent detection. For jamming frequency estimation, we have also considered two types of schemes – differential frequency estimation and the ESPRIT algorithm. To further reduce the error in jamming detection and estimation, we make use of iterative jamming detection and estimation by removing the reconstructed data signal component from the received samples.

In the fading channel, we have designed a robust pilot sequence for the estimation of the channel state information for the data signal. The eigenvalue-based jamming detection requires that the pilot sequence have evenly distributed power in all dimensions so that it would not be treated as a jamming tone since it can not differentiate between a constant pilot sequence and a jamming tone whose frequency coincides with the carrier frequency of the pilot subchannel. Even if the jamming detection does make false-alarm errors in the pilot subchannel, the pilot sequence is little affected by the jamming estimation and cancellation process because its power is spread evenly over the entire bandwidth. Thus removing one frequency component will not cause much distortion. In addition, we have also included iterative channel estimation so that the receiver have better estimates of the channel state information after the first iteration.

Simulation results have shown that our design of the anti-jamming multi-carrier receiver are very effective in suppressing the jamming signal and that the iterative processing greatly improves the BER performance. It works for all the simulated $J/S$ values ranging from $-10$ to 30 dB. Although not simulated, it should also work with $J/S$ values below $-10$ dB as the jamming signal is

too weak to affect the receiver performance at this range. On the other hand, we have simulated the system at up to 40 dB and it still works in the AWGN channel.

In the AWGN channel, the anti-jamming design based on the ESPRIT algorithm displays no error floor above $10^{-5}$ bit error rate while the design based on differential frequency estimation has error floors at $J/S = -10\ dB$ and $J/S = -5\ dB$, though it performs as well as the former at high $J/S$ values. In the fading channel, both designs have error floors, but error floors of the ESPRIT algorithm is one magnitude lower than those of differential frequency estimation. This implies that better performance can be achieved with better algorithms for estimating jamming frequencies such as the MUSIC algorithm.

Although we have only simulated the anti-jamming system design against the partial-band tone jamming, we expect it has similar performance in the case of the partial-time pulse jamming because of the duality between them. The anti-jamming design for multicarrier communications can also be used for M-QAM signals since it does not require constant envelope property of MPSK signals.

Chapter 5

# Power Control and Adaptive Modulation for OFDM with Transmit and Receive Diversity

High data-rate mobile communications have received great interests in the past several years. One of the main problems in mobile communications is how to maximize the system throughput against frequency-selective multipath fading. Another important practical issue is how to mitigate cochannel interference in a wireless network. In this chapter, we first apply adaptive modulation and transmit diversity techniques to OFDM signals in a hexagonal cellular system and use a distributed water-pouring algorithm (DWPA) [25] and a centralized power control algorithm (CPCA) based on active set strategy to combat fading and suppress cochannel interference. Our objective is to achieve high spectral efficiency and high throughput under the constraints on maximum transmission power. Then we will study the performance of the system in hostile environments with deliberate jamming signals. The system performance will be assessed using simulation methods.

Compared to single carrier serial transmission schemes, which require lengthy equalizers to mitigate frequency-selective fading, orthogonal frequency-division

multiplexing (OFDM) makes the equalizer obsolete by dividing the transmission bandwidth into multiple subchannels so that the channel gain within each subchannel is flat – approximately constant. With OFDM, the problem of maximizing the system throughput against frequency-selective fading in a wireless channel can be achieved through power allocation and adaptive modulation among subchannels. When there is only a single cell, the optimization problem can be solved using water-pouring. In a multi-cell mobile communication environment, in order to increase the spectral efficiency with given bandwidth one would tend to increase the frequency reuse, which, however, introduces severe cochannel interferences and makes the problem of maximizing the system throughput intractable.

For wireless communications, Su [25] proposed the distributed power allocation algorithm for adaptive modulation which is executed independently by the cochannel interfering users. It was shown that the DWPA could effectively suppress cochannel interference and improve the system throughput. Since the optimization of a multi-cell system is complicated and computationally intensive, this heuristic distributed algorithm is more practical and much easier to implement. The idea was based on the fact that in many practical situations, a feedback channel with limited bandwidth from the receiver to the transmitter is usually available. Therefore channel state information can not only be obtained (estimated) at the receiver but is also available at the transmitter. Adaptive modulation can thus be used together with power control to improve the OFDM throughput for a given QoS. Previous works on distributed power control can also be found in [56], [57], [58], [59], and [60]. Besides, Chow [61] proposed power allocation algorithms to maximize the throughput under maximum power and

QoS constraints for wireline communications.

In addition to distributed algorithms, there also exists extensive interest in centralized power control algorithms. In [62], centralized power allocation algorithms were proposed for TDMA single carrier systems. Compared to distributed systems, centralized controllers have information from all cochannel cells and are capable of better coordinating the transmit power of the entire network. In this chapter, we develop a centralized power control algorithm based on the active set strategy and the gradient projection method. The proposed CPCA outperforms the DWPA in all cases, albeit with much higher computational complexity.

Another effective method to mitigate fading, especially deep slow one, is to use spatial diversity – multiple transmit and receive antennas. Transmit and receive antenna diversity has been an area of intensive research with the invention of trellis-based space-time codes by Tarokh, etc in [26]. Later, full-rate space-time block codes have also been proposed. Among them, Alamouti [28] proposed a simple transmit diversity technique. For our problem of interest, space-time coded OFDM systems have been explored by Agrawal, etc. [29] and Li [22].

In this chapter, we first extend Su's distributed algorithm from single transmit and receive antenna to multiple antennas in order to mitigate fading and cochannel interference, where multiple transmit antennas also cause an increase in the number of cochannel interfering sources. For simplicity, we will consider only the uplink communications in this chapter, although the algorithm is applicable to both uplink and downlink communications.

In the second part of this chapter, we will develop the centralized power control algorithm for different antenna combinations. In the case of multiple transmit antennas, the number of parameters to be controlled doubles and simply

splitting the power evenly to two transmit antennas as in the space-time code usually does not give good performance.

In the third part of this chapter, we will study the performance of the system in hostile jamming environments. The jammer randomly selects a subset of the OFDM subchannels and sends the jamming signals in those subchannels. Because both the DWPA and the CPCA allows the transmitter to remove the subchannel that does not satisfy the service requirements and reallocate the power to the subchannels with better channel conditions – large channel gains, small cochannel interference and no jamming signals, we expect the system to be robust in the presence of strong jamming signals.

This chapter is organized as follows. In Section 5.1, a brief description will be given to the cellular OFDM system, the channel model and adaptive modulation. In Section 5.2, we describe different diversity schemes for the space-time coded OFDM system to be considered in this chapter. In Section 5.3, we present the distributed water-pouring power allocation algorithm for the OFDM system. In Section 5.4, we develop the centralized power allocation algorithm. In Section 5.5, we present the jamming models. In Section 5.6, we will demonstrate the simulation results and have some discussions. Finally, Section 5.7 summarizes and concludes this chapter.

## 5.1   Channel and System Model

The system considered here is a multi-cell OFDM system. Users within a cell transmit OFDM signals and the multiple access scheme among them is either TDMA or FDMA. While same frequency bands are reused by multiple cells

in order to achieve high spectral efficiency, the degree of reuse is determined by the reuse factor, which usually takes the number of 3, 4, or 7. The higher the frequency of the frequency reuse, the smaller the value of the reuse factor. Because of the frequency reuse, cells assigned with the same frequency band interfere with each other.

We assume that the fading on each subchannel can be treated as flat fading and that the mobile speed is sufficiently low so that the Doppler effect and the inter-channel interference can be ignored.
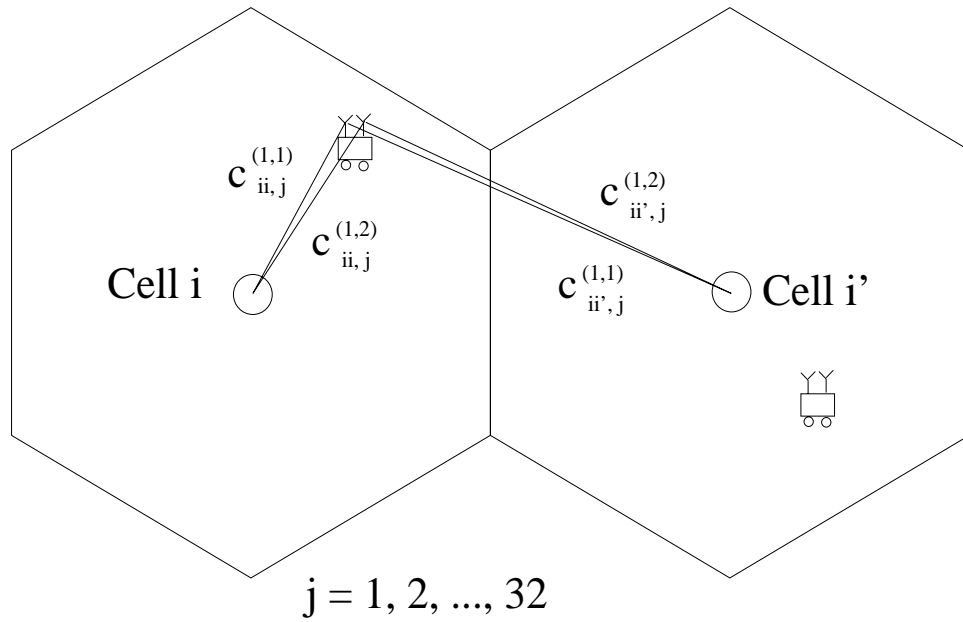


Figure 5.1: Channel Gains for Space-Time Coded OFDM

Suppose there are $N_C$ cochannel cells and there is one mobile within the boundary of each cell. All the mobiles have $N_{TX}$ transmit antennas and all the base stations have $N_{RX}$ receive antenna as shown in Fig. 5.1. We use $s_{i,j}(k)$ to denote the information symbol to be sent from the $j$the subchannel of the $i$th mobile at time $k$ while $s_{i,j}^{(u)}(k)$ the symbol to be transmitted from the $u$th transmit antenna from the same subchannel of the same mobile. In space-time coded

systems, the former represents the uncoded symbol while the latter the coded symbols; they are equal in the absence of space-time codes. For convenience, we normalize $s_{i,j}(k)$ and $s_{i,j}^{(u)}(k)$ so that

$$E\left[|s_{i,j}(k)|^2\right] = E\left[|s_{i,j}^{(u)}(k)|^2\right] = 1.0. \tag{5.1}$$

We use $P_{i,j}$ to denote the total power assigned to the $j$the subchannel of the $i$th mobile and $P_{i,j}^{(u)}$ the corresponding power on the $u$th transmit antenna.

$$P_{i,j} = \sum_{u=1}^{N_{TX}} P_{i,j}^{(u)}. \tag{5.2}$$

If at time $k$, symbols $s_{i,j}^{(1)}(k), \cdots, s_{i,j}^{(N_{TX})}(k)$ are transmitted through subchannel $j$ from $N_{TX}$ antennas of the mobile in cell $i$ to its base station, the received signal at subchannel $j$ on the $v$th antenna can be written as

$$r_{i,j}^{(v)}(k) = \sum_{u=1}^{N_{TX}} c_{ii,j}^{u,v}(k)\sqrt{P_{i,j}^{(u)}}s_{i,j}^{(u)}(k) + \sum_{\substack{i'=1 \\ i'\neq i}}^{N_C} \sum_{u=1}^{N_{TX}} c_{i'i,j}^{u,v}(k)\sqrt{P_{i',j}^{(u)}}\zeta_{i',j}^{(u)}(k) + n_{i,j}^{(v)}(k),$$

$$\tag{5.3}$$

where $n_{i,j}^{(v)}(k)$ is the additive white Gaussian noise; the second term on the right-hand side of the equation

$$i_{i,j}^{(v)}(k) = \sum_{\substack{i'=1 \\ i'\neq i}}^{N_C} \sum_{u=1}^{N_{TX}} c_{i'i,j}^{u,v}(k)\sqrt{P_{i',j}^{(u)}}\zeta_{i',j}^{(u)}(k) \tag{5.4}$$

is the total interference from other cochannel cells with $\zeta_{i',j}^{(u)}(k)$ the interference from the $u$th antenna of the $j$th subchannel of the $i'$th mobile; $c_{i'i,j}^{u,v}(k)$ is the channel state information of subchannel $j$ from the $u$th antenna of the transmitting mobile in cell $i'$ to the $v$th receive antenna of the base station in cell $i$. In the practical situation, it is reasonable to assume that channel gains are Gaussian random variables and that all $N_{TX}$ paths from the

$N_{TX}$ transmit antennas to receiver antenna $v$ have the same statistics, i.e., $E\left[|c_{ii,j}^{1,v}|^2\right] = E\left[|c_{ii,j}^{2,v}|^2\right] = \cdots = E\left[|c_{ii,j}^{N_{TX},v}|^2\right]$. In addition, we assume that channel gains will not change throughout the process of power control. For this purpose, we will drop the time index for channel gains hereafter when doing so will not cause ambiguity, i.e., we will simply write $c_{i'i,j}^{u,v}(k)$ as $c_{i'i,j}^{u,v}$.

The channel state information includes the joint effect of multipath fading, distance loss and shadowing. The spaced-frequency correlation function of the multipath channel is given by

$$\Phi_c(\Delta f) = \frac{1}{1 + j2\pi\Delta f \lambda}, \tag{5.5}$$

where the parameter $\lambda$ is defined as the mean access delay (MED). The distance loss usually follows the reverse $\alpha$th ($\alpha = 2 \sim 5$ [63]) power rule with respect to distance. The shadowing factor is log-normally distributed with 0 dB mean and a standard deviation ranging from 4 to 12 dB [64].

### 5.1.1   Adaptive Modulation

The main task in this chapter is to maximize the throughput under maximum power constraints given a modulation technique and symbol error rate (SER) requirements. The throughput will be obtained through power allocation and variable modulation constellations. Since the derivation of the throughput is the same as in  [65], we only give a concise description in the following to help understanding the algorithms to be discussed later.

We assume that an $M_{i,j}$-QAM two-dimensional constellation is used on the $jth$ subchannel of the $ith$ cell. We also assume that for each subchannel, the modulation is fixed within a frame but may vary from one frame to another

126

depending on the channel conditions and power allocation.

The number of bits transmitted on this subchannel is

$$b_{i,j} = \log_2 M_{i,j}. \tag{5.6}$$

The symbol error probability on this subchannel is [1]

$$SER_{i,j} \approx 4\,Q\left(\sqrt{\frac{3 \cdot SINR_{i,j}}{M_{i,j} - 1}}\right), \tag{5.7}$$

where $SINR_{i,j}$ is the signal-to-interference ratio of the $j$th subchannel in the $i$th cell and $Q(x) = \int_x^\infty \frac{1}{\sqrt{2\pi}} e^{-\frac{x^2}{2}} dx$. It is obvious that when the SER requirement is given, the function inside $Q(\cdot)$ is fixed. Let us define a service requirement $\gamma_{i,j}$ such that

$$\gamma_{i,j} = \frac{3 \cdot SINR_{i,j}}{M_{i,j} - 1}. \tag{5.8}$$

Then we have

$$M_{i,j} = 1 + \frac{3 \cdot SINR_{i,j}}{\gamma_{i,j}},$$

and

$$
\begin{aligned}
b_{i,j} &= \log_2 M_{i,j} \\
&= \log_2\left(1 + \frac{3 \cdot SINR_{i,j}}{\gamma_{i,j}}\right) \\
&= \log_2\left(1 + \frac{SINR_{i,j}}{\Gamma_{i,j}}\right), \tag{5.9}
\end{aligned}
$$

where $\Gamma_{i,j} = \gamma_{i,j}/3$. The final equation resembles the expression for Shannon capacity [66] in the AWGN channel. The factor $\Gamma_{i,j}$ is defined as the SINR gap, which relates the performance of a quadrature amplitude modulated signal to the Shannon capacity of the channel.

For simplicity, we assume for the rest of this chapter that there is a common service requirement $\gamma$ for every cell and every subchannel, and that the corresponding SINR gap is $\Gamma$. By allowing noninteger number of bits per channel symbol – justification of noninteger bits per channel symbol can be found in [67], the optimization problem can be recast as

$$\max_{P_{i,j}^{(u)}} \sum_{i,j} \log\left(1 + \frac{SINR_{i,j}}{\Gamma}\right), \quad \text{subject to} \quad \begin{cases} \sum_{j,u} P_{i,j}^{(u)} \leq P_i, \ \forall\, i, \\ P_{i,j}^{(u)} \geq 0, \ \forall\, i,j,u. \end{cases} \tag{5.10}$$

## 5.2  Transmit and Receive Diversity

In this section we consider diversity combining in the case of transmit and receive diversity and derive the effective signal-to-interference ratio. For fair comparison, we use normalized channel gains so that

$$E\left[\sum_{u,v} |c_{i'i,j}^{u,v}|^2\right] = \text{Constant}. \tag{5.11}$$

Also, the power of the AWGN noise level is the same at each receive antenna, i.e., $E|n_{i,j}^v(k)|^2 = N_{i,j}, \forall v = 1, 2, \cdots, N_{RX}$. We start with single transmit and receive antenna, Then we move to receive diversity and maximal ratio combining. At last we consider transmit diversity, using the space-time block code proposed by Alamouti [28]. We assume that the propagation delay only depends on the direct distance between the source and the destination so the signals from multiple transmit antennas of a mobile or base station arrive at the multiple receive antennas of another base station or mobile at the same time. Based on this assumption, we discuss how to calculate the power of cochannel interference in detail, a major issue in deriving the SINR for transmit diversity.

## 5.2.1 Single Transmit and Receive Antenna

In the case of single transmit and receive antenna, the SINR is given by

$$SINR_{i,j} = \frac{|c_{ii,j}^{1,1}|^2 P_{i,j}}{N_{i,j} + \sum_{\substack{i'=1 \\ i' \neq i}}^{N_C} |c_{i'i,j}^{1,1}|^2 P_{i',j}} \tag{5.12}$$

For convenience, let

$$\xi_{i'i,j} = \begin{cases} \frac{1}{\Gamma} |c_{ii,j}^{1,1}|^2, & i' = i, \\[2mm] |c_{i'i,j}^{1,1}|^2, & i' \neq i. \end{cases} \tag{5.13}$$

Then the SINR becomes

$$SINR_{i,j} = \frac{\Gamma \xi_{ii,j} P_{i,j}}{N_{i,j} + \sum_{\substack{i'=1 \\ i' \neq i}}^{N_C} \xi_{i'i,j} P_{i',j}}. \tag{5.14}$$

And the maximizing problem becomes

$$\max_{P_{i,j}} \sum_{i,j} \log \left( 1 + \frac{\xi_{ii,j} P_{i,j}}{N_{i,j} + \sum_{\substack{i'=1 \\ i' \neq i}}^{N_C} \xi_{i'i,j} P_{i',j}} \right)$$

subject to

$$\begin{cases} \sum_j P_{i,j} \leq P_i, \ \forall \, i, \\[2mm] P_{i,j} \geq 0, \ \forall \, i, j. \end{cases} \tag{5.15}$$

The original problem is a nonlinear optimization problem with linear inequality constraints. As $P_{i,j}^{(u)}$ is always nonnegative, we can let $P_{i,j}^{(u)} = \left[ q_{i,j}^{(u)} \right]^2$ and work on another form of the problem

$$\max_{q_{i,j}^{(1)}} \sum_{i,j} \log \left( 1 + \frac{\xi_{ii,j} [q_{i,j}^{(1)}]^2}{N_{i,j} + \sum_{\substack{i'=1 \\ i' \neq i}}^{N_C} \xi_{i'i,j} [q_{i',j}^{(1)}]^2} \right),$$

subject to

$$\sum_j [q_{i,j}^{(1)}]^2 \leq P_i, \ \forall \, i, \tag{5.16}$$

Now the problem becomes a nonlinear optimization problem with nonlinear inequality constraints. But since it has much fewer inequality constraints, it is more suitable for the active set method in nonlinear optimization.

Define

$$\underline{q}_i = \left[ q_{i,1}^{(1)} \cdots q_{i,1}^{(N_{TX})} \cdots q_{i,N}^{(1)} \cdots q_{i,N}^{(N_{TX})} \right]^T, \underline{q} = \left[ \underline{q}_1 \cdots \underline{q}_M \right]^T. \tag{5.17}$$

and

$$J(\underline{q}) \triangleq - \sum_{i,j} \log \left( 1 + \frac{\xi_{ii,j}[q_{i,j}^{(1)}]^2}{N_{i,j} + \sum_{i' \neq i} \xi_{i'i,j}[q_{i',j}^{(1)}]^2} \right). \tag{5.18}$$

Then the equivalent problem becomes

$$\min_{\underline{q}} J(\underline{q}) \quad \text{subject to} \quad \sum_{j,u}[q_{i,j}^{(u)}]^2 \leq P_i, \ \forall i \tag{5.19}$$

To find the optimum solution to (5.19), we need to derive the first and the second order derivatives of the objective function $J(\underline{q})$. For convenience we first make a few definitions.

$$I_{i,j}(\underline{q}) \triangleq N_{i,j} + \sum_{i' \neq i} \xi_{i'i,j}[q_{i',j}^{(2)}]^2, \tag{5.20}$$

$$b_{i,j}(\underline{q}) \triangleq \log \left( 1 + \frac{\xi_{ii,j}[q_{i,j}^{(1)}]^2}{N_{i,j} + \sum_{i' \neq i} \xi_{i'i,j}[q_{i',j}^{(1)}]^2} \right). \tag{5.21}$$

Then the first order derivative is given by

$$\frac{\partial J(\underline{q})}{\partial q_{m,n}^{(1)}} = \frac{q_{m,n}^{(1)}}{\ln 2} \left\{ \sum_{i=1}^{M} \frac{\xi_{mi,n}}{I_{i,n}(\underline{q})} \left[ 1 - e^{-b_{i,n}(\underline{q})} \right] - \frac{\xi_{mm,n}}{I_{m,n}(\underline{q})} \right\} \tag{5.22}$$

The second order derivative is given by

$$\frac{\partial^2 J(\underline{q})}{\partial q_{k,l}^{(1)} \partial q_{m,n}^{(1)}} = 0, \ l \neq n. \tag{5.23}$$

$$\frac{\partial^2 J(\underline{q})}{\partial q_{k,n}^{(1)} \partial q_{m,n}^{(1)}} = -\frac{2q_{m,n}^{(1)}q_{k,n}^{(1)}}{\ln 2} \left\{ \sum_{i=1}^{M} \frac{\xi_{mi,n}\xi_{ki,n}}{[I_{i,n}(\underline{q})]^2} \left[ 1 - e^{-2b_{i,n}(\underline{q})} \right] \right.$$

$$
\left. - \frac{\xi_{mk,n}\xi_{kk,n}}{\left[I_{k,n}(\underline{q})\right]^2} - \frac{\xi_{mm,n}\xi_{km,n}}{\left[I_{m,n}(\underline{q})\right]^2} \right\} , \ k \neq m; \tag{5.24}
$$

$$
\frac{\partial^2 J(\underline{q})}{\partial q_{m,n}^{(1)} \partial q_{m,n}^{(1)}} = \frac{1}{\ln 2} \left\{ \sum_{i=1}^{M} \frac{\xi_{mi,n}}{I_{i,n}(\underline{q})} \left[1 - e^{-b_{i,n}(\underline{q})}\right] - \frac{\xi_{mm,n}}{I_{m,n}(\underline{q})} \right\}
$$
$$
- \frac{2[q_{m,n}^{(1)}]^2}{\ln 2} \left\{ \sum_{i=1}^{M} \left[\frac{\xi_{mi,n}}{I_{i,n}(\underline{q})}\right]^2 \left[1 - e^{-2b_{i,n}(\underline{q})}\right] - \left[\frac{\xi_{mm,n}}{I_{m,n}(\underline{q})}\right]^2 \right\}. 
$$
$$
\tag{5.25}
$$

### 5.2.2 Receive Diversity

In the case of receive diversity, one transmit and $N_{RX}$ receiver antennas are used. If at time $k$, the $i$th mobile sends a symbol $s_{i,j}^1(k)$ through subchannel $j$ from its transmit antenna to the multiple antennas at the $i$th base station. The received signal at the $N_{RX}$ receive antennas can be written as

$$
\begin{cases}
r_{i,j}^{(1)}(k) & = \ c_{ii,j}^{1,1}\sqrt{P_{i,j}^{(1)}}\, s_{i,j}^{(1)}(k) + i_{i,j}^{(1)}(k) + n_{i,j}^{(1)}(k), \\[2mm]
r_{i,j}^{(2)}(k) & = \ c_{ii,j}^{1,2}\sqrt{P_{i,j}^{(1)}}\, s_{i,j}^{(1)}(k) + i_{i,j}^{(2)}(k) + n_{i,j}^{(2)}(k), \\[2mm]
\vdots & \quad \vdots \ \ \vdots \\[2mm]
r_{i,j}^{(N_{RX})}(k) & = \ c_{ii,j}^{1,N_{RX}}\sqrt{P_{i,j}^{(1)}}\, s_{i,j}^{(1)}(k) + i_{i,j}^{(N_{RX})}(k) + n_{i,j}^{(N_{RX})}(k).
\end{cases}
\tag{5.26}
$$

By using maximal-ratio combining, we can form a decision variable for $s_{i,j}^1(k)$ as follows

$$
\begin{aligned}
y_{i,j}(k) & = \ \sum_{v=1}^{N_{RX}} c_{ii,j}^{1,v\,*} \sqrt{P_{i,j}^{(1)}}\ r_{i,j}^{(1)}(k) \\[2mm]
& = \ \left(\sum_{v=1}^{N_{RX}} |c_{ii,j}^{1,v}|^2\right) P_{i,j}^{(1)} s_{i,j}^{(1)}(k) + \sqrt{P_{i,j}^{(1)}} \sum_{v=1}^{N_{RX}} c_{ii,j}^{1,v\,*}\, i_{i,j}^{(v)}(k) \\[2mm]
& \quad + \sqrt{P_{i,j}^{(1)}} \sum_{v=1}^{N_{RX}} c_{ii,j}^{1,v\,*}\, n_{i,j}^{(v)}(k) \\[2mm]
& = \ \left(\sum_{v=1}^{N_{RX}} |c_{ii,j}^{1,v}|^2\right) P_{i,j}^{(1)} s_{i,j}^{(1)}(k) + \sqrt{P_{i,j}^{(1)}} \sum_{v=1}^{N_{RX}} c_{ii,j}^{1,v\,*} \sum_{\substack{i'=1 \\ i'\neq i}}^{N_C} c_{i'i,j}^{1,v}\, \zeta_{i',j}^{(1)}(k)
\end{aligned}
$$

$$+\sqrt{P_{i,j}^{(1)}} \sum_{v=1}^{N_{RX}} c_{ii,j}^{1,v \, *} \, n_{i,j}^{(v)}(k)$$

$$= \left( \sum_{v=1}^{N_{RX}} \left| c_{ii,j}^{1,v} \right|^2 \right) P_{i,j}^{(1)} s_{i,j}^{(1)}(k) + \sqrt{P_{i,j}^{(1)}} \sum_{\substack{i'=1 \\ i' \neq i}}^{N_C} \left( \sum_{v=1}^{N_{RX}} c_{ii,j}^{1,v \, *} \, c_{i'i,j}^{1,v} \right) \zeta_{i',j}^{(1)}(k)$$

$$+\sqrt{P_{i,j}^{(1)}} \sum_{v=1}^{N_{RX}} c_{ii,j}^{1,v \, *} \, n_{i,j}^{(v)}(k), \tag{5.27}$$

where $\zeta_{i',j}^{(1)}$ is the interference due to transmission of the $i$th mobile on the $j$th subchannel. Since the signals $s_{i',j}^{(1)}(k)$ transmitted from different mobiles are mutually independent, so are the interference $\zeta_{i',j}^{(1)}(k)$'s. As $E\left[ |\zeta_{i',j}^{(u)}|^2 \right] = P_{i',j}^{(u)}$, the signal-to-interference ratio at the $j$the subchannel of the $i$th base station can be written as

$$SINR_{i,j}^r = \frac{\left( \sum_{v=1}^{N_{RX}} \left| c_{ii,j}^{1,v} \right|^2 \right)^2 P_{i,j}^{(1)}}{\left( \sum_{v=1}^{N_{RX}} \left| c_{ii,j}^{1,v} \right|^2 \right) N_{i,j} + \sum_{\substack{i'=1 \\ i' \neq i}}^{N_C} \left| \sum_{v=1}^{N_{RX}} c_{ii,j}^{1,v \, *} \, c_{i'i,j}^{1,v} \right|^2 P_{i',j}^{(1)}} \tag{5.28}$$

For convenience, define

$$\eta_{i'i,j} \triangleq \begin{cases} \frac{1}{\Gamma} \sum_{v=1}^{N_{RX}} |c_{ii,j}^{1,v}|^2, & i' = i, \\[2ex] \sum_{v=1}^{N_{RX}} c_{ii,j}^{1,v \, *} \, c_{i'i,j}^{1,v} / \sum_{v=1}^{N_{RX}} |c_{ii,j}^{1,v}|^2, & i' \neq i. \end{cases} \tag{5.29}$$

Then the effective SINR becomes

$$SINR_{i,j}^r = \frac{\Gamma \, \eta_{ii,j} P_{i,j}^{(1)}}{N_{i,j} + \sum_{\substack{i'=1 \\ i' \neq i}}^{N_C} \eta_{i'i,j} P_{i',j}^{(1)}}. \tag{5.30}$$

As (5.30) has the same form as (5.14), the rest of the problem is the same as in the case of single transmit and receive antenna.

## 5.2.3 Transmit Diversity

To exploit the transmit diversity, we adopt Alamouti's [28] approach, which involves two transmit antennas and one receive antenna, i.e., $N_{TX} = 2$ and

$N_{RX} = 1$. Suppose there are symbols $s_{i,j}(2k)$ and $s_{i,j}(2k+1)$ to be transmitted at time $2k$ and $2k+1$ from subchannel $j$ of the $i$th mobile. To make use of the transmit diversity, at time $2k$, after the inverse Fourier transform, $s_{i,j}(2k)$ is transmitted through one of the antennas and $s_{i,j}(2k+1)$ transmitted through the other antenna; at time $2k+1$, $-s_{i,j}^*(2k+1)$ and $s_{i,j}^*(2k)$ are transmitted through two antennas after the inverse Fourier transform.

At the $ith$ base station, the signals are first passed through the Fourier transform. At time $2k$, the output of subchannel $j$ at antenna $v$ can be written as

$$
\begin{aligned}
r_{i,j}^{(v)}(2k) &= c_{ii,j}^{1,v}\sqrt{P_{i,j}^{(1)}}s_{i,j}(2k) + c_{ii,j}^{2,v}\sqrt{P_{i,j}^{(2)}}s_{i,j}(2k+1) \\
&\quad + i_{i,j}^{(v)}(2k) + n_{i,j}^{(v)}(2k).
\end{aligned}
\tag{5.31}
$$

The output of subchannel $j$ at time $2k+1$ is given by

$$
\begin{aligned}
r_{i,j}^{(v)}(2k+1) &= c_{ii,j}^{1,v}\sqrt{P_{i,j}^{(1)}}\left[-s_{i,j}^*(2k+1)\right] + c_{ii,j}^{2,v}\sqrt{P_{i,j}^{(2)}}s_{i,j}^*(2k) \\
&\quad + i_{i,j}^{(v)}(2k+1) + n_{i,j}^{(v)}(2k+1).
\end{aligned}
\tag{5.32}
$$

Let

$$
\begin{cases}
y_{i,j}^{(v)}(2k) = c_{ii,j}^{1,v\,*}\sqrt{P_{i,j}^{(1)}}r_{i,j}^{(v)}(k) + c_{ii,j}^{2,v}\sqrt{P_{i,j}^{(2)}}r_{i,j}^{(v)\,*}(k+1), \\
y_{i,j}^{(v)}(2k+1) = c_{ii,j}^{2,v\,*}\sqrt{P_{i,j}^{(2)}}r_{i,j}^{(v)}(k) - c_{ii,j}^{1,v}\sqrt{P_{i,j}^{(1)}}r_{i,j}^{(v)\,*}(k+1).
\end{cases}
\tag{5.33}
$$

Then we have

$$
\begin{cases}
\begin{aligned}
y_{i,j}^{(v)}(2k) &= (|c_{ii,j}^{1,v}|^2 P_{i,j}^{(1)} + |c_{ii,j}^{2,v}|^2 P_{i,j}^{(2)})s_{i,j}(2k) \\
&\quad + c_{ii,j}^{1,v\,*}\sqrt{P_{i,j}^{(1)}}i_{i,j}^{(v)}(k) + c_{ii,j}^{2,v}\sqrt{P_{i,j}^{(2)}}i_{i,j}^{(v)\,*}(k+1) \\
&\quad + c_{ii,j}^{1,v\,*}\sqrt{P_{i,j}^{(1)}}n_{i,j}^{(v)}(k) + c_{ii,j}^{2,v}\sqrt{P_{i,j}^{(2)}}n_{i,j}^{(v)\,*}(k+1), \\
y_{i,j}^{(v)}(2k+1) &= (|c_{ii,j}^{1,v}|^2 P_{i,j}^{(1)} + |c_{ii,j}^{2,v}|^2 P_{i,j}^{(2)})s_{i,j}(2k+1) \\
&\quad + c_{ii,j}^{2,v\,*}\sqrt{P_{i,j}^{(2)}}i_{i,j}^{(v)}(k) - c_{ii,j}^{1,v}\sqrt{P_{i,j}^{(1)}}i_{i,j}^{(v)\,*}(k+1)) \\
&\quad + c_{ii,j}^{2,v\,*}\sqrt{P_{i,j}^{(2)}}n_{i,j}^{(v)}(k) - c_{ii,j}^{1,v}\sqrt{P_{i,j}^{(1)}}n_{i,j}^{(v)\,*}(k+1).
\end{aligned}
\end{cases}
\tag{5.34}
$$

$y_{i,j}^{(v)}(2k)$ and $y_{i,j}^{(v)}(2k+1)$ can be used for the demodulation of the signals $s_{i,j}(2k)$ and $s_{i,j}(2k+1)$ respectively. Here we can treat $y_{i,j}^{(v)}(2k)$ and $y1_{i,j}^{(v)}(2k+1)$ as received samples of a virtual subchannel $j$ with $|c_{ii,j}^{1,v}|^2 P_{i,j}^{(1)} + |c_{ii,j}^{2,v}|^2 P_{i,j}^{(2)}$ as its channel state information.

Power of Cochannel Interference

In the case of space-time coded OFDM systems, the transmitted signals from multiple transmit antennas are not independent of each other, which poses the question of how to analyze the power of cochannel interference. We assume that the propagation delay only depends on the direct distance between the source and the destination so the signals from multiple transmit antennas of a mobile or base station arrive at the multiple receive antennas of another base station or mobile at the same time. The remaining issue is, because the intended signal and the cochannel interference come from difference sources, we must consider delays between the intended signals and the cochannel interferences in analyzing the power of cochannel interference.

For simplicity, we first consider only one interfering source, i.e.,

$$i_{i,j}^{(v)}(k) = c_{i'i,j}^{1,v}\sqrt{P_{i',j}^{(1)}}\zeta_{i',j}^{(1)}(k) + c_{i'i,j}^{2,v}\sqrt{P_{i',j}^{(2)}}\zeta_{i',j}^{(2)}(k), \ i' \neq i. \tag{5.35}$$

Substitute into (5.31), we have

$$
\begin{cases}
r_{i,j}^{(v)}(2k) & = c_{ii,j}^{1,v}\sqrt{P_{i,j}^{(1)}}s_{i,j}(2k) + c_{ii,j}^{2,v}\sqrt{P_{i,j}^{(2)}}s_{i,j}(2k+1)+ \\
& \quad c_{i'i,j}^{1,v}\sqrt{P_{i',j}^{(1)}}\zeta_{i',j}^{(1)}(2k) + c_{i'i,j}^{2,v}\sqrt{P_{i',j}^{(2)}}\zeta_{i',j}^{(2)}(2k) + n_{i,j}^{(v)}(2k), \\
r_{i,j}^{(v)}(2k+1) & = c_{ii,j}^{1,v}\sqrt{P_{i,j}^{(1)}}[-s_{i,j}^*(2k+1)] + c_{ii,j}^{2,v}\sqrt{P_{i,j}^{(2)}}s_{i,j}^*(2k)+ \\
& \quad c_{i'i,j}^{1,v}\sqrt{P_{i',j}^{(1)}}\zeta_{i',j}^{(1)}(2k+1) + c_{i'i,j}^{2,v}\sqrt{P_{i',j}^{(2)}}\zeta_{i',j}^{(2)}(2k+1) \\
& \quad +n_{i,j}^{(v)}(2k+1).
\end{cases}
\tag{5.36}
$$

Note here that the cochannel interference terms $\zeta_{i',j}^{(u)}(2k) \neq s_{i',j}^{(u)}(2k)$ because the OFDM receiver is supposed to be synchronized to the intended signal $s_{i,j}(k)$ instead of the interference $s_{i',j}^{(u)}(k)$. We denote the delay between the intended signal and the CCI being considered as $\tau_{i'i,j}$. For convenience, let

$$g_{ii,j}^{u,v} = c_{ii,j}^{u,v} \sqrt{P_{i,j}^{(u)}}, \tag{5.37}$$

and

$$
\begin{cases}
z_{i',j}^{(1)}(2k) & = \zeta_{i',j}^{(1)}(2k), \\
z_{i',j}^{(2)}(2k) & = \zeta_{i',j}^{(2)}(2k), \\
z_{i',j}^{(1)}(2k+1) & = -\zeta_{i',j}^{(1)\,*}(2k+1), \\
z_{i',j}^{(2)}(2k+1) & = \zeta_{i',j}^{(2)\,*}(2k+1).
\end{cases}
\tag{5.38}
$$

Then (5.36) becomes

$$
\begin{cases}
r_{i,j}^{(v)}(2k) & = \; g_{ii,j}^{1,v} s_{i,j}(2k) + g_{ii,j}^{2,v} s_{i,j}(2k+1) + \\
& \quad g_{i'i,j}^{1,v} z_{i',j}^{(1)}(2k) + g_{i'i,j}^{2,v} z_{i',j}^{(2)}(2k) + n_{i,j}^{(v)}(2k), \\
r_{i,j}^{(v)}(2k+1) & = \; g_{ii,j}^{1,v}[-s_{i,j}^{*}(2k+1)] + g_{ii,j}^{2,v} s_{i,j}^{*}(2k) + \\
& \quad g_{i'i,j}^{1,v}[-z_{i',j}^{(1)\,*}(2k+1)] + g_{i'i,j}^{2,v} z_{i',j}^{(2)\,*}(2k+1) \\
& \quad + n_{i,j}^{(v)}(2k+1).
\end{cases}
\tag{5.39}
$$

Without loss of generality, we consider $0 \leq \tau_{i'i,j} < 2T$. We first solve for $s_{i,j}(2k)$.

$$
\begin{aligned}
y_{i,j}^{(v)}(2k) & = \; g_{ii,j}^{1,v\,*} r_{i,j}^{v}(2k) + g_{ii,j}^{2,v} r_{i,j}^{v\,*}(2k+1) \\
& = \; \left( |g_{ii,j}^{1,v}|^2 + |g_{ii,j}^{2,v}|^2 \right) s_{i,j}(2k) + \\
& \quad g_{ii,j}^{1,v\,*} g_{i'i,j}^{1,v} z_{i',j}^{(1)}(2k) + g_{ii,j}^{1,v\,*} g_{i'i,j}^{2,v} z_{i',j}^{(2)}(2k) - \\
& \quad g_{ii,j}^{2,v} g_{i'i,j}^{1,v\,*} z_{i',j}^{(1)}(2k+1) + g_{ii,j}^{2,v} g_{i'i,j}^{2,v\,*} z_{i',j}^{(2)}(2k+1) + \\
& \quad g_{ii,j}^{1,v\,*} n_{i,j}^{(v)}(2k) + g_{ii,j}^{2,v} n_{i,j}^{(v)\,*}(2k+1)
\end{aligned}
\tag{5.40}
$$

In modeling the power of cochannel interference, we should analyze the correlation of $z_{i',j}^{(1)}(2k)$, $z_{i',j}^{(2)}(2k)$, $z_{i',j}^{(1)}(2k+1)$, and $z_{i',j}^{(2)}(2k+1)$.



Figure 5.2: Cochannel Interference, $\tau_{i'i,j} = 0$

*Case A*   As shown in Fig. 5.2, $\tau_{i'i,j} = 0$. In this case, we have

$$z_{i',j}^{(1)}(2k) = z_{i',j}^{(2)}(2k+1) = s_{i',j}(2k), \tag{5.41}$$

$$z_{i',j}^{(2)}(2k) = z_{i',j}^{(1)}(2k+1) = s_{i',j}(2k+1). \tag{5.42}$$

So the total interference can be written as

$$
\begin{aligned}
I_{i,j}^{(v)}(2k) &= g_{ii,j}^{1,v\,*}g_{i'i,j}^{1,v}z_{i',j}^{(1)}(2k) + g_{ii,j}^{1,v\,*}g_{i'i,j}^{2,v}z_{i',j}^{(2)}(2k) - \\
&\quad g_{ii,j}^{2,v}g_{i'i,j}^{1,v\,*}z_{i',j}^{(1)}(2k+1) + g_{ii,j}^{2,v}g_{i'i,j}^{2,v\,*}z_{i',j}^{(2)}(2k+1) \\
&= g_{ii,j}^{1,v\,*}g_{i'i,j}^{1,v}s_{i',j}(2k) + g_{ii,j}^{1,v\,*}g_{i'i,j}^{2,v}s_{i',j}(2k+1) - \\
&\quad g_{ii,j}^{2,v}g_{i'i,j}^{1,v\,*}s_{i',j}(2k+1) + g_{ii,j}^{2,v}g_{i'i,j}^{2,v\,*}s_{i',j}(2k) \\
&= \left(g_{ii,j}^{1,v\,*}g_{i'i,j}^{1,v} + g_{ii,j}^{2,v}g_{i'i,j}^{2,v\,*}\right)s_{i',j}(2k) + \\
&\quad \left(g_{ii,j}^{1,v\,*}g_{i'i,j}^{2,v} - g_{ii,j}^{2,v}g_{i'i,j}^{1,v\,*}\right)s_{i',j}(2k+1). \tag{5.43}
\end{aligned}
$$

And the power of the total interference is given by

$$
E\left[|I_{i,j}^{(v)}(2k)|^2\right] = \left|g_{ii,j}^{1,v\,*}g_{i'i,j}^{1,v} + g_{ii,j}^{2,v}g_{i'i,j}^{2,v\,*}\right|^2 E\left[|s_{i',j}(2k)|^2\right] +
$$

$$\left|g_{ii,j}^{1,v\,*}g_{i'i,j}^{2,v} - g_{ii,j}^{2,v}g_{i'i,j}^{1,v\,*}\right|^2 E\left[\left|s_{i',j}(2k+1)\right|^2\right]$$

$$= \left|g_{ii,j}^{1,v\,*}g_{i'i,j}^{1,v} + g_{ii,j}^{2,v}g_{i'i,j}^{2,v\,*}\right|^2 + \left|g_{ii,j}^{1,v\,*}g_{i'i,j}^{2,v} - g_{ii,j}^{2,v}g_{i'i,j}^{1,v\,*}\right|^2$$

$$= |g_{ii,j}^{1,v}|^2|g_{i'i,j}^{1,v}|^2 + |g_{ii,j}^{2,v}|^2|g_{i'i,j}^{2,v}|^2 + |g_{ii,j}^{1,v}|^2|g_{i'i,j}^{2,v}|^2 + |g_{ii,j}^{2,v}|^2|g_{i'i,j}^{1,v}|^2$$

$$= \left(|g_{ii,j}^{1,v}|^2 + |g_{ii,j}^{2,v}|^2\right)\left(|g_{i'i,j}^{1,v}|^2 + |g_{i'i,j}^{2,v}|^2\right)$$

$$= \left(|c_{ii,j}^{1,v}|^2 P_{i,j}^{(1)} + |c_{ii,j}^{2,v}|^2 P_{i,j}^{(2)}\right)\left(|c_{i'i,j}^{1,v}|^2 P_{i',j}^{(1)} + |c_{i'i,j}^{2,v}|^2 P_{i',j}^{(2)}\right).(5.44)$$
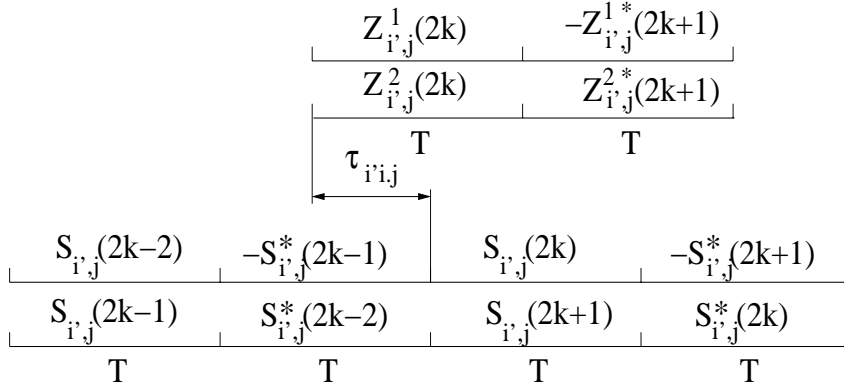


Figure 5.3: Cochannel Interference, $0 < \tau_{i'i,j} < T$

*Case B*    As shown in Fig. 5.3, $0 < \tau_{i'i,j} < T$. In this case, obviously $z_{i',j}^{(1)}(2k)$ and $z_{i',j}^{(2)}(2k)$ are independent. For further analysis, we assume that the input symbols to the space-time encoder are independent with each other and that the inphase and the quadrature components of data symbols are independent and balanced in power. Under this assumption, even though both $z_{i',j}^{(1)}(2k)$ and $-z_{i',j}^{(1)\,*}(2k+1)$ contains $s_{i',j}(2k)$, $z_{i',j}^{(1)}(2k)$ and $z_{i',j}^{(1)}(2k+1)$ are uncorrelated because

$$E\left[s_{i',j}(2k)\left(s_{i',j}^{*}(2k)\right)^{*}\right] = E[s_{i',j}^2(2k)] = E[x_{i',j}^2(2k)] - E[y_{i',j}^2(2k)] = 0, (5.45)$$

where $x_{i',j}(2k)$ and $y_{i',j}(2k)$ are real and imaginary parts of $s_{i',j}(2k)$ respectively. Although we did not include the FFT and IFFT in the argument, but since they are linear transforms, they do not affect the result. Using similar arguments, we

can prove that $z^{(2)}_{i',j}(2k)$ and $z^{(2)}_{i',j}(2k+1)$ are uncorrelated, and that $z^{(1)}_{i',j}(2k+1)$ and $z^{(2)}_{i',j}(2k+1)$ are also uncorrelated. Therefore,

$$
\begin{aligned}
& E\left[|I^{(v)}_{i,j}(2k)|^2\right] \\
= \; & E\left[|g^{1,v\,*}_{ii,j}g^{1,v}_{i'i,j}z^{(1)}_{i',j}(2k) + g^{1,v\,*}_{ii,j}g^{2,v}_{i'i,j}z^{(2)}_{i',j}(2k)- \right. \\
& \left. g^{2,v}_{ii,j}g^{1,v\,*}_{i'i,j}z^{(1)}_{i',j}(2k+1) + g^{2,v}_{ii,j}g^{2,v\,*}_{i'i,j}z^{(2)}_{i',j}(2k+1)|^2\right] \\
= \; & E\left[|g^{1,v\,*}_{ii,j}g^{1,v}_{i'i,j}z^{(1)}_{i',j}(2k) + g^{2,v}_{ii,j}g^{2,v\,*}_{i'i,j}z^{(2)}_{i',j}(2k+1)|^2\right] + \\
& E\left[|g^{1,v\,*}_{ii,j}g^{2,v}_{i'i,j}z^{(2)}_{i',j}(2k) - g^{2,v}_{ii,j}g^{1,v\,*}_{i'i,j}z^{(1)}_{i',j}(2k+1)|^2\right] \\
= \; & |g^{1,v}_{ii,j}|^2|g^{1,v}_{i'i,j}|^2 + |g^{2,v}_{ii,j}|^2|g^{2,v}_{i'i,j}|^2 + |g^{1,v}_{ii,j}|^2|g^{2,v}_{i'i,j}|^2 + |g^{2,v}_{ii,j}|^2|g^{1,v}_{i'i,j}|^2 \\
& + g^{1,v\,*}_{ii,j}g^{1,v}_{i'i,j}g^{2,v\,*}_{ii,j}g^{2,v}_{i'i,j}E|z^{(1)}_{i',j}(2k)z^{(2)\,*}_{i',j}(2k+1)| \\
& + g^{1,v}_{ii,j}g^{1,v\,*}_{i'i,j}g^{2,v}_{ii,j}g^{2,v\,*}_{i'i,j}E|z^{(1)\,*}_{i',j}(2k)z^{(2)}_{i',j}(2k+1)| \\
& - g^{1,v\,*}_{ii,j}g^{2,v}_{i'i,j}g^{2,v\,*}_{ii,j}g^{1,v}_{i'i,j}E|z^{(2)}_{i',j}(2k)z^{(1)\,*}_{i',j}(2k+1)| \\
& - g^{1,v}_{ii,j}g^{2,v\,*}_{i'i,j}g^{2,v}_{ii,j}g^{1,v\,*}_{i'i,j}E|z^{(2)\,*}_{i',j}(2k)z^{(1)}_{i',j}(2k+1)| \\
= \; & \left(|g^{1,v}_{ii,j}|^2 + |g^{2,v}_{ii,j}|^2\right)\left(|g^{1,v}_{i'i,j}|^2 + |g^{2,v}_{i'i,j}|^2\right) \\
& + g^{1,v\,*}_{ii,j}g^{1,v}_{i'i,j}g^{2,v\,*}_{ii,j}g^{2,v}_{i'i,j}\left[E|z^{(1)}_{i',j}(2k)z^{(2)\,*}_{i',j}(2k+1)| - E|z^{(2)}_{i',j}(2k)z^{(1)\,*}_{i',j}(2k+1)|\right] \\
& + g^{1,v}_{ii,j}g^{1,v\,*}_{i'i,j}g^{2,v}_{ii,j}g^{2,v\,*}_{i'i,j}\left[E|z^{(1)\,*}_{i',j}(2k)z^{(2)}_{i',j}(2k+1)| - E|z^{(2)\,*}_{i',j}(2k)z^{(1)}_{i',j}(2k+1)|\right]
\end{aligned}
$$

(5.46)

Since the correlation $E\left[|z^{(1)}_{i',j}(2k)z^{(2)\,*}_{i',j}(2k+1)|\right]$ and $E\left[|z^{(2)}_{i',j}(2k)z^{(1)\,*}_{i',j}(2k+1)|\right]$ only depends on the delay $\tau_{i'i,j}$, they are equal by symmetry, which is true even when the transmit power on the two antennas are different. Similarly, $E\left[|z^{(1)\,*}_{i',j}(2k)z^{(2)}_{i',j}(2k+1)|\right]$ is equal to $E\left[|z^{(2)\,*}_{i',j}(2k)z^{(1)}_{i',j}(2k+1)|\right]$. So we have

$$
\begin{aligned}
E\left[|I^{(v)}_{i,j}(2k)|^2\right] = \; & \left(|g^{1,v}_{ii,j}|^2 + |g^{2,v}_{ii,j}|^2\right)\left(|g^{1,v}_{i'i,j}|^2 + |g^{2,v}_{i'i,j}|^2\right) \\
= \; & \left(|c^{1,v}_{ii,j}|^2 P^{(1)}_{i,j} + |c^{2,v}_{ii,j}|^2 P^{(2)}_{i,j}\right)\left(|c^{1,v}_{i'i,j}|^2 P^{(1)}_{i',j} + |c^{2,v}_{i'i,j}|^2 P^{(2)}_{i',j}\right).
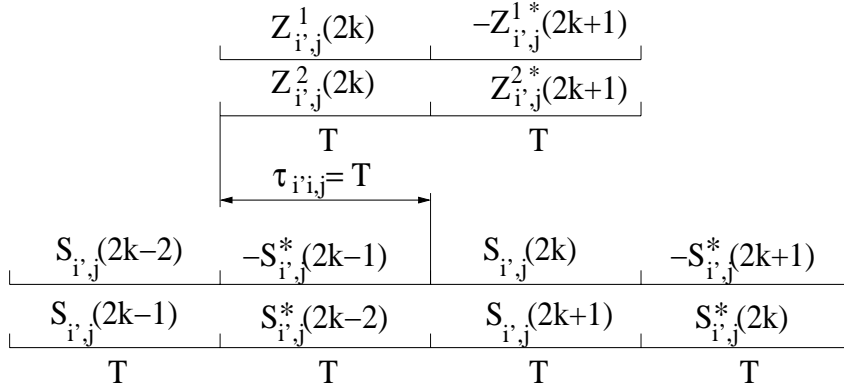\end{aligned}
$$

138

Figure 5.4: Cochannel Interference, $\tau_{i'i,j} = T$

*Case C*   As shown in Fig. 5.4, $\tau_{i'i,j} = T$. In this case, we have

$$z_{i',j}^{(1)}(2k) = -s_{i',j}^*(2k-1), \tag{5.48}$$

$$z_{i',j}^{(2)}(2k) = s_{i',j}^*(2k-2), \tag{5.49}$$

$$z_{i',j}^{(1)}(2k+1) = -s_{i',j}^*(2k), \tag{5.50}$$

$$z_{i',j}^{(2)}(2k+1) = s_{i',j}^*(2k+1). \tag{5.51}$$

Since $s_{i',j}(2k-2)$, $s_{i',j}(2k-1)$, $s_{i',j}(2k)$, and $s_{i',j}(2k+1)$ are mutually independent, $z_{i',j}^{(1)}(2k)$, $z_{i',j}^{(2)}(2k)$, $z_{i',j}^{(1)}(2k+1)$, and $z_{i',j}^{(2)}(2k+1)$ are also mutually independent of each other. Therefore

$$
\begin{aligned}
E\left[|I_{i,j}^{(v)}(2k)|^2\right] &= E\left[|g_{ii,j}^{1,v\,*}g_{i'i,j}^{1,v}z_{i',j}^{(1)}(2k) + g_{ii,j}^{1,v\,*}g_{i'i,j}^{2,v}z_{i',j}^{(2)}(2k) - \right.\\
&\qquad \left. g_{ii,j}^{2,v}g_{i'i,j}^{1,v\,*}z_{i',j}^{(1)}(2k+1) + g_{ii,j}^{2,v}g_{i'i,j}^{2,v\,*}z_{i',j}^{(2)}(2k+1)|^2\right]\\
&= |g_{ii,j}^{1,v}|^2|g_{i'i,j}^{1,v}|^2 + |g_{ii,j}^{1,v}|^2|g_{i'i,j}^{2,v}|^2 + |g_{ii,j}^{2,v}|^2|g_{i'i,j}^{1,v}|^2 + |g_{ii,j}^{2,v}|^2|g_{i'i,j}^{2,v}|^2\\
&= \left(|g_{ii,j}^{1,v}|^2 + |g_{ii,j}^{2,v}|^2\right)\left(|g_{i'i,j}^{1,v}|^2 + |g_{i'i,j}^{2,v}|^2\right)\\
&= \left(|c_{ii,j}^{1,v}|^2 P_{i,j}^{(1)} + |c_{ii,j}^{2,v}|^2 P_{i,j}^{(2)}\right)\left(|c_{i'i,j}^{1,v}|^2 P_{i',j}^{(1)} + |c_{i'i,j}^{2,v}|^2 P_{i',j}^{(2)}\right). \tag{5.52}
\end{aligned}
$$

$$\text{Z}^{1}_{\text{i',j}}(2k) \qquad -\text{Z}^{1\,*}_{\text{i',j}}(2k+1)$$

$$\text{Z}^{2}_{\text{i',j}}(2k) \qquad \text{Z}^{2\,*}_{\text{i',j}}(2k+1)$$

$$\text{T} \qquad\qquad \text{T}$$

$$\tau_{\text{i'i,j}}$$

$$S_{\text{i',j}}(2k-2) \quad -S^{*}_{\text{i',j}}(2k-1) \qquad S_{\text{i',j}}(2k) \quad -S^{*}_{\text{i',j}}(2k+1)$$

$$S_{\text{i',j}}(2k-1) \qquad S^{*}_{\text{i',j}}(2k-2) \qquad S_{\text{i',j}}(2k+1) \qquad S^{*}_{\text{i',j}}(2k)$$

$$\text{T} \qquad\qquad \text{T} \qquad\qquad \text{T} \qquad\qquad \text{T}$$
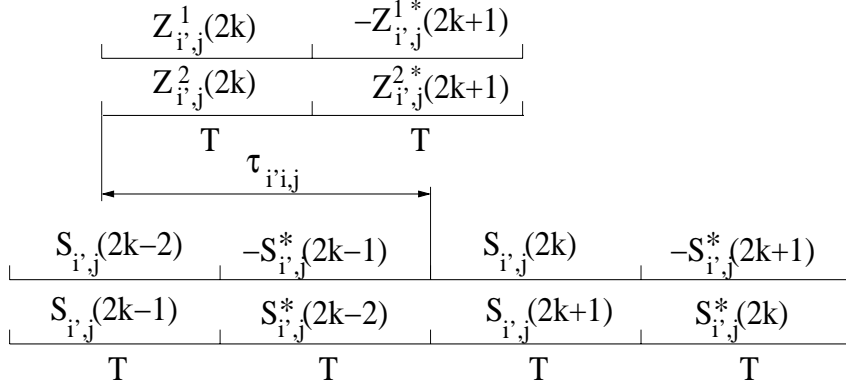
Figure 5.5: Cochannel Interference, $T < \tau_{i'i,j} < 2T$

*Case D*  As shown in Fig. 5.5, $T < \tau_{i'i,j} < 2T$. Using the same argument as in Case B, we have

- $z^{(1)}_{i',j}(2k)$ and $z^{(1)}_{i',j}(2k+1)$ are uncorrelated;

- $z^{(1)}_{i',j}(2k)$ and $z^{(2)}_{i',j}(2k)$ are uncorrelated;

- $z^{(2)}_{i',j}(2k)$ and $z^{(2)}_{i',j}(2k+1)$ are uncorrelated;

- $z^{(1)}_{i',j}(2k+1)$ and $z^{(2)}_{i',j}(2k+1)$ are independent.

And similar to Case B, the power of interference is given by

$$E\left[|I^{(v)}_{i,j}(2k)|^2\right] = \left(|c^{1,v}_{ii,j}|^2 P^{(1)}_{i,j} + |c^{2,v}_{ii,j}|^2 P^{(2)}_{i,j}\right)\left(|c^{1,v}_{i'i,j}|^2 P^{(1)}_{i',j} + |c^{2,v}_{i'i,j}|^2 P^{(2)}_{i',j}\right). \tag{5.53}$$

In summary, the power of an interfering signal from a single cochannel cell is given by (5.53) in all cases. In the case of multiple CCI sources, as they are mutually independent of each other, the power of the total CCI is simply the sum of the power of every interfering source. So the SINR for virtual subchannel $j$ at the $i$th base station can be written as

$$SINR^{t}_{i,j} = \frac{|c^{1,1}_{ii,j}|^2 P^{(1)}_{i,j} + |c^{2,1}_{ii,j}|^2 P^{(2)}_{i,j}}{N_{i,j} + \sum_{i'\neq i}\left(|c^{1,1}_{i'i,j}|^2 P^{(1)}_{i',j} + |c^{2,1}_{i'i,j}|^2 P^{(2)}_{i',j}\right)}. \tag{5.54}$$

140

For simplicity, let

$$\kappa_{i'i,j}^{(u)} = \begin{cases} \frac{1}{\Gamma}|c_{i'i,j}^{u,1}|^2, & i' = i, \\ |c_{i'i,j}^{u,1}|^2, & i' \neq i, \end{cases} \tag{5.55}$$

Then

$$SINR_{i,j}^t = \frac{\Gamma \sum_{u=1}^2 \kappa_{ii,j}^{(u)} \left[q_{i,j}^{(u)}\right]^2}{N_{i,j} + \sum_{i' \neq i} \sum_{u=1}^2 \kappa_{i'i,j}^{(u)} \left[q_{i',j}^{(u)}\right]^2} \tag{5.56}$$

The first and second derivatives of the objective function

In the case of dual transmit antennas, the number of parameters doubles. The objective function now becomes

$$J(\underline{q}) = -\sum_{i,j} \log \left\{ 1 + \frac{\sum_{u=1}^2 \kappa_{ii,j}^{(u)} \left[q_{i,j}^{(u)}\right]^2}{N_{i,j} + \sum_{i' \neq i} \sum_{u=1}^2 \kappa_{i'i,j}^{(u)} \left[q_{i',j}^{(u)}\right]^2} \right\}, \tag{5.57}$$

where $\underline{q}$ is as defined before. The optimization problem can now be recast as

$$\min_{\underline{q}} J(\underline{q}) \quad \text{subject to} \quad \sum_j \sum_u \left[q_{i,j}^{(u)}\right]^2 \leq P_i, \forall i. \tag{5.58}$$

To derive the first and the second order derivatives of the objective function. First we redefine $I_{i,j}(\underline{q})$ and $b_{i,j}(\underline{q})$

$$I_{i,j}(\underline{q}) \triangleq N_{i,j} + \sum_{i' \neq i} \sum_{u=1}^2 \kappa_{i'i,j}^{(u)} \left[q_{i',j}^{(u)}\right]^2, \tag{5.59}$$

$$b_{i,j}(\underline{q}) \triangleq \log \left(1 + \frac{\sum_{u=1}^2 \kappa_{ii,j}^{(u)} \left[q_{i,j}^{(u)}\right]^2}{N_{i,j} + \sum_{i' \neq i} \sum_{u=1}^2 \kappa_{i'i,j}^{(u)} \left[q_{i',j}^{(u)}\right]^2} \right). \tag{5.60}$$

Then the first order derivative is given by

$$\frac{\partial J(\underline{q})}{\partial q_{m,n}^{(u)}} = \frac{q_{m,n}^{(u)}}{\ln 2} \left[\sum_{i=1}^M \frac{\kappa_{mi,n}^{(u)}}{I_{i,n}(\underline{q})} \left(1 - e^{-b_{i,n}(\underline{q})}\right) - \frac{\kappa_{mm,n}^{(u)}}{I_{m,n}(\underline{q})} \right] \tag{5.61}$$

141

The second order derivative is given by

$$
\frac{\partial^2 J(\underline{q})}{\partial q_{k,l}^{(u)} \partial q_{m,n}^{(v)}} = 0, \, l \neq n. \tag{5.62}
$$

$$
\frac{\partial^2 J(\underline{q})}{\partial q_{k,n}^{(u)} \partial q_{m,n}^{(v)}} = -\frac{2q_{k,n}^{(u)} q_{m,n}^{(v)}}{\ln 2} \left\{ \sum_i \frac{\kappa_{ki,n}^{(u)} \kappa_{mi,n}^{(v)}}{\left[ I_{i,n}(\underline{q}) \right]^2} \left[ 1 - e^{-2b_{i,n}(\underline{q})} \right] \right.
$$
$$
\left. -\frac{\kappa_{kk,n}^{(u)} \kappa_{mk,n}^{(v)}}{\left[ I_{k,n}(\underline{q}) \right]^2} - \frac{\kappa_{km,n}^{(u)} \kappa_{mm,n}^{(v)}}{\left[ I_{m,n}(\underline{q}) \right]^2} \right\}, \, \forall k \neq m, u \neq v. \tag{5.63}
$$

$$
\frac{\partial^2 J(\underline{q})}{\partial q_{k,n}^{(u)} \partial q_{m,n}^{(u)}} = -\frac{2q_{m,n}^{(u)} q_{k,n}^{(u)}}{\ln 2} \left\{ \sum_{i=1}^{M} \frac{\kappa_{mi,n}^{(u)} \kappa_{ki,n}^{(u)}}{\left[ I_{i,n}(\underline{q}) \right]^2} \left[ 1 - e^{-2b_{i,n}(\underline{q})} \right] \right.
$$
$$
\left. -\frac{\kappa_{mk,n}^{(u)} \kappa_{kk,n}^{(u)}}{\left[ I_{k,n}(\underline{q}) \right]^2} - \frac{\kappa_{mm,n}^{(u)} \kappa_{km,n}^{(u)}}{\left[ I_{m,n}(\underline{q}) \right]^2} \right\}, \, k \neq m. \tag{5.64}
$$

$$
\frac{\partial^2 J(\underline{q})}{\partial q_{m,n}^{(u)} \partial q_{m,n}^{(v)}} = -\frac{2q_{m,n}^{(u)} q_{m,n}^{(v)}}{\ln 2} \left\{ \sum_i \frac{\kappa_{mi,n}^{(u)} \kappa_{mi,n}^{(v)}}{\left[ I_{i,n}(\underline{q}) \right]^2} \left[ 1 - e^{-2b_{i,n}(\underline{q})} \right] - \frac{\kappa_{mm,n}^{(u)} \kappa_{mm,n}^{(v)}}{\left[ I_{k,n}(\underline{q}) \right]^2} \right\},
$$
$$
\forall u \neq v. \tag{5.65}
$$

$$
\frac{\partial^2 J(\underline{q})}{\partial q_{m,n}^{(u)} \partial q_{m,n}^{(u)}} = \frac{1}{\ln 2} \left\{ \sum_{i=1}^{M} \frac{\kappa_{mi,n}^{(u)}}{I_{i,n}(\underline{q})} \left[ 1 - e^{-b_{i,n}(\underline{q})} \right] - \frac{\kappa_{mm,n}^{(u)}}{I_{m,n}(\underline{q})} \right\}
$$
$$
-\frac{2 \left[ q_{m,n}^{(u)} \right]^2}{\ln 2} \left\{ \sum_{i=1}^{M} \left[ \frac{\kappa_{mi,n}^{(u)}}{I_{i,n}(\underline{q})} \right]^2 \left[ 1 - e^{-2b_{i,n}(\underline{q})} \right] - \left[ \frac{\kappa_{mm,n}^{(u)}}{I_{m,n}(\underline{q})} \right]^2 \right\}. \tag{5.66}
$$

## 5.3   Distributed Power Allocation Algorithm with Transmit and Receive Diversity

In this section, we consider the DWPA for improving the total throughput against frequency-selective fading and cochannel interference. We first assume that each base station can accurately measure the channel state information – $c_{ii,j}^{u,v}$ – for all the intended signal paths and the total interference plus noise power

appearing during demodulation. We further assume that the computed power allocation information can be fed back to the mobile without any distortion. We first consider the case with one transmit antenna. Then we move to two transmit antennas.

## 5.3.1 Single Transmit Antenna

We first extend the DWPA from single receive antenna to multiple receive antennas. The distributed water-pouring algorithm is as follows:

For cochannel base station $i$,

1. Define a set of active subchannels

$$\mathcal{G}_i = \{j : \ SINR_{i,j}^r > \eta\},$$

   where $\eta$ is the least SINR requirement and $SINR_{i,j}^r$ is defined in (5.28).

2. Initially set the set $\mathcal{G}_i$ to include all subchannels.

3. Base station $i$ first measures the subchannel gains $c_{ii,j}^{u,v}$ and computes $\eta_{ii,j}$, $\forall j \in \mathcal{G}_i$ (5.29). It then measures the virtual interference plus noise power

$$I_{i,j} = N_{i,j} + \sum_{\substack{i' \neq 1 \\ i' \neq i}}^{N_C} \eta_{i'i,j} P_{i',j}, \ \forall j \in \mathcal{G}_i$$

   of its own link and forms the virtual effective noise level as

$$I'_{i,j} = \frac{\Gamma}{\eta_{ii,j}} I_{i,j}, \ \forall j \in \mathcal{G}_i$$

4. Apply water-pouring algorithm to all subchannels in $\mathcal{G}_i$

$$\hat{P}_{i,j} = \begin{cases} \frac{P_i + \sum_{j \in \mathcal{G}_i} I'_{i,j}}{n_{\mathcal{G}_i}} - I'_{i,j}, & \forall j \in \mathcal{G}_i \ \& \ \frac{P_i + \sum_{j \in \mathcal{G}_i} I'_{i,j}}{n_{\mathcal{G}_i}} \geq I'_{i,j}, \\ 0, & \text{otherwise}, \end{cases}$$

   where $n_{\mathcal{G}_i}$ is the size of the set $\mathcal{G}_i$.

5. Update the set of active subchannel $\mathcal{G}_i$. Go to step 4 if $\mathcal{G}_i$ is changed; otherwise continue.

6. Feedback $\hat{P}_{i,j}$ to the corresponding mobile. The mobile then adjusts the power and modulation according to this information. Go to step 1.

The algorithm is executed independently by all cochannel base stations. Since there is no analytical approach on how to choose the least SINR requirement $\eta$, it will be selected through simulation.

## 5.3.2 Dual Transmit Antenna

In the case of dual transmit antennas, a new question arises on how to assign the power between the two transmit antennas. A better solution to this problem will be presented in Section 5.4, where the gradient of the objective function is used to balance the power between the two antennas. Given the limited information the receiver has in the DWPA, however, the best way is to use selective diversity (SD) and assign all the power for that subchannel to the antenna with larger channel gain. For comparison, we will also include the approach used in the space-time code, that is, to split the power evenly to two transmit antennas – equal power diversity (EPD), which is the best solution when the channel state information is not available at the transmitter.

Selective Diversity

In this case, the transmitter assigns all the power of $P_{i,j}$ to the antenna with better channel conditions. (5.54) can be written as

$$SINR_{i,j}^t = \frac{\max(|c_{ii,j}^{1,1}|^2, |c_{ii,j}^{2,1}|^2)P_{i,j}}{N_{i,j} + \sum_{i' \neq i} \max\left(|c_{i'i,j}^{1,1}|^2, |c_{i'i,j}^{2,1}|^2\right) P_{i',j}}. \tag{5.67}$$

Replace $\eta_{i'i,j}$ with $\max\left(|c_{i'i,j}^{1,1}|^2, |c_{i'i,j}^{2,1}|^2\right)$, we can apply the DWPA.

**Equal Power Diversity**

In this case, we let $P_{i,j}^{(1)} = P_{i,j}^{(2)} = P_{i,j}/2, \forall i, j$. Then (5.54) becomes

$$SINR_{i,j}^t = \frac{\left(\frac{|c_{ii,j}^{1,1}|^2+|c_{ii,j}^{2,1}|^2}{2}\right) P_{i,j}}{N_{i,j} + \sum_{i'\neq i} \left(\frac{|c_{i'i,j}^{1,1}|^2+|c_{i'i,j}^{2,1}|^2}{2}\right) P_{i',j}}. \tag{5.68}$$

Replace $\eta_{i'i,j}$ with $\frac{|c_{i'i,j}^{1,1}|^2+|c_{i'i,j}^{2,1}|^2}{2}$, we can also apply the DWPA.

## 5.4 Centralized Power Control Algorithm with Transmit Diversity

In this section, we present the centralized power control algorithm with transmit diversity. We will first discuss the gradient projection method and how to reduce the computational complexity given the large dimension of the vector $\underline{q}$. Then we will describe the centralized power control algorithm based on the active set strategy.

### 5.4.1 Gradient Projection Method

The problem in (5.58) is a constrained nonlinear optimization problem. We adopt the gradient projection method to handle the active inequality constraints. Let $\Omega_a$ be the set of all active constraints and $M_a$ the number of elements in the set $\Omega_a$. First, define

$$h_i \triangleq \sum_j \sum_u P_{i,j}^{(u)} - P_i, \forall i \in \Omega_a, \tag{5.69}$$

$$h = \left[ h_{i_1}, h_{i_2}, \cdots, h_{i_{M_a}} \right]^T, \; i_1, \cdots, i_{M_a} \in \Omega_a. \tag{5.70}$$

Let $\nabla h$ be the Jacobian matrix of the matrix $h$

$$\nabla h \triangleq \begin{bmatrix} \left( \frac{\partial h_{i_1}}{\partial \underline{q}} \right)^T \\ \left( \frac{\partial h_{i_2}}{\partial \underline{q}} \right)^T \\ \vdots \\ \left( \frac{\partial h_{i_{M_a}}}{\partial \underline{q}} \right)^T \end{bmatrix}. \tag{5.71}$$

We will use subscript $(\cdot)$ to indicate the index of the algorithm step. According to [68], the projection matrix and the search direction at step $k$ are given by

$$\mathcal{R}_{(k)} = I - \nabla h_{(k)}^T (\nabla h_{(k)} \nabla h_{(k)}^T)^{-1} \nabla h_{(k)}, \tag{5.72}$$

$$\underline{s}_{(k)} = \mathcal{R}_{(k)} \nabla J_{(k)} \tag{5.73}$$

The vector $\underline{q}$ are then updated by

$$\underline{q}'_{(k+1)} = \underline{q}_{(k)} - \alpha_{(k)} \underline{s}_{(k)}. \tag{5.74}$$

We then use Newton-Raphson iterations to return $\underline{q}_{k+1}$ to the active constraint surface

$$[\underline{q}_{(k+1)}]_{(j+1)} = [\underline{q}_{(k+1)} - \nabla h_{(k+1)}^T (\nabla h_{(k+1)} \nabla h_{(k+1)}^T)^{-1} h_{(k+1)}]_{(j)}, \tag{5.75}$$

with $[\underline{q}_{(k+1)}]_{(0)} = \underline{q}'_{(k+1)}$. This Newton-Raphson iterations are terminated when $\|\mathcal{R}_{(k)} \nabla J_{(k)}\| \leq \epsilon$.

The step size $\alpha_{(k)}$ is given by

$$\alpha_{(k)} = \frac{\nabla J_{(k)}^T \nabla J_{(k)}}{\nabla J_{(k)}^T H_{(k)} \nabla J_{(k)}}, \tag{5.76}$$

where $H$ is the Hessian of the objective function given by

$$H = \frac{\partial}{\partial \underline{q}} \left( \frac{\partial J(\underline{q})}{\partial \underline{q}} \right)^T \tag{5.77}$$

As we have found in the numerical experiments, the Hessian $H_{(k)}$ often turns out to be indefinite, which can lead to negative step size $\alpha_{(k)}$. To avoid this situation, we use modified Hessian instead. We first perform eigenvalue decomposition for the Hessian

$$H_{(k)} = Q_{(k)}\Lambda_{(k)}Q_{(k)}^T. \tag{5.78}$$

Let $\lambda_{min}$ be the minimum diagonal element of the matrix $\Lambda_{(k)}$. Then the modified Hessian is determined by

$$\hat{H}_{(k)} = \begin{cases} H_{(k)}, \ \lambda_{min} > 0; \\ Q_{(k)}\left(\Lambda_{(k)} - \lambda_{min}I + \delta\right)Q_{(k)}^T, \ \lambda_{min} \leq 0, \end{cases} \tag{5.79}$$

where $\delta$ is a small positive number. Therefore the step size $\alpha_{(k)}$ is computed by

$$\alpha_{(k)} = \frac{\nabla J_{(k)}^T \nabla J_{(k)}}{\nabla J_{(k)}^T \hat{H}_{(k)} \nabla J_{(k)}}. \tag{5.80}$$

*Complexity Reduction* In the simulation, we use 19 cochannel cells and 32 OFDM subchannels. As a result, the dimension of $\underline{q}$ is as much as 608. Since the gradient projection method involves eigenvalue decomposition for the Hessian $H_k$ in each step. So the complexity will be in the order of $(NM)^3 \approx 2.25 \times 10^8$ operations. To reduce the computational complexity, we first let

$$\underline{\hat{q}}_j = \left[q_{1,j}^{(1)} \cdots q_{1,j}^{(N_{TX})} \cdots q_{M,j}^{(1)} \cdots q_{M,j}^{(N_{TX})}\right]^T, \underline{\hat{q}} = \left[\underline{\hat{q}}_1 \cdots \underline{\hat{q}}_N\right]^T. \tag{5.81}$$

Obviously $\underline{\hat{q}}$ is a linear transformation of $\underline{\hat{q}}$.

$$\underline{\hat{q}} = A\underline{q}. \tag{5.82}$$

Define

$$H_j' = \frac{\partial}{\partial \underline{\hat{q}}_j}\left(\frac{\partial J(\underline{\hat{q}})}{\partial \underline{\hat{q}}_j}\right)^T, \tag{5.83}$$

$$H' = \frac{\partial}{\partial \hat{\underline{q}}} \left( \frac{\partial J(\hat{\underline{q}})}{\partial \hat{\underline{q}}} \right)^T \tag{5.84}$$

From (5.23), it is obvious that $H'$ consists of $N$ $M \times M$ diagonal matrix

$$H' = \begin{bmatrix} H'_1 & & & \\ & H'_2 & & \\ & & \ddots & \\ & & & H'_N \end{bmatrix} \tag{5.85}$$

So instead of decompose $H'$, which needs $(NM)^3$ multiplications, we decompose $H'_j$, $\forall j = 1, \cdots, N$, which only needs $NM^3$ operations. And the step size is actually given by

$$\alpha_{(k)} = \frac{\nabla J_{(k)}^T \nabla J_{(k)}}{\nabla J_{(k)}^T \hat{H}'_{(k)} \nabla J_{(k)}}, \tag{5.86}$$

Another term that needs huge amount of computation is the calculation of $\nabla h_{(k)}^T (\nabla h_{(k)} \nabla h_{(k)}^T)^{-1} \nabla h_{(k)}$ that involves $(NM)^2 + M^3 + M^2 + NM$ operations. In fact,

$$\nabla h_{(k)} = \begin{bmatrix} \nabla h_{i_1,(k)}^T & & & \\ & \nabla h_{i_2,(k)}^T & & \\ & & \vdots & \\ & & & \nabla h_{i_M,(k)}^T \end{bmatrix} \tag{5.87}$$

Therefore

$$\nabla h_{(k)}^T (\nabla h_{(k)} \nabla h_{(k)}^T)^{-1} \nabla h_{(k)}$$

$$= \begin{bmatrix} \nabla h_{i_1,(k)}^T (\nabla h_{i_1,(k)} \nabla h_{i_1,(k)}^T)^{-1} \nabla h_{i_1,(k)} & & \\ & \ddots & \\ & & \nabla h_{i_M,(k)}^T (\nabla h_{i_M,(k)} \nabla h_{i_M,(k)}^T)^{-1} \nabla h_{i_M,(k)} \end{bmatrix} \tag{5.88}$$

The number of multiplications is reduced to $MN^2 + M^3 + M^2 + NM$.

## 5.4.2 Active Set Strategy

*Estimation of Lagrangian Multipliers*   According to the Karush-Kuhn-Tucker conditions (KKT) [69], at a KKT point $\underline{q}_*$

$$\nabla J_* + \sum_{i=1}^{M} \mu_i \nabla h_{i*} = 0, \ \mu_i \geq 0, \ \forall i = 1, \cdots, M. \tag{5.89}$$

This is the same as

$$\nabla J_* + \mu_i \nabla h_{i*} = 0, \ \mu_i \geq 0, \ \forall i = 1, \cdots, M. \tag{5.90}$$

For inactive constraints, $\mu_i = 0$; for active constraints, $\mu_i > 0$, and can be estimated by

$$\min_{\mu_i} \|\nabla J_* + \mu_i \nabla h_{i*}\| \tag{5.91}$$

So we have

$$\hat{\mu}_i = -\frac{\nabla J_*^T \nabla h_{i*}}{\nabla h_{i*}^T \nabla h_{i*}} \tag{5.92}$$

*Discussion on Step Size in Dealing with Inactive constraints*   After the step size is computed by (5.80), for active constraints, the $q_{i,j}$ are forced to the constraint surface by the Newton-Raphson iterations. Note due to the particular structure, all the $q_{i,j}$ in inactive constraints are not affected by this iterative process. But we must check whether $\alpha_{(k)}$ is so large that some of the inactive constraints would be violated. We must ensure for every inactive constraints $i$

$$\|\underline{q}_i - \alpha_{(k)} \nabla \underline{q}_i\| \leq P_i \tag{5.93}$$

i.e.,

$$\left(\underline{q}_i^T - \alpha_{(k)} \nabla \underline{q}_i^T\right) \left(\underline{q}_i - \alpha_{(k)} \nabla \underline{q}_i\right) - P_i$$

$$= \|\underline{q}_i\| - 2\alpha_{(k)}\nabla \underline{q}_i^T \underline{q}_i + \alpha_{(k)}^2 \|\nabla \underline{q}_i\| - P_i \tag{5.94}$$

$$= \|\nabla \underline{q}_i\| \alpha_{(k)}^2 - 2\nabla \underline{q}_i^T \underline{q}_i \alpha_{(k)} + \|\underline{q}_i\| - P_i \leq 0. \tag{5.95}$$

Solve the above inequality, we obtain

$$\frac{2\nabla \underline{q}_i^T \underline{q}_i - \sqrt{(2\nabla \underline{q}_i^T \underline{q}_i)^2 - 4\|\nabla \underline{q}_i\|(\|\underline{q}_i\| - P_i)}}{2\|\nabla \underline{q}_i\|} \leq \alpha_{(k)}$$

$$\leq \frac{2\nabla \underline{q}_i^T \underline{q}_i + \sqrt{(2\nabla \underline{q}_i^T \underline{q}_i)^2 - 4\|\nabla \underline{q}_i\|(\|\underline{q}_i\| - P_i)}}{2\|\nabla \underline{q}_i\|} \tag{5.96}$$

Since $\|\underline{q}_i\| - P_i \leq 0$,

$$\frac{2\nabla \underline{q}_i^T \underline{q}_i - \sqrt{(2\nabla \underline{q}_i^T \underline{q}_i)^2 - 4\|\nabla \underline{q}_i\|(\|\underline{q}_i\| - P_i)}}{2\|\nabla \underline{q}_i\|} \leq 0$$

$$\frac{2\nabla \underline{q}_i^T \underline{q}_i + \sqrt{(2\nabla \underline{q}_i^T \underline{q}_i)^2 - 4\|\nabla \underline{q}_i\|(\|\underline{q}_i\| - P_i)}}{2\|\nabla \underline{q}_i\|} \geq 0 \tag{5.97}$$

Since $\alpha_{(k)}$ must be positive, so we have bounded $\alpha_{(k)}$ in both directions

$$0 \leq \alpha_{(k)} \leq \frac{2\nabla \underline{q}_i^T \underline{q}_i + \sqrt{(2\nabla \underline{q}_i^T \underline{q}_i)^2 - 4\|\nabla \underline{q}_i\|(\|\underline{q}_i\| - P_i)}}{2\|\nabla \underline{q}_i\|}. \tag{5.98}$$

*Centralized Power Control Algorithm* Let $\Omega_a$ be the set of active constraint indices.

1. Initially set all $M$ constraints to be active. Let $q_{i,j}^{(u)} = \sqrt{\frac{P_i}{N_{TX}N}}, \forall i, j, u$.

2. Compute $\nabla J_{(k)}$ (5.61) and $\mathcal{R}_{(k)}$ (5.72).

3. If $\|\mathcal{R}_{(k)} \nabla J_{(k)}\| \geq \epsilon_1$, continue the inside loop; otherwise go to step 4.

   (a) Compute the step size $\alpha_{(k)}$ (5.86). If $\alpha_{(k)}$ violates any inactive constraints, let

$$\alpha_{(k)} = \min_i \frac{2\nabla \underline{q}_i^T \underline{q}_i + \sqrt{(2\nabla \underline{q}_i^T \underline{q}_i)^2 - 4\|\nabla \underline{q}_i\|(\|\underline{q}_i\| - P_i)}}{2\|\nabla \underline{q}_i\|}$$

and set the constraint

$$\arg\min_i \frac{2\nabla \underline{q}_i^T \underline{q}_i + \sqrt{(2\nabla \underline{q}_i^T \underline{q}_i)^2 - 4\|\nabla \underline{q}_i\|(\|\underline{q}_i\| - P_i)}}{2\|\nabla \underline{q}_i\|}$$

to be active.

(b) Set $\underline{q}_{(k+1)} = \underline{q}_{(k)} - \alpha_{(k)}\mathcal{R}_{(k)}\nabla J_{(k)}$

(c) If $\|h_{(k+1)}\| \geq \epsilon_2$, continue the inside loop; otherwise go to step 3(d).

    i. $[\underline{q}_{(k+1)}]_{(j+1)} = [\underline{q}_{(k+1)} - \nabla h_{(k+1)}^T (\nabla h_{(k+1)} \nabla h_{(k+1)}^T)^{-1} h_{(k+1)}]_{(j)}$

(d) Compute $\nabla J_{(k)}$ (5.61) and $\mathcal{R}_{(k)}$ (5.72).

4. Estimate $\hat{\mu}_i$, $\forall i \in \Omega_a$. Let $j = \arg\min_{i \in \Omega_a} \hat{\mu}_i$.

5. If $\hat{\mu}_j \geq 0$, terminate; otherwise, deactivate constraint $j$ and go to step 2.

In the simulation, we observe that the algorithm often oscillates between the positive and negative values of a subset of the vector $\underline{q}$, leading to extremely slow convergence. Considering that changing the sign of $q_{i,j}$ will not change the actual power allocation, which is equal to $q_{i,j}^2$, and subsequently the throughput, we deliberately randomize the step size $\alpha_{(k)}$ after step 3($a$). Specifically, we first generate a Bernoulli random variable with equal probability. If the result is one, let

$$\alpha_{(k)} = \frac{\alpha_{(k)}}{2}. \tag{5.99}$$

If the result is zero, leave $\alpha_{(k)}$ unchanged. This modification has proved to be very effective in preventing the CPCA from getting stuck at oscillation and has significantly improved the convergence speed in the simulation.

## 5.5 Power Control in the Presence of Jamming

In this section, we consider the DWPA and the CPCA in the case of strong jamming signals. We will describe the jamming model. The simulation result and discussions will be give in Section 5.6.

### 5.5.1 Jamming Model

In the case of jamming, we assume that there is a random noise jammer located inside the cellular network. We assume that the jammer's position is uniformly distributed inside the boundary of the cellular network as in [70]. The jammer randomly selects a subset of OFDM subchannels and transmits the jamming signals – additive white Gaussian noise – through those subchannels. As a result, all the cochannel cells are affected to a certain degree depending on the distance. The jammer uses a single antenna to transmit jamming signals. As the jammer has no knowledge of the channel conditions, it distributes its power evenly over the entire subset of selected subchannels.

With the presence of the jammer, the equation for the received signal, (5.3), can be rewritten as

$$
\begin{aligned}
r_{i,j}^{v}(k) &= \sum_{u=1}^{N_{TX}} c_{ii,j}^{u,v}(k)s_{i,j}^{u}(k) + \sum_{\substack{i'=1\\i'\neq i}}^{N_C}\sum_{u=1}^{N_{TX}} c_{i'i,j}^{u,v}(k)s_{i',j}^{u}(k) + d_{i,j}^{v}(k)j(k)\\
&+ n_{i,j}^{v}(k),
\end{aligned}
\tag{5.100}
$$

where $d_{i,j}^{v}(k)$ is the channel gain of the $j$th subchannel from the jammer to the $v$th receive antenna of the $i$th base station; $j(k)$ is the jamming signal at time $k$. The jammer signals are subject to distance loss, shadowing, and frequency-selective fading as the data signals. Based on this new equation, we derive the

expressions for the signal-to-interference ratio. Again, we omit the time index $k$ for the jamming channel state information $d_{i,j}^v(k)$ as we did to $c_{ii,j}^{u,v}(k)$ in Section 5.1.

In the case of single transmit (mobile) and receive antenna (base station), the SINR in the $j$th subchannel of the $i$ base station now becomes

$$SINR_{i,j} = \frac{\Gamma \xi_{ii,j} P_{i,j}}{N_{i,j} + \sum_{\substack{i'=1 \\ i' \neq i}}^{N_C} \xi_{i'i,j} P_{i',j} + \xi_{Ji,j} \mathcal{I}_j P_J / N_J}. \tag{5.101}$$

where $\xi_{Ji,j} = |d_{i,j}^1|^2$, $\mathcal{I}_j$ is the indication function – it equals one when subchannel $j$ has jamming signals and zero otherwise, $N_J$ is the number of subchannels that have jamming signals, and $P_J$ is the total jamming power.

In the case of receive diversity, the SINR is

$$SINR_{i,j}^r = \frac{\Gamma \eta_{ii,j} P_{i,j}}{N_{i,j} + \sum_{\substack{i'=1 \\ i' \neq i}}^{N_C} \eta_{i'i,j} P_{i',j} + \eta_{Ji,j} \mathcal{I}_j P_J / N_J} \tag{5.102}$$

where

$$\eta_{Ji,j} = \frac{\left| \sum_{v=1}^{N_{RX}} c_{ii,j}^{1,v\,*} d_{i,j}^v \right|^2}{\sum_{v=1}^{N_{RX}} \left| c_{ii,j}^{1,v} \right|^2}. \tag{5.103}$$

In the case of transmit diversity, the SINR is

$$SINR_{i,j}^t = \frac{\Gamma \sum_{u=1}^2 \kappa_{ii,j}^{(u)} \left[ q_{i,j}^{(u)} \right]^2}{N_{i,j} + \sum_{i' \neq i} \sum_{u=1}^2 \kappa_{i'i,j}^{(u)} \left[ q_{i',j}^{(u)} \right]^2 + \kappa_{Ji,j} \mathcal{I}_j P_J / N_J}, \tag{5.104}$$

where $\kappa_{Ji,j} = |d_{i,j}^1|^2$.

## 5.6   Simulation Results

We consider a hexagonal cellular system with frequency reuse factor 4 as shown in Fig. 5.6. Around a central cell, we consider 6 cochannel cells in the second

total cochannel cells: 19
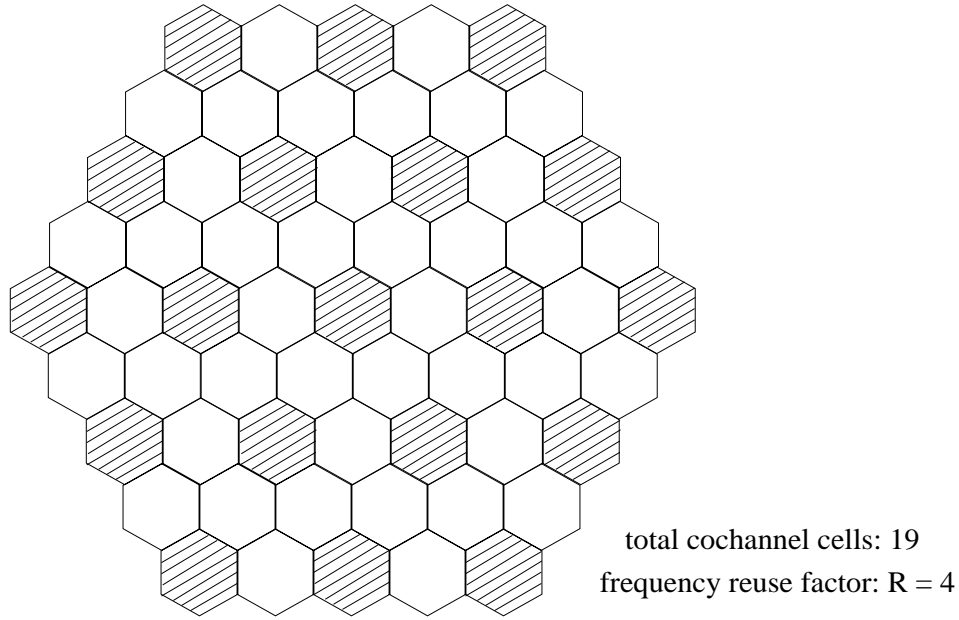
frequency reuse factor: R = 4

Figure 5.6: A Hexagonal Cellular System

tier and 12 cochannel cells in the fourth tier. In each of the 19 cochannel cells, a base station is located in the center and is communicating with one mobile within the cell. The mobiles are uniformly distributed in their corresponding cells for each simulation instance. Path distance loss obeys a decay law with exponent $\alpha = 3.5$, whose gain is normalized to one at a reference distance that is equal to 0.01 times the radius of the cell. No mobiles are allowed within this reference distance from the base station. A lognormal fading with 0 dB mean and 8 dB standard deviation is used to simulate shadowing effect. There are a total of 32 OFDM subchannels for each cochannel cell. The adjacent subchannel cross-correlation coefficient is 0.5. The total transmission power for each mobile is normalized to 1.0 Watt and the power of AWGN at the receiver end is $10^{-10}$ Watt. The SINR gap $\Gamma$ is set to be 10.8276, which corresponds to a symbol error probability of $10^{-3}$.

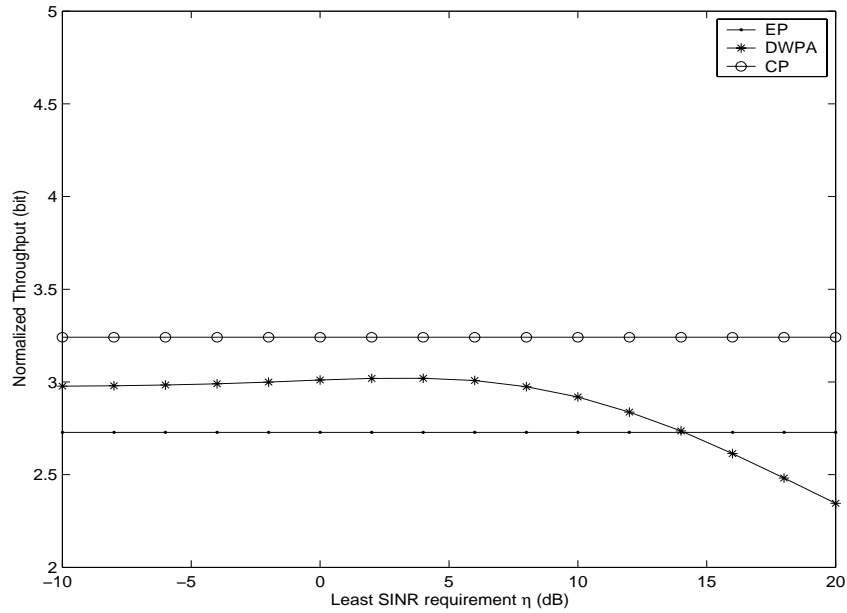We simulate three antenna combinations: 1 transmit antenna and 1 receive

Figure 5.7: Normalized Throughput of the Cellular System, 1 TX antenna, 1 RX antenna, $\sigma = 8$ dB

antenna; 1 transmit antenna and 2 receive antennas; 2 transmit antennas and 1 receive antenna. For each antenna combination, we simulate three algorithms: EP, DWPA, and CPCA. For transmit diversity, both EP and DWPA have two cases: one is to split power evenly between two transmit antennas, which is referred to as EPD (equal power diversity); the other assigns full power to the transmit antenna with larger channel gain in that subchannel, referred to as SD (selective diversity). For each simulation, 1000 samples are generated and the results are shown in Fig. 5.7, 5.8, 5.9. We use the normalized throughput, which is equal to the total throughput divided by the product of the number of cochannel cells and the number of OFDM subchannels.

*Comparison of Power Control Algorithms*    The first observation is that in terms of the normalized throughput the CPCA always gives the best performance, the
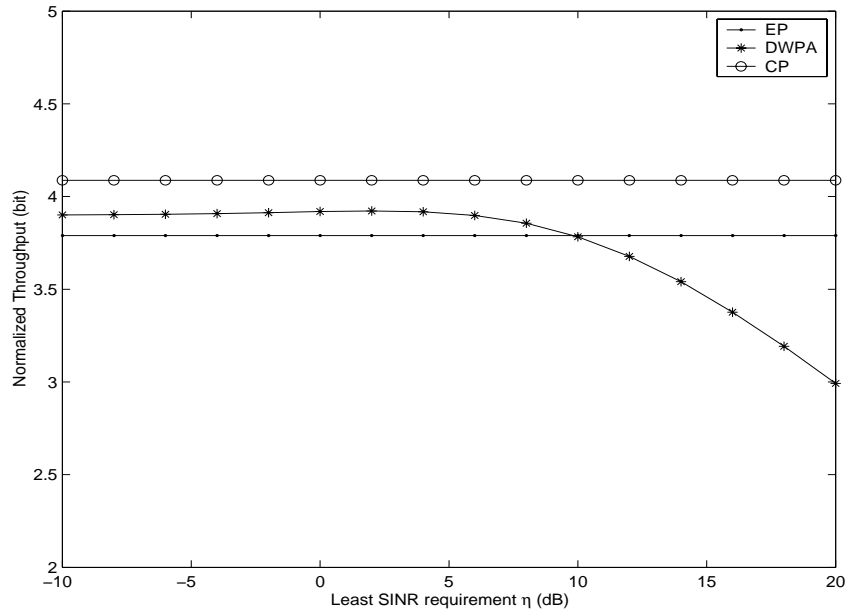
Figure 5.8: Normalized Throughput of the Cellular System, 1 TX antenna, 2 RX antennas, $\sigma = 8$ dB

DWPA the second at low $\eta$ values, and the EP the third. This is reasonable because both the CPCA and the DWPA exploit feedback information to improve the normalized throughput with the CPCA having the most information on channel conditions and the AWGN noise level. The performance of the DWPA also relies heavily on the $\eta$ value. It reaches the peak at about 4 dB and descends quickly after 6 dB.

*Comparison of Diversity Schemes* The second observation is that among three diversity schemes: the receive diversity gives the best performance, the transmit diversity with selective diversity slightly worse, the transmit diversity with equal power diversity the third, and the no diversity case the worst. The reason that the receive diversity has an edge over the transmit diversity with SD is because the former actually has larger channel gains because it has two paths from each
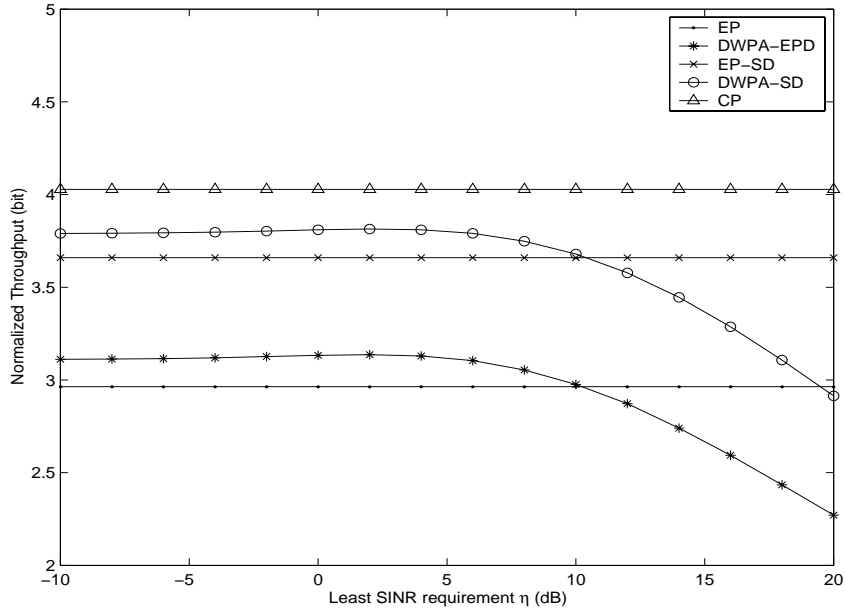
156

Figure 5.9: Normalized Throughput of the Cellular System, 2 TX antennas, 1 RX antenna, $\sigma = 8$ dB

transmit antenna while in the latter, only the stronger one is used. As for why the SD is much better than the EPD, the reason is that the SD puts all power in the stronger path so the receiving power is larger than that of the EPD.

*Convergence of the DWPA and the CPCA*   In Fig. 5.10, we study the percentage of convergence the DWPA. For the DWPA, we stop the algorithm if the difference of any two consecutive power vectors has a norm smaller than $10^{-8}$ and consider that it has reached convergence; or when the number of iterations reaches 100 and consider that it diverges. The reason we set the maximum number of iterations to be 100 is because we have observed that when the algorithm converges, it usually converges in fewer than 10 iterations; otherwise it will not converge anyway. From Fig. 5.10, we can see that the percentage of convergence of the DWPA is a function of the threshold value $\eta$ – it has a higher percentage of
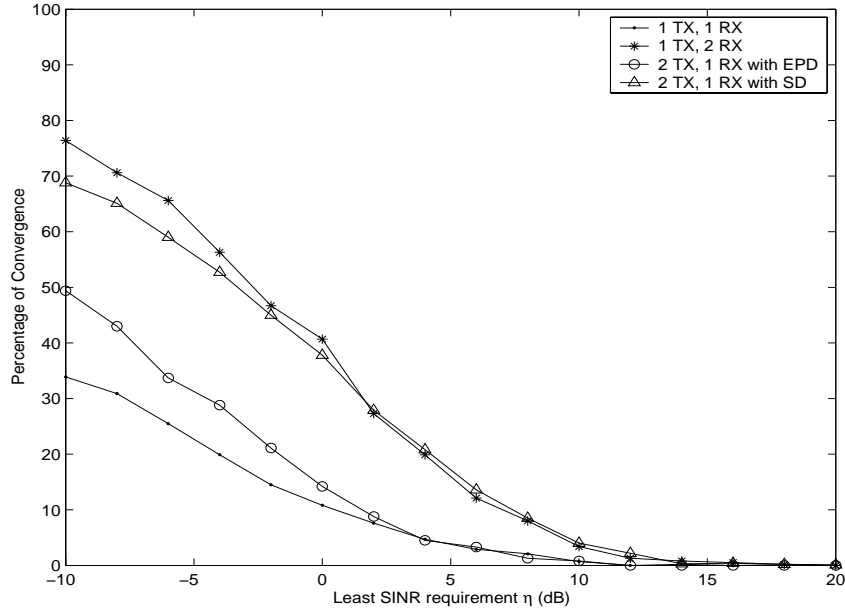
Figure 5.10: Convergence Rate of the DWPA Algorithm, $\sigma = 8$ dB

convergence at very low $\eta$ values. Also, diversity helps improve the percentage of convergence. Among different diversity schemes, the receive diversity and the transmit diversity with SD have the best percentage of convergence for the DWPA.

|  | $\sigma = 6$ dB | $\sigma = 8$ dB | $\sigma = 10$ dB |
|---|---|---|---|
| No Diversity | 336 | 1032 | 3023 |
| Receive Diversity | 95 | 364 | 1330 |
| Transmit Diversity with EPD | 164 | 550 | 1459 |
| Transmit Diversity with SD | 134 | 448 | 1190 |

Table 5.1: Number of Iterations Needed for Convergence of the CPCA

For the CPCA, we stop the algorithm when the KKT conditions are satisfied. In the simulation, $\epsilon_1 = 10^{-3} \cdot$ length of $\underline{q}$ and $\epsilon_2 = 10^{-8}$. The algorithm has converged in all the simulations we have run. In Table 5.1, we show the average
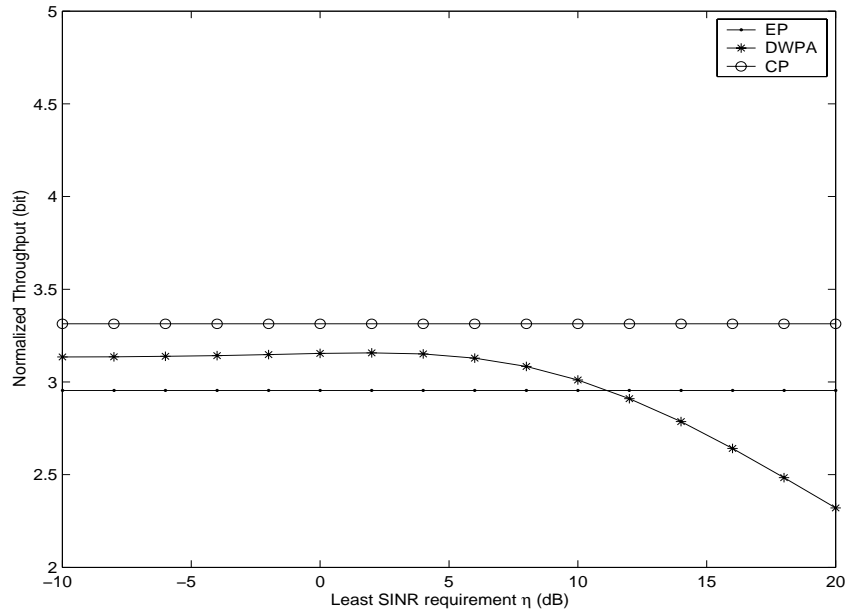
Figure 5.11: Normalized Throughput of the Cellular System, 1 TX antenna, 1 RX antenna, $\sigma = 6$ dB

number of iterations it takes to converge for different shadowing parameters. A complete iteration is defined as a step taken towards the negative direction of the gradient. The general trend for the CPCA is that as the standard deviation of the shadowing goes higher, so goes the number of iterations needed for convergence. As in the DWPA, the CPCA converges faster when there is diversity. The common characteristics is that when the channel variation is small, the CPCA converges in fewer iterations.

*Effect of Shadowing Deviation on DWPA*  To obtain a better understanding of these algorithms, we vary the standard shadowing deviation $\sigma$ and simulate the sensitivity of the three algorithms to this parameter. The results are shown in Fig. 5.11, 5.12, 5.13 for $\sigma = 6$ dB and 5.14, 5.15, 5.16 for $\sigma = 10$ dB. As the standard deviation of the shadowing goes higher, the normalized throughput
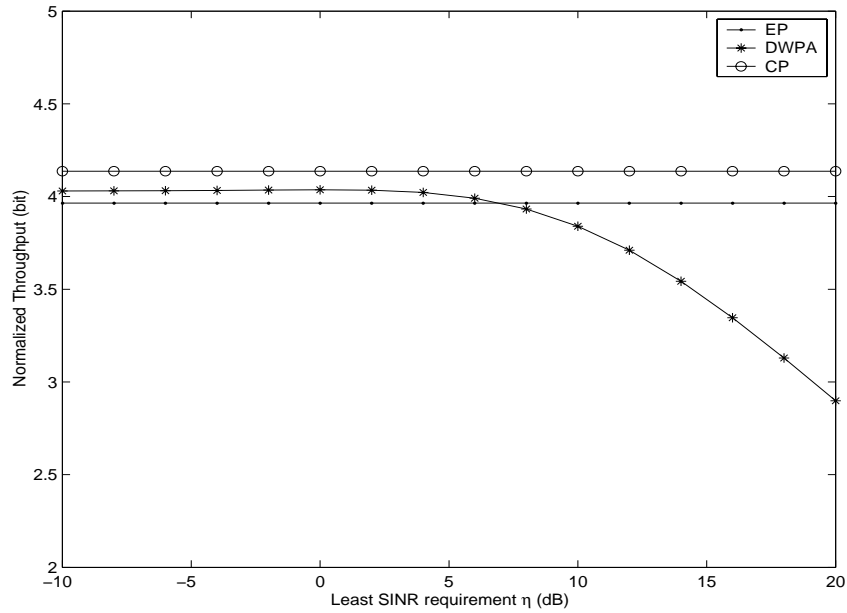
159

Figure 5.12: Normalized Throughput of the Cellular System, 1 TX antenna, 2 RX antennas, $\sigma = 6$ dB

experiences a slight decrease due to the increased cochannel interference. But the advantages of the CPCA and the DWPA over the EP become more prominent as $\sigma$ increases. The same is true between the CPCA and the DWPA. For instance, in the one transmit antenna and one receive antenna case, the throughput of the DWPA ($\eta = 4$ dB) and the CPCA are 7% and 12% more than that of the EP at $\sigma = 6$ dB. The numbers change to 11% and 19% at $\sigma = 8$ dB and 17% and 28% at $\sigma = 10$ dB.

*Power Control in the Presence of Jamming* We use the same hexagonal cellular system as before. And all the system parameters are the same if not specified. The jammer roams inside the network area. The jamming power is 30 dB as high as the maximum transmit power of a single mobile. For each simulation, 1000 samples are generated.

Figure 5.13: Normalized Throughput of the Cellular System, 2 TX antennas, 1 RX antenna, $\sigma = 6$ dB



Figure 5.14: Normalized Throughput of the Cellular System, 1 TX antenna, 1 RX antenna, $\sigma = 10$ dB

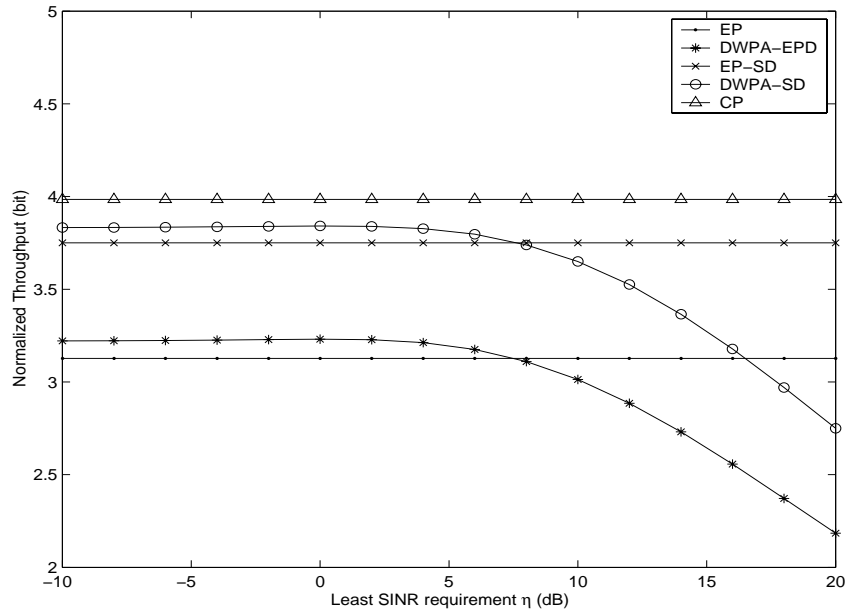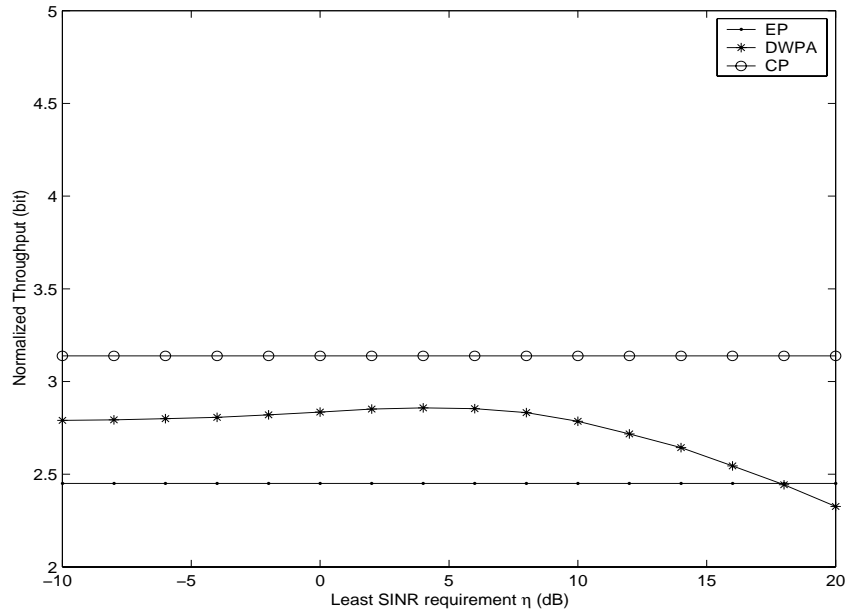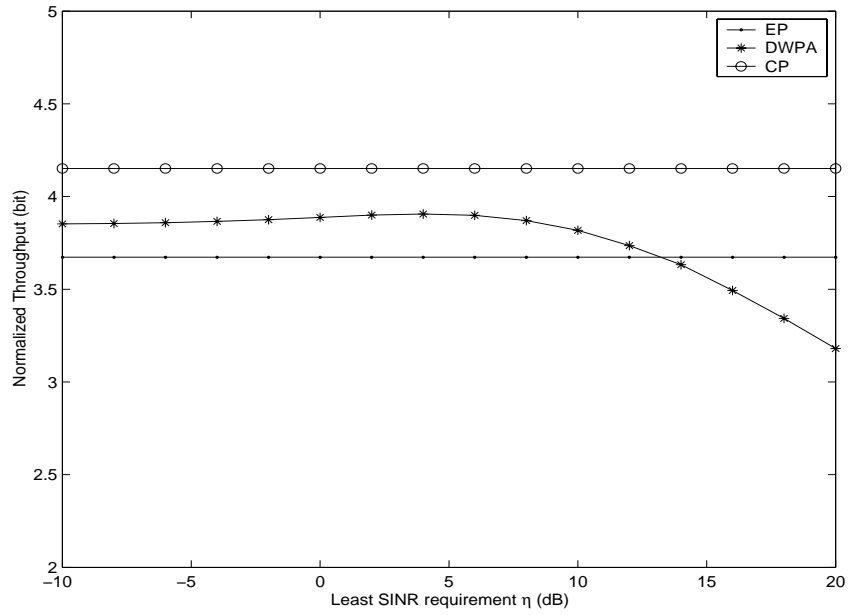Figure 5.15: Normalized Throughput of the Cellular System, 1 TX antenna, 2 RX antennas, $\sigma = 10$ dB
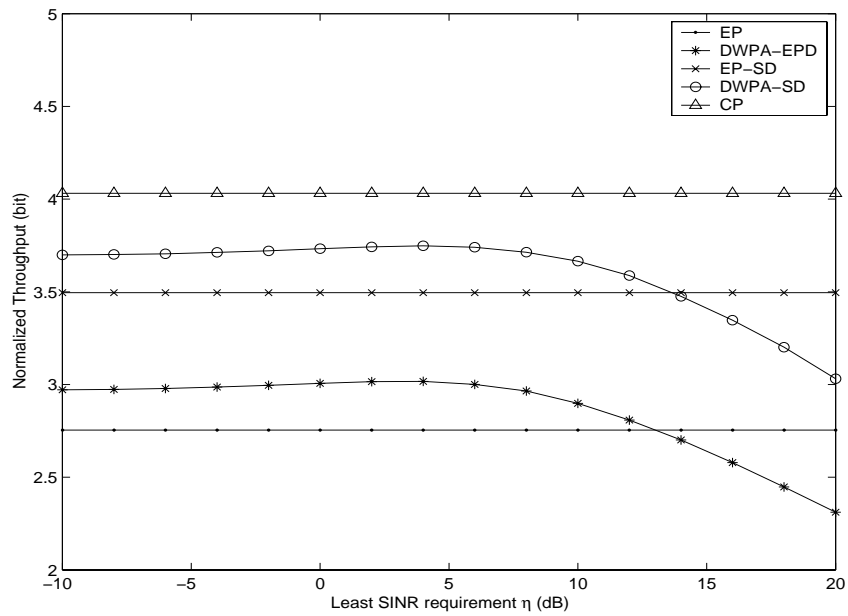


Figure 5.16: Normalized Throughput of the Cellular System, 2 TX antennas, 1 RX antenna, $\sigma = 10$ dB

162
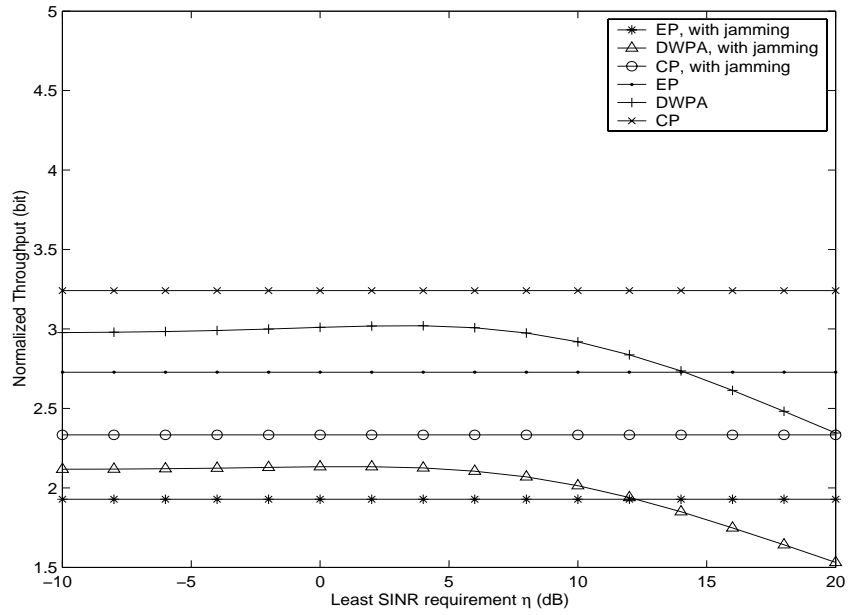
Figure 5.17: Normalized Throughput Under Jamming, 1 TX antenna, 1 RX antenna, $\sigma = 8$ dB
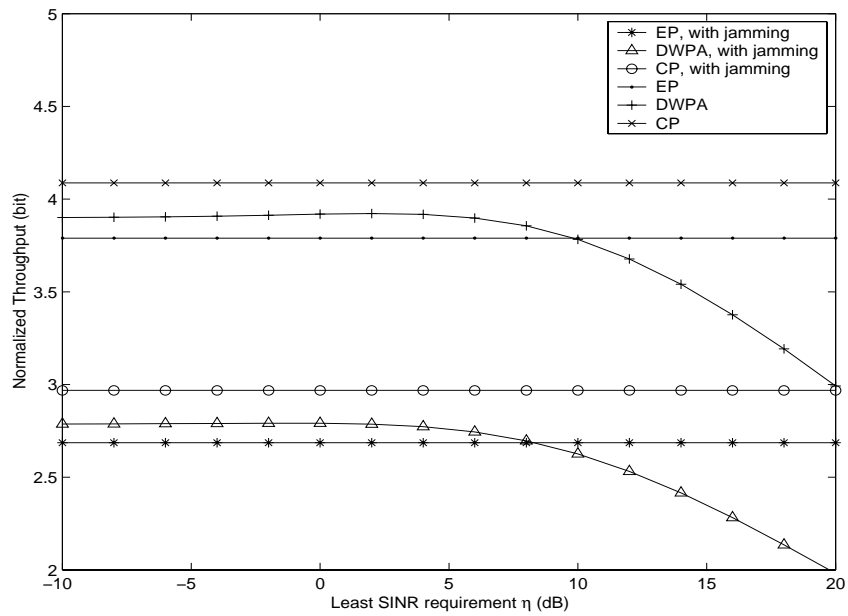


Figure 5.18: Normalized Throughput Under Jamming, 1 TX antenna, 2 RX antenna, $\sigma = 8$ dB
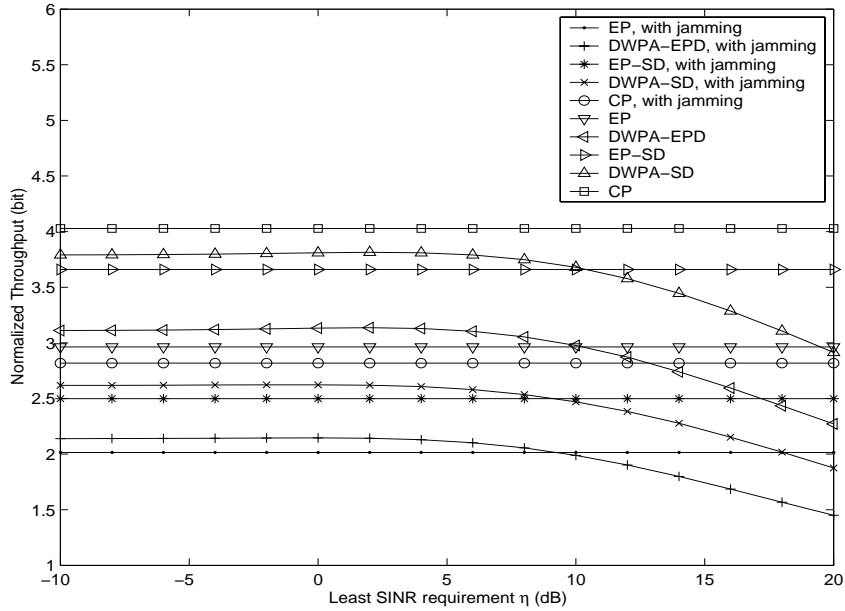
Figure 5.19: Normalized Throughput Under Jamming, 2 TX antenna, 1 RX antenna, $\sigma = 8$ dB

Shown in Fig. 5.17 - 5.19 are the throughput of the cellular network for three antenna combinations under hostile jamming. We can see that although the performance of all the three algorithms – EP, DWPA, CP – deteriorate by $20 - 30\%$ due to the jamming, all of them are very robust against random jamming in terms of the normalized throughput.

## 5.7 Conclusions

In this chapter, we dealt with the problem of optimizing throughput for a hexagonal cellular OFDM system with transmit and receive diversity. We first extended the DWPA initially proposed by Su [25] from single transmit and receive antenna to multiple antennas. Then we developed a centralized power control algorithm based on the gradient projection method and the active set strategy. To increase

the convergence rate, randomization of the step size was proposed.

Several conclusions can be drawn from the simulation results. First, among three power control algorithms, the CPCA always produces the best performance in terms of the normalized throughput, the DWPA the second, and the EP the last. In terms of complexity, however, the CPCA is the most complicated. It requires all the information on the channel and the cochannel cells as well as sophisticated processing to allocate the transmit power. Although we did not prove its convergence analytically, it has converged in all the simulations we have run. As for the DWPA, it only needs to estimate the channel gains for the intended signal and measure the total cochannel interference plus noise level for each subchannels. The processing of the information is relatively simple – only water pouring is needed. It somehow achieves a balance between the complexity and the performance when compared with the CPCA and the EP. The main issue remained for the DWPA, however, is that it cannot guarantee convergence, although it does give better performance than the EP even when it diverges. Still, it is a good heuristic algorithm to exploit frequency selectivity when the additive white Gaussian noise dominates the total interference.

Second, among different diversity schemes, receive diversity and transmit diversity with SD have similar performances that are better than others. On both cases, however, the advantages of the DWPA and the CPCA over the EP are less obvious. This is because there is less channel variation when there is diversity.

Third, the shadowing parameter also affects the performance of the three power control algorithms. When the standard deviation of the shadowing goes higher, the advantages of the DWPA and the CPCA over the EP are more

prominent. In other words, the complexity of the DWPA and the CPCA are more acceptable on severe shadowing channels.

In the end, we simulated the effect of a single noise jammer on the system throughput. Although it did cause a $20 - 30\%$ decrease in the normalized throughput with overwhelming jamming power – 30 dB as high as the maximum transmit power of a single mobile, the system remained in working conditions.

Chapter 6

# Conclusions and Future Work

In this dissertation, we have studied joint detection and decoding of high-order modulation schemes for CDMA and OFDM wireless communications. We have proposed various joint detection and decoding schemes to improve power and bandwidth efficiency, to mitigate the effect of fading, interference, and jamming. In the following, we summarize our work in this dissertation and point out some directions for future work.

Specifically, in Chapter 2, we have designed coherent and noncoherent iterative receivers for high-order CPM signals. Both of them make use of the memory inherent in CPM signals and have a structure similar to that of a serial concatenated convolutional decoder. For the coherent receiver, pilot symbols are used as references for channel estimation. Simulation results have shown significant improvement in BER performance for both PSAM and PSAM-IF receivers. And the PSAM-IF receiver further improves the BER performance by 1.0 dB over the PSAM receiver at high SNR since it involves iteratively estimating the channel state information on reconstructed CPM phase trajectories. The noncoherent MDD receiver that applies multiple-symbol differential detection in the CPM

demodulator also benefits significantly from iterative processing.

The BER performance of noncoherent MDD receiver is largely determined by the length of the linear predictor, which, however, would incur huge increase in computational complexity and memory requirement. Reduced-state MDD demodulator using the techniques described in [39] is a direction for further research. We might be able to achieve better performance under the same computational complexity and memory requirements by balancing between the number of trellis states and the linear predictor length.

In Chapter 3, we have proposed joint iterative channel estimation and decoding systems for pilot symbol-assisted QAM communications over Doppler fading channels, including both the flat-fading channel and the multipath frequency-selective channel. In the flat-fading channel, we have designed a threshold-controlled iterative channel estimation scheme, simulated the scheme using a wide range of threshold values and determined that the best results are achieved at very low threshold values. To reduce the polynomial complexity of the threshold-controlled scheme, we also proposed another simplified scheme that has similar performance but with only linear complexity.

In the multipath channel, our focus is on the comparison between pilot symbol-assisted demodulation and pilot-aided demodulation under various transmit and receive diversity combinations. We concluded from the simulation results that iterative channel estimation always provides remarkable performance improvement and that transmit diversity should only be used when the number of multiple paths is small. As the total number of paths increases, the performance of PSAM, PSAM-IF, PAD, and PAD-IF all improves initially, reaches peak at some points, and then starts to degrade. Finally, when the normalized

Doppler frequency is around 0.01 or higher, PSAM performs better than PAD, and PSAM-IF performs better than PAD-IF.

In Chapter 4, we have designed anti-jamming systems for multicarrier communications against partial-band tone jamming and partial-time pulse jamming. The design of the anti-jamming systems is illustrated by using the multi-tone jamming. Specifically, we have proposed a hard jamming detector based on eigenvalues and a soft detector based on the correlation of the jamming estimator output. We proposed to use differential frequency estimation and the ESPRIT algorithm for jamming frequency estimation. To further reduce the error in jamming detection and estimation, we make use of iterative jamming detection and estimation by removing the reconstructed data signal component from the received samples.

In the fading channel, we have designed the pilot symbol sequence robust to jamming detection and estimation for channel estimation. Furthermore, we have also included iterative channel estimation in the design so that the receiver has better estimates of the channel state information after the first iteration. Simulation results have shown that our design of the anti-jamming multicarrier receiver is very effective in suppressing the jamming signal and that the iterative processing greatly improves the BER performance. It works for all the simulated $J/S$ values ranging from $-10$ to 30 dB.

Future work includes the design for more reliable jamming detection and more accurate jamming estimation schemes. Exploring the anti-jamming capability of multicarrier communication systems against jamming signals of other types, such as noise jamming, is another interesting topic.

In Chapter 5, we dealt with the problem of optimizing throughput for a

hexagonal cellular OFDM system with transmit and receive diversity. We first extended the DWPA initially proposed by Su [25] from single transmit and receive antenna to multiple antennas. We have studied both selective diversity and equal power diversity on the transmitter side. Then we developed a centralized power control algorithm based on the gradient projection method and the active set strategy. To increase the convergence rate, we randomized the step size.

Among three power control algorithms – EP, DWPA, and CPCA, the CPCA always produces the best performance in terms of the normalized total throughput, the DWPA the second, and the EP the last. In terms of complexity, however, the CPCA is the most complicated. The processing of the information for the DWPA is relatively simple – only water pouring is needed. The main issue remained for the DWPA, however, is that it cannot guarantee convergence, although it does give better performance than the EP even when it diverges.

Among different diversity schemes, receive diversity and transmit diversity with selective diversity have similar performances that are better than others. On both cases, however, the advantages of the DWPA and the CPCA over the EP are less obvious.

One of the remaining issues for power control and adaptive modulation in cellular wireless network is to prove analytically the convergence of the CPCA algorithm. Another issue is to find algorithms for constrained optimization that converges faster than the current gradient projection method.

In all, we have covered a wide range of important issues in the physical layer wireless communications. These issues are essential to the development of high data rate, power and bandwidth efficient wireless communication systems in the future.

# BIBLIOGRAPHY

[1] J. G. Proakis, *Digital Communications*, McGraw Hill, New York, 1995.

[2] Michael J. Gertsman and John H. Lodge, "Symbol-by-symbol MAP demodulation of CPM and PSK signals on Rayleigh flat-fading channels," *IEEE Transactions on Communications*, vol. 45, no. 7, pp. 788–799, 1997.

[3] Paul Ho and Jae Hyung Kim, "Pilot symbol-assisted detection of CPM schemes operating in fast fading channels," *IEEE Transactions on Communications*, vol. 44, no. 3, pp. 337–347, 1996.

[4] J. Hagenauer, "The turbo principle: Tutorial introduction and state of the art," in *Proceedings of International Symposium on Turbo Codes and Related Topics*, 1997, pp. 1–9.

[5] Bixio Romoldi, "A decomposition approach to CPM," *IEEE Transactions on Information Theory*, vol. 34, no. 2, pp. 260–270, 1988.

[6] Gottfried Ungerboeck, "Channel coding with multilevel phase signals," *IEEE Transactions on Information Theory*, vol. 28, no. 1, pp. 55–67, Jan. 1982.

[7] Claude Berrou, Alain Glavieux, and Punya Thitimajshima, "Near shannon limit error-correcting coding and decoding: Turbo codes (1)," in *Proceed-*

*ings of IEEE International Conference on Communications*, May 1993, pp. 1064–1070.

[8] S. Benedetto, D. Divsalar, G. Montorsi, and F. Pollara , "Parallel concatenated trellis-coded modulation," in *Proceedings of IEEE International Conference on Communications*, 1996, pp. 974–978.

[9] Patrick Robertson, "Bandwidth-efficient turbo trellis-coded modulation using punctured component codes," *IEEE Journal on Selected Areas in Communications*, vol. 16, no. 2, pp. 206–218, 1998.

[10] Dariush Divsalar and Marvin K. Simon, "The design of trellis coded MPSK for fading channels: performance criteria," *IEEE Transactions on Communications*, vol. 36, pp. 1004–1012, 1988.

[11] Andrew J. Viterbi, Jack K. Wolf, Ephraim Zehavi, and Roberto Padovani, "A pragmatic approach to trellis-coded modulation," *IEEE Communications Magazine*, pp. 11–19, July, 1989.

[12] Stephane Le Goff, Alain Glavieux, and Claude Berrou , "Turbo-codes and high spectral efficiency modulation," in *Proceedings of IEEE International Conference on Communications*, May 1994, pp. 645–649.

[13] Giuseppe Caire, Giorgio Taricco, and Ezio Biglieri, "Bit-interleaved coded modulation," *IEEE Transactions on Communications*, vol. 44, no. 3, pp. 927–946, May 1998.

[14] E. Zehavi, "8-PSK trellis codes for a Rayleigh fading channel," *IEEE Transactions on Information Theory*, vol. 40, pp. 873–884, May 1992.

[15] J. P. McGeehan and A. J. Bateman, "Phase locked transparent-tone-in-band (TTIB): a new spectrum configuration particularly suited to the transmission of data over SSB mobile radio networks," *IEEE Transactions on Communications*, vol. 32, pp. 81–87, 1984.

[16] A. J. Bateman, "Speech and data communications over 942 MHz TAB and TTIB single sideband mobile radio systems incorporating feed-forward signal generation," *IEEE Transactions on Vehicular Technology*, vol. 34, pp. 13–21, 1985.

[17] F. Davarian, "Mobile digital communications via tone calibration," *IEEE Transactions on Vehicular Technology*, vol. 36, pp. 55–62, May 1987.

[18] James K. Cavers, "An analysis of pilot symbol-assisted modulation for Rayleigh fading channels," *IEEE Transactions on Vehicular Technology*, vol. 40, no. 4, pp. 686–693, Nov. 1991.

[19] Xiaoyi Tang, Mohamed-Slim Alouini, and Andrea Goldsmith, "Effect of channel estimation error on M-QAM BER performance in Rayleigh fading," *IEEE Transactions on Communications*, vol. 47, no. 12, pp. 1856–1864, 1999.

[20] Leonard J. Cimini, "Analysis and simulation of a digital mobile channel using orthogonal frequency division multiplexing," *IEEE Transactions on Communications*, vol. 33, pp. 665–675, 1985.

[21] John A. C. Bingham, "Multicarrier modulation for data transmission: an idea whose time has come," *IEEE Communications Magazine*, pp. 5–14, May 1990.

[22] Ye Li, N. Seshadri , and S. Ariyavisitakul, "Channel estimation for OFDM systems with transmitter diveristy in mobile wireless channels," *IEEE Journal on Selected Areas in Communications*, vol. 17, no. 3, pp. 461–471, 1999.

[23] Peter Hoeher, Stefan Kaiser, and Patrick Robertson, "Two-dimensional pilot-symbol-aided channel estimation by Wiener filtering," in *Proceedings of IEEE International Conference on Acoustics, Speech and Signal Processing*, 1997, pp. 1845–1848.

[24] Veli-Pekka Kaasila, "Performance analysis of an OFDM system using data-aided channel estimation," in *Proceedings of IEEE Vehicular Technology Conference*, 1999, pp. 2303–2307.

[25] Hsuan-Jung Su, and Evaggelos Geraniotis, "A distributed power allocation algorithm with adaptive modulation for multi-cell OFDM systems," in *Proceedings of IEEE 1988 International Symposium on Spread Spectrum Techniques and Applications*, 1998, vol. 3, pp. 474–478.

[26] Vahid Tarokh, Nambi Seshadri, and A. R. Calderbank, "Space-time codes for high data rate wireless communication: performance criterion and code construction," *IEEE Transactions on Information Theory*, vol. 44, no. 2, pp. 744–765, 1998.

[27] Vahid Tarokh, Hamid Jafarkhani, and A. R. Calderbank, "Space-time block codes from orthogonal designs," *IEEE Transactions on Information Theory*, vol. 45, no. 5, pp. 1456–1467, 1999.

[28] Siavash M. Alamouti, "A simple transmit diversity technique for wireless communications," *IEEE Journal on Selected Areas in Communications*, vol. 16, no. 8, pp. 1451–1458, 1998.

[29] Dakshi Agrawal, Vahid Tarokh, Ayman Naguib, and Nambi Seshadri, "Space-time coded OFDM for high date-rate wireless communication over wideband channels," in *Proceedings of 48th IEEE Vehicular Technology Conference*, 1998, pp. 2232–2236.

[30] J. Hagenauer, and P. Hoeher, "A Viterbi algorithm with soft-decision outputs and its applications," in *Proceedings of IEEE Globecom Telecommunications Conference*, 1989, pp. 1680–1686.

[31] L. R. Bahl, J. Cocke, F. Jelinek, and J. Raviv, "Optimal decoding of linear codes for minimizing symbol error rate," *IEEE Transactions on Information Theory*, vol. 20, pp. 284–287, Mar. 1974.

[32] Krishna R. Narayanan, and Gordon L. Stuber, "A serial concatenation approach to iterative demodulation and decoding," *IEEE Transactions on Communications*, vol. 47, no. 7, pp. 956–961, 1999.

[33] Par Moqvist, and Tor M. Aulin, "Serially concatenated continuous phase modulation with iterative decoding," *IEEE Transactions on Communications*, vol. 49, no. 11, pp. 1901–1915, 2001.

[34] Peter Hoeher, and John H. Lodge, ""Turbo DPSK": Iterative differential PSK demodulation and channel decoding," *IEEE Transactions on Communications*, vol. 47, no. 6, pp. 837–843, 1999.

[35] William Lee, *Mobile Communications Engineering*, McGraw-Hill, New York, 1982.

[36] Joachim Hagenauer, "Iterative decoding of binary block and convolutional codes," *IEEE Transactions on Information Theory*, vol. 42, no. 2, pp. 429–445, Mar. 1996.

[37] Simon S. Haykin, *Adaptive Filter Theory*, Prentice Hall, New York, 3rd edition, 1996.

[38] Patrick Robertson, E. Villebrun, P. Hoeher, "A comparison of optimal and sub-optimal MAP decoding algorithms operating in the log domain," in *Proceedings of IEEE International Conference on Communications*, 1995, pp. 1009–1013.

[39] M. V. Eyuboglu, and S. U. H. Qureshi, "Reduced state sequence estimation with set partitioning and decision feedback," *IEEE Transactions on Communications*, vol. 36, no. 1, pp. 13–20, 1988.

[40] Hsuan-Jung Su and Evaggelos Geraniotis, "Low complexity joint channel estimation and decoding for pilot symbol-assisted modulation and multiple differential detection systems with correlated Rayleigh fading," *IEEE Transactions on Communications*, vol. 50, pp. 249–261, 2002.

[41] Mohamed Khairy, *Combating Fading and Interference for Wireless and Wireline Communication Systems*, Ph.D. dissertation, University of Maryland, College Park, 2000.

[42] Massimiliano Lenardi, Abdelkader Mdeles, and Dirk T.M. Slock, "Comparison of downlink transmit diversity schemes for rake and SINR maximizing

receivers," in *Proceedings of IEEE International Conference on Communications*, 2001, vol. 3, pp. 1679–1683.

[43] Peter Schulz-Rittich, Jens Baltersee, and Gunnar Fock, "Channel estimation for DS-CDMA with transmit diversity over frequency selective fading channels," in *Proceedings of IEEE Vehicular Technology Conference*, 2001, vol. 3, pp. 1973–1977.

[44] H. Vincent Poor, and Xiaodong Wang, "Blind multiuser detection: A subspace approach," *IEEE Transactions on Information Theory*, vol. 44, No. 2, pp. 677–690, 1998.

[45] Hesham El Gamal and Evaggelos Geraniotis, "Iterative multiuser detection for coded CDMA signals in AWGN and fading channels," *IEEE Journal on Selected Areas in Communications*, vol. 18, no. 1, pp. 30–41, 2000.

[46] M. Pursley, "Performance evaluation of phase coded spread spectrum multiple access communications, Part I: System analysis," *IEEE Transactions on Communications*, vol. COM-25, pp. 795–799, 1977.

[47] Evaggelos Geraniotis, "Performance of noncoherent direct sequence spread spectrum multiple access communications," *IEEE Journal on Selected Areas in Communications*, vol. SAC-3, pp. 687–694, 1985.

[48] Robert C. Dixon, *Spread Spectrum Systems*, John Wiley & Sons, New York, 1984.

[49] Jun Tan, and Gordon L. Stuber, "Anti-jamming performance of multi-carrier spread spectrum with constant envelope," in *Proceedings of IEEE International Conference on Communications*, 2003, vol. 1, pp. 743–747.

[50] Steve Tretter, "Estimating the frequency of a noisy sinusoid by linear regression," *IEEE Transactions on Information Theory*, vol. 31, pp. 832–835, 1985.

[51] Simon Haykin, *Adaptive Filter Theory*, Prentice Hall, New York, 2nd edition, 1991.

[52] Richard Roy and Thomas Kailath, "ESPRIT - estimation of signal parameter via rotational invariance techniques," *IEEE Transactions on Acoustics, Speech, and Signal Processing*, vol. 7, pp. 984–995, 1989.

[53] Steven Kay, *Modern Spectral Estimation: Theory and Application*, Prentice Hall, New York, 1988.

[54] Irving Kalet, "The multitone channel," *IEEE Transactions on Communications*, vol. 37, no. 2, pp. 119–124, 1989.

[55] Yingjiu Xu, Hsuan-Jung Su, and Evaggelos Geraniotis, "Pilot symbol assisted QAM with iterative filtering and turbo decoding over Rayleigh flat-fading channels," in *IEEE Military Communications Conference Proceedings*, 1999, vol. 1, pp. 86–91.

[56] J. Zander, "Performance of optimal transmitter power control in cellular radio systems," *IEEE Transactions on Vehicular Technology*, vol. 41, no. 1, pp. 57–62, 1992.

[57] J. Zander, "Distributed cochannel interference control in cellular radio systems," *IEEE Transactions on Vehicular Technology*, vol. 41, no. 3, pp. 305–311, 1992.

[58] G. J. Foschini and Z. Miljanic, "A simple distributed autonomous power control algorithm and its convergence," *IEEE Transactions on Vehicular Technology*, vol. 42, no. 4, pp. 641–646, 1993.

[59] R. D. Yates and Ching-Yao Huang, "Integrated power control and base station assignment," *IEEE Transactions on Vehicular Technology*, vol. 44, no. 3, pp. 638–644, 1995.

[60] R. D. Yates, "A framework for uplink power control in cellular radio systems," *IEEE Journal on Selected Areas in Communications*, vol. 13, no. 7, pp. 1341–1347, 1995.

[61] P. S. Chow, J. Tu, and J. M. Cioffi, "A discrete multitone transceiver system for HDSL application," *IEEE Journal on Selected Areas in Communications*, vol. 9, no. 6, pp. 895–908, 1991.

[62] X. Qiu, and K. Chawla, "On the performance of adaptive modulation in cellular systems," *IEEE Transactions on Communications*, vol. 47, no. 6, pp. 884–895, 1999.

[63] T. S. Rappaport, *Wireless Communications: Principles and Practice*, Prentice Hall, New York, 1996.

[64] David Parsons, *The Mobile Radio Propagation Channel*, John Wiley & Sons, New York, 1992.

[65] M. Barton and M. L. Honig, "Optimization of discrete multitone to maintain spectrum compatibility with other transmission systems on twisted copper pair," *IEEE Journal on Selected Areas in Communications*, vol. 13, no. 9, pp. 1558–1563, 1995.

[66] T. M. Cover and J. A. Thomas, *Elements of Information Theory*, John Wiley & Sons, New York, 1991.

[67] G. D. Forney Jr., R. G. Gallager, G. R. Lang, F. M. Longstaff, and S. U. Qureshi, "Efficient modulation for band-limited channels," *IEEE Journal on Selected Areas in Communications*, vol. 2, no. 5, pp. 632–647, 1984.

[68] Panos Papalambrosand Douglass J. Wilde, *Principles of Optimal Design – Modeling and Computation*, Cambridge University Press, New York, 1988.

[69] Garth P. Mccormick, *Nonlinear Programming*, John Wiley & Sons, New York, 1982.

[70] Hsuan-Jung Su and Evaggelos Geraniotis, "Power allocation and adaptive modulation for multicell OFDM systems with random multi-tone jammers," in *Proceedings of ATIRP 1999*, 1999, pp. 141–146.